Dynamic Stability Evaluation of an Automotive Turbocharger Rotor-Bearing System

by

Ali A. Alsaeed

Thesis submitted to the Faculty of the
Virginia Polytechnic Institute and State University
in partial fulfillment of the requirements for the degree of

Master of Science
in
Mechanical Engineering

R. Gordon Kirk, Chair
Mary E. Kasarda
Daniel J. Inman

May 3, 2005
Blacksburg, Virginia

Keywords: turbocharger, stability, linear, nonlinear, fluid-film bearings, rotordynamics

Dynamic Stability Evaluation of an Automotive Turbocharger Rotor-Bearing System

Ali A. Alsaeed

(ABSTRACT)

This project was initiated to more fully understand the dynamic stability of an automotive turbocharger rotor-bearing system using both linear and nonlinear analyses. The capabilities of a commercial Finite Element Analysis (FEA) code (computer program) were implemented in the investigation process. Several different hydrodynamic journal bearings were employed in the study of the turbocharger linearized dynamic stability. The research demonstrates how the linear analysis of a turbocharger rotordynamics can be very beneficial for the design evaluation and maintenance purposes.

Acknowledgments

I would like to express my deepest gratitude to my academic and research advisor Dr. Gordon Kirk for his guidance and constant support in helping me to conduct and complete this work. I would like also to thank Dr. Daniel J. Inman and Dr. Mary E. Kasarda for serving on my committee. Many thanks to Eigen Technologies Inc., RODYN Vibration Analysis Inc. and Holset Co. for their contributions to the research.

I also thank all my colleges I worked with in the Rotor Dynamics Laboratory at Virginia Tech, and specially Dr. Zenglin Guo and Giridhar Sabnavis for their cooperation and kindness. A special thank goes to Graduate Services Coordinator Cathy Hill.

I owe my sincere appreciation to my beloved parents, mother-in-law, father-in-law, and my wife for their constant support and prayers.

Table of Contents

List of Figures

Chapter 1

Introduction

Turbochargers are a vital class of turbomachinery intended to increase the power of internal combustion engines. Their total design, as in the other turbomachines, involves different types of analyses such as mechanical, thermal and acoustical. Engineers and researchers are still searching for ways to improve their designs while keeping the balance between the needs and costs.

1.1 Background and Motivation

The first turbocharger (Figure 1.1) was invented in the early twentieth century by the Swiss engineer Alfred Buchi who introduced a prototype to increase the power of a diesel engine. The idea of turbocharging at that time was very little accepted. However, in the last few decades, turbocharging has become essential part in almost all diesel engines (Figure 1.2), with the exception being very small diesel engines [18]. Their use in the petrol (gasoline) engines (Figure 1.3) has also shown good boost for the power output. Figure 1.4 represents a turbocharger used in an aircraft engine.

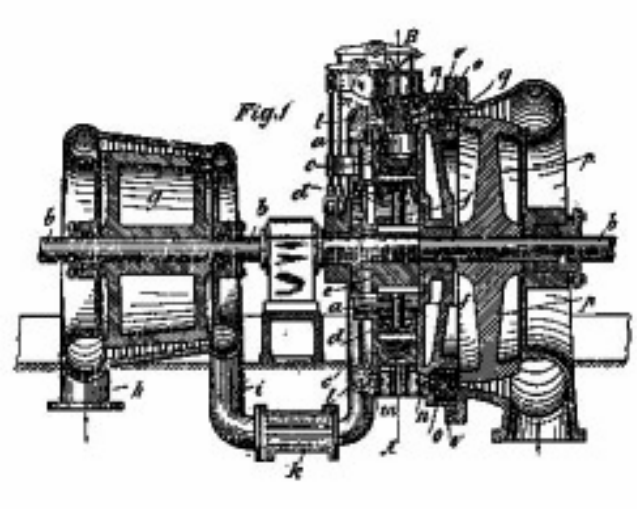

Figure 1.1 Early Turbocharger [4]

Since the earliest turbocharger prototypes, researchers have attempted to develop the design to be more reliable for users. These studies were conducted on the output performance of the turbochargers with focus on the thermodynamics of the process. Although thermal analysis is an important part of the design process, thorough rotordynamics investigations of the turbochargers did not have a great attention at the early time. There were relatively few studies presented for the rotordynamics analysis of turbochargers.

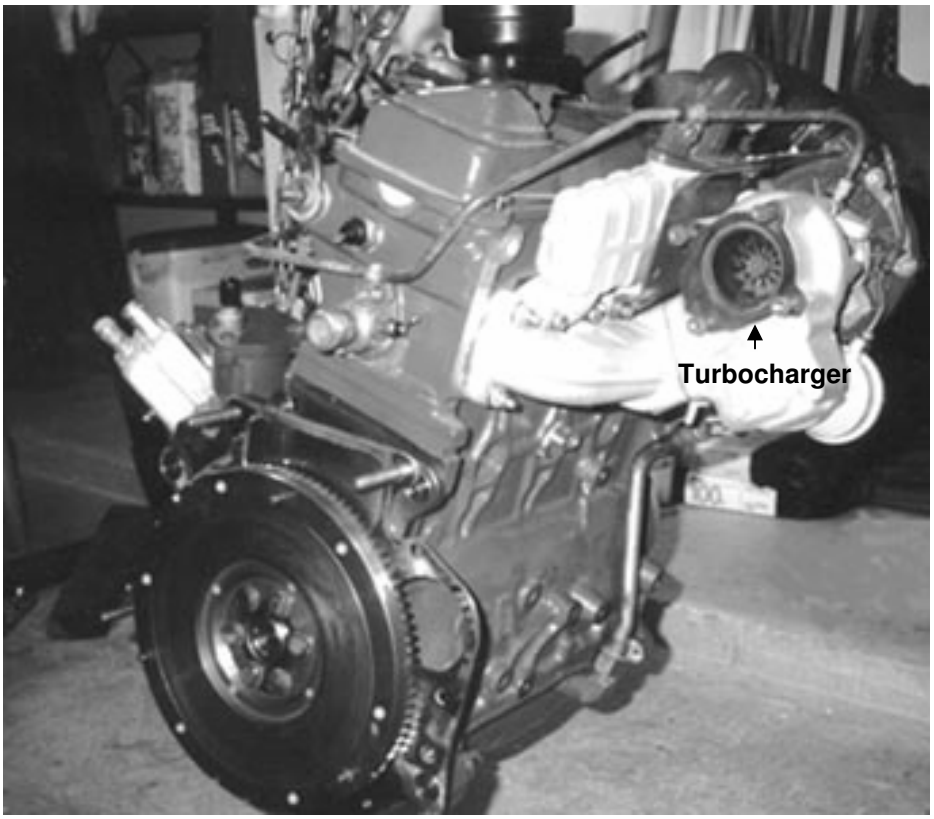

Figure 1.2 Turbocharger Used in Diesel Engine [17]

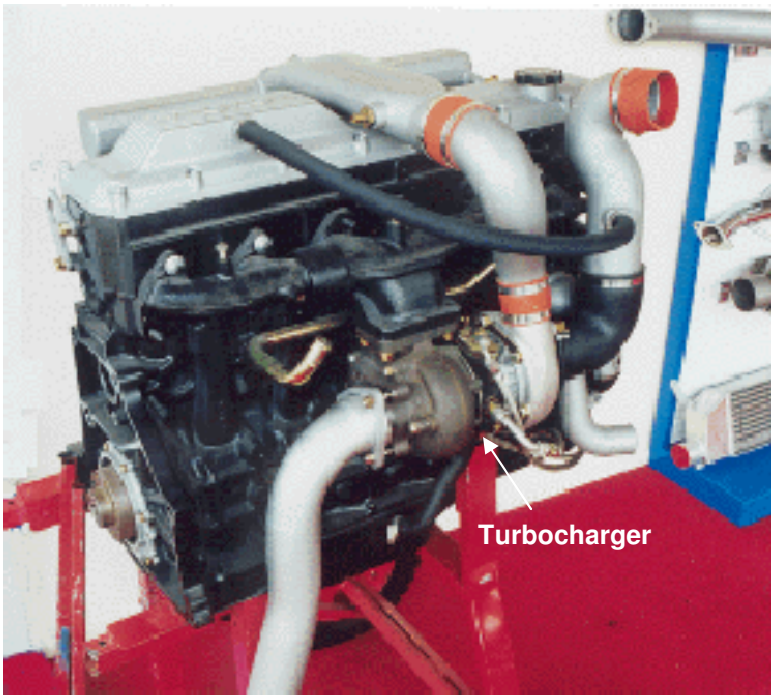

Figure 1.3 Turbocharger Used in Gas Engine [2]

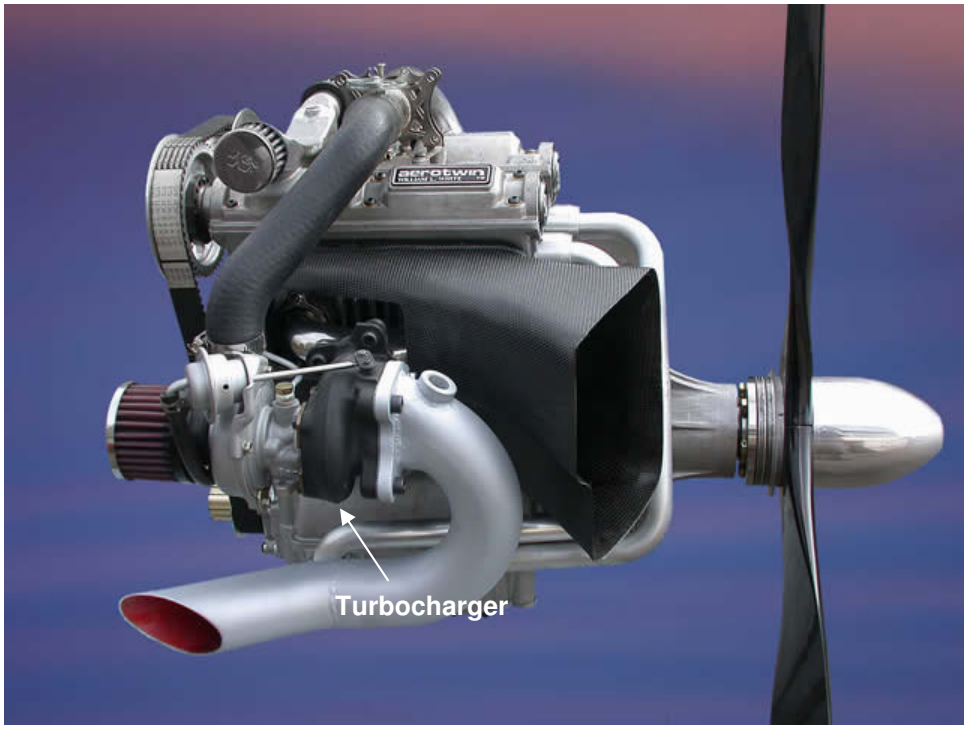

Figure 1.4 Turbocharger Used in Aircraft Engine [1]

The advances in rotordynamics analysis using the up-to-date computation technology have made the dynamics of turbochargers rotor-bearing system a rich area for investigation. Vendors are still looking for ways to have more dynamically stable turbochargers for the benefit of their business and customers satisfaction. More contributions are needed to have optimum design stability while assuring continued low cost production.

1.2 Research Goals and Approach

The proposed research aims to evaluate the dynamic stability of an automotive turbocharger rotor-bearing system using both linear and nonlinear analysis. The capabilities of a commercial Finite Element Analysis (FEA) code (computer program) will be implemented in the investigation process. The research will demonstrate how linear analysis of turbocharger rotordynamics can be very beneficial for the design and maintenance purposes.

1.3 Thesis Outline

The current thesis consists of five main chapters. Chapter 1 is an introduction to turbochargers with background and motivation in addition to research goals and approach followed by the thesis outline. Chapter 2 gives a short literature review on turbocharging and turbochargers. The turbocharging theory is first introduced followed by elaboration on automotive turbochargers and their rotordynamics analysis. Chapter 3 discusses the nonlinear dynamical response of turbochargers. The use of floating ring bearings in turbochargers will be summarized followed by a discussion of experimental investigation of the whirl instabilities. Nonlinear analytical prediction of whirling is then performed using the FEA code. In Chapter 4, the results of a linear analysis of turbocharger rotordynamic stability are presented, beginning with floating ring bearings. Turbocharger dynamical performance is also analytically examined for several other types of fluid film journal bearings. By the end of Chapter 4 an attempt to create a method to stabilize the turbocharger rotor-bearing system using damped supports is introduced. Conclusions of the current research work and recommendations of future work are presented in Chapter 5.

Chapter 2

Literature Review

The rotordynamics of high-speed rotating machinery has been always a challenging, and more often the most interesting, part of the design process. Almost all machinery exhibit vibration problems and need frequent maintenance to extend their operation.

2.1 Introduction to Turbocharging

Turbocharging is a way to increase the power output of an engine by introducing air into the engine cylinder with higher density than ambient. This can be achieved by a compressor driven by a turbine. The engine hot exhaust gas boost is used to drive the turbine. A general description of the turbocharger process is shown in Figure 2.1.

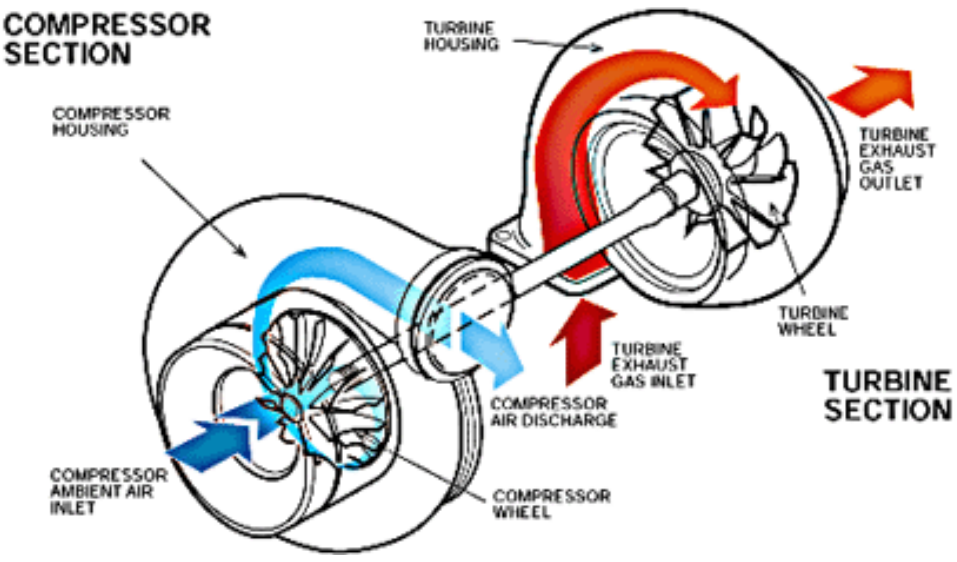

Figure 2.1 Cutaway View of a Typical Turbocharger Showing the Compressor and Turbine Flow [4]

In fact, increasing the power output of the engine (also called supercharging) does not always come with a better efficiency. There is a recognized practice to supercharge the automotive engine by using the mechanical power of the engine itself. In other words, a belt can transfer the engine torque to a compressor that boosts the pressure of the intake air going into the engine cylinder. Obviously that method would take from the engine power itself, while the supercharging is being performed. However, turbochargers can utilize the wasted hot exhaust gas to increase the engine power, without as much loss of efficiency.

The commercially available turbochargers can be subdivided into two principal groups: those primarily designed for use on automotive and truck engines (Figure 2.2), and those for use on medium-speed and low speed diesel engines for railway traction, electricity-generating sets, industrial and marine applications (Figure 2.3). The difference between the two principal groups can be summed up as a contrast between small, simple and cheaply mass-produced units, and larger, more complex, expensive and reliable industrial or large marine units. [18]

Figure 2.2 Holset HX35 Turbocharger [16]

Figure 2.3 Large Turbocharger [12]

2.2 Automotive Turbochargers

Turbochargers are widely used in trucks and diesel engines. There are also some gasoline fueled cars and other special purposes vehicles that use turbochargers. A small turbocharger (Figure 2.4 and Figure 2.5) consists basically of a compressor and a turbine coupled on a common shaft.

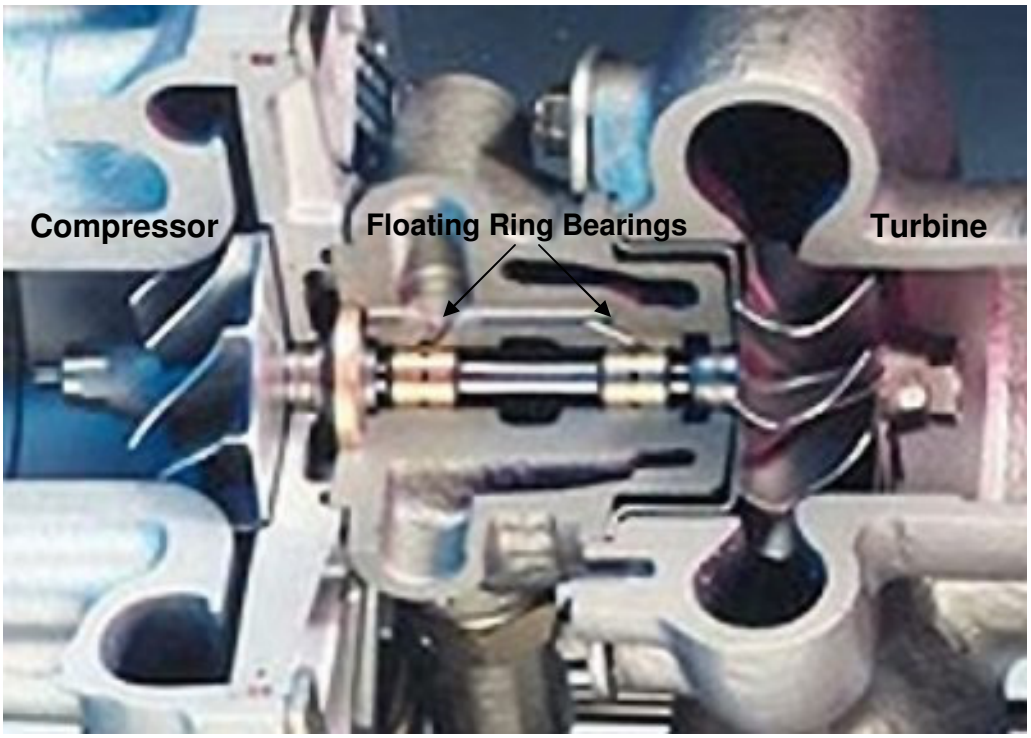

Figure 2.4 Turbocharger Cross Section [4]

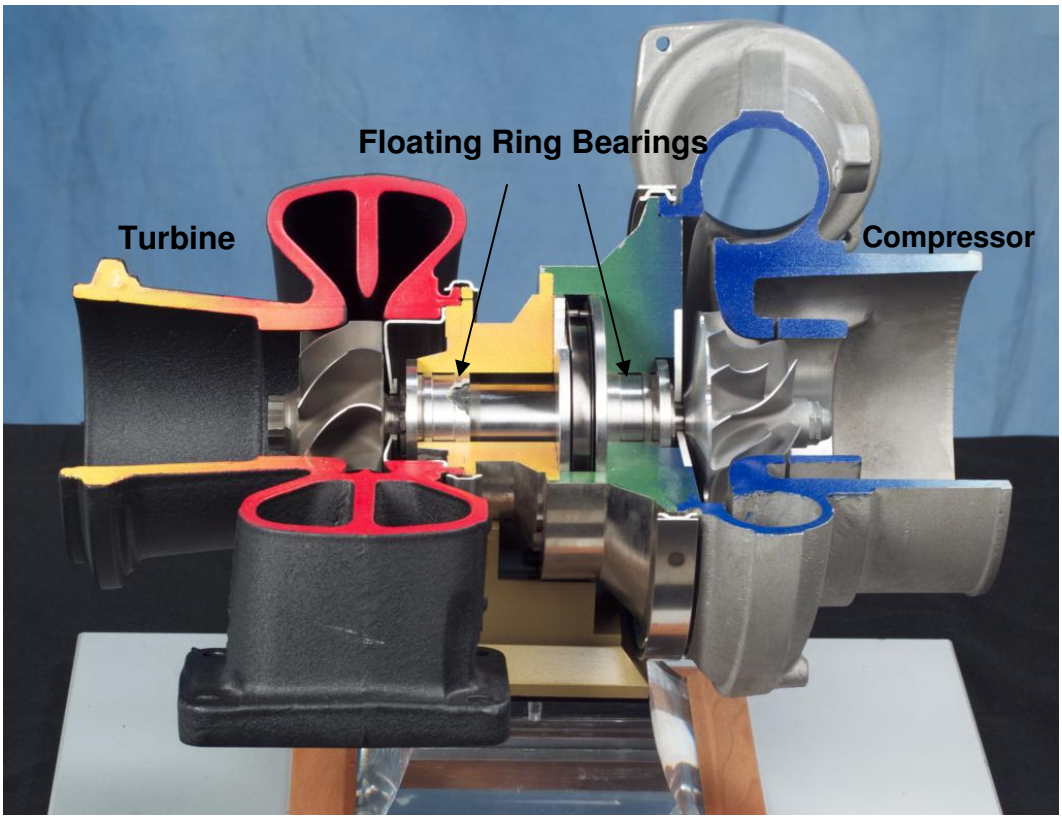

Figure 2.5 Turbocharger with twin-entry turbine [11]

The most important factor in the design of an automotive turbocharger is the initial cost. Engineers aim to undercut the cost of producing larger engines capable of providing the same power. Even though truck engines operate at modest break-mean-effective-pressure (~14 bar) and hence at lower boost pressure (up to 2.5:1), they work at much higher exhaust temperature [18]. Because of truck engines heavy operations, they demand good acceleration and high torque over a wide speed range. They also require a high level of reliability and efficiency.

There are several ways to reduce the costs of turbochargers. However, the best way to achieve that is to keep the design as simple as possible. Figure 2.6, shows a very frequent assembly of automotive turbochargers. It has a simple inboard bearing mounting arrangement with a radial outflow compressor and a radial inflow turbine on a single shaft.

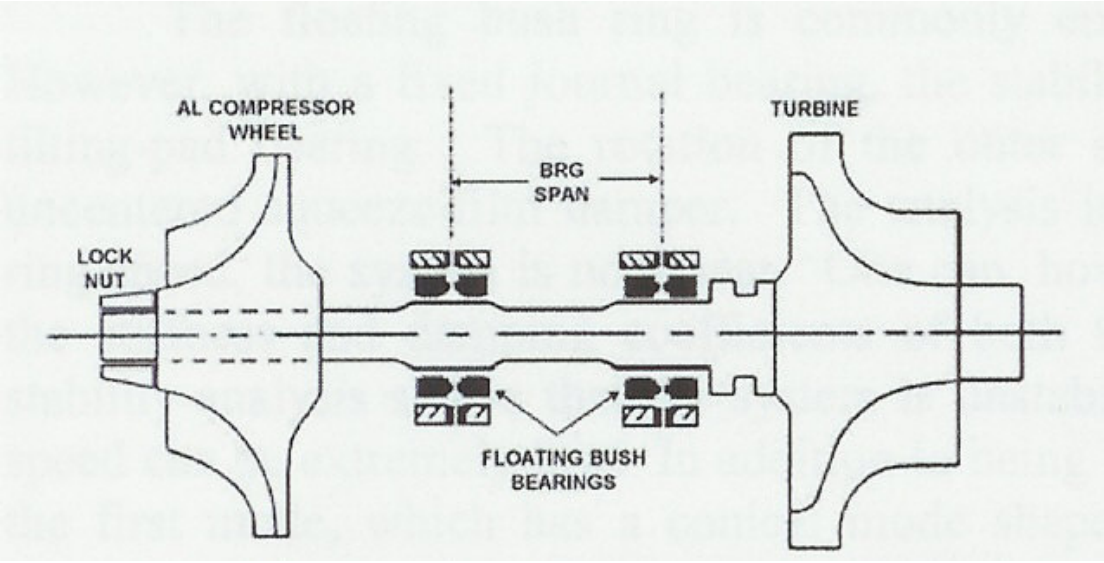

Figure 2.6 Turbocharger Rotor-Bearing System [6]

The compressor impeller (Figure 2.7) in most automotive type turbochargers is made of aluminum (LM-16-WP or C-355T61). Aluminum LM-27-M is also used for the compressor casing, unless the compressor impeller is made from other material than aluminum. On the other hand, the turbine rotor should withstand a much higher operating temperatures that could be as high as 1000 K (1340.6° F), or more. Therefore, the most convenient material to use for that purpose is 713C Inconel (a high nickel alloy). The turbine rotor casing should also withstand high temperatures, but not resist as high pressure as the turbine. There are three different types of materials used for the turbine rotor casing depending on their operating temperatures. S.G. iron (spheroidal graphite) is used for operating temperatures up to 975 K, high-silicon S.G. iron is for temperatures up to 1000 K, and high nickel cast iron for temperatures above 1000 K. The shaft is usually made of high-carbon steel (C1144 steel, EN 19C) to allow induction hardening of journals.

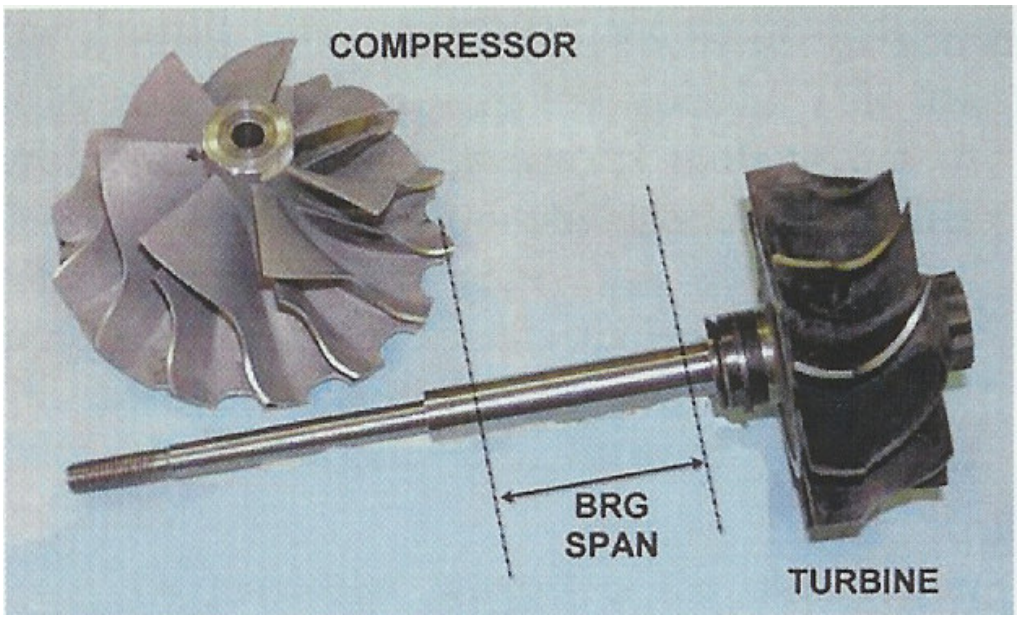

Figure 2.7 Disassembled Turbocharger [6]

The turbine rotor in most common automotive turbochargers is connected to its shaft by using friction welding or an electron beam welding method. The compressor is usually a loose or very light interference fit on the other end of the shaft. A self locking nut is used to hold the impeller against an abutment on the shaft. A friction created between the shaft and compressor is sufficient to transmit the torque. Therefore, no splines or keys are needed.

Most of automotive-size turbochargers, if not all of them, incorporate simple journal bearings. They use the engine lubricating oil system for their bearings to assure low cost and simplicity of maintenance, instead of having a separate system. Ball bearings are not used for most commercial engine applications because of their short life and difficult access for replacement. Special high performance engines in automotive racing applications, can afford the added expense of ball bearings. Current designs make use of ceramic ball elements. A more detailed elaboration on this subject will be the main interest in the following chapters.

2.3 Turbocharger Rotordynamics

Since the early times of turbocharger evolution, engineers have attempted to design more efficient, low cost turbochargers. They also tried to redesign the compressor and turbine stages for a higher flow capacity. This can not be done without altering the original rotor-bearing system.

The primary consideration in the design of high-speed rotating machinery in the context of rotordynamics is to control and minimize response to forced vibration (and in particular, rotor unbalance). But there exists another class of vibration - rotordynamic instability and self excited vibration - which involves an additional set of design approaches, requirements, and constraints to ensure trouble-free, quiet, and durable rotating machinery. [5]

Almost all rotors of automotive turbochargers exhibit strong subsynchronous vibrations as well as the more usual unbalance vibrations found in other rotating machinery. These vibrations are undesirable as they cause noise (rumble) and can be of large amplitude, causing rotor-stator rub. [8]

Unbalance generally arises in rotors by two main causes: mass eccentricity and shaft bow. Mass eccentricity is a natural phenomenon in all rotors due to the offset of mass centroid, whereas shaft bow is commonly caused by thermal effects. Unbalance vibrations are harmonic (or synchronous) with shaft speed. They can be mainly solved by balancing the rotor (correcting the centroid offset) or by straightening the shafts that been bowed by thermal effects.

Self-excited vibrations, on the other hand, are different from the forced or unbalance vibrations. They often developed during the operation of the rotor, but they do not naturally exist there. In other words, when the rotor stops running, the mechanical unbalance will still exist, however, the sources of self-excited vibrations will not.

Rotordynamic instabilities that caused by self-excited lateral vibrations occur at the system critical (natural) frequencies, and below the running speed (subsynchronous). They usually increase as the running speed increase until nonlinearities in the system forbid higher amplitudes. The mechanism of self-excitation can be categorized as: whipping and whirling, parametric instabilities, stick-slip rubs and chatter and instabilities in forced vibrations [5].

Subsynchronous instabilities in turbochargers are commonly referred to as whirling or whipping. The main sources of whirling and whipping in turbochargers are: internal rotor damping (hysteretic whirl), fluid-film journal bearings, and aerodynamic cross-coupling. This research will highlight the fluid film bearings affects on the rotordynamic instabilities of turbochargers.

Whirling and whipping arise in turbochargers in fluid film bearings as the viscous fluid (usually engine oil) circulates in the bearing clearance with an average velocity of about one-half the shaft's surface speed. Figure 2.8 demonstrate the tangential force component developed from the high pressure bearing fluid. This force induces the forward whirl of the rotor. Instability occurs when this force exceeds the inherent stabilizing damping forces.

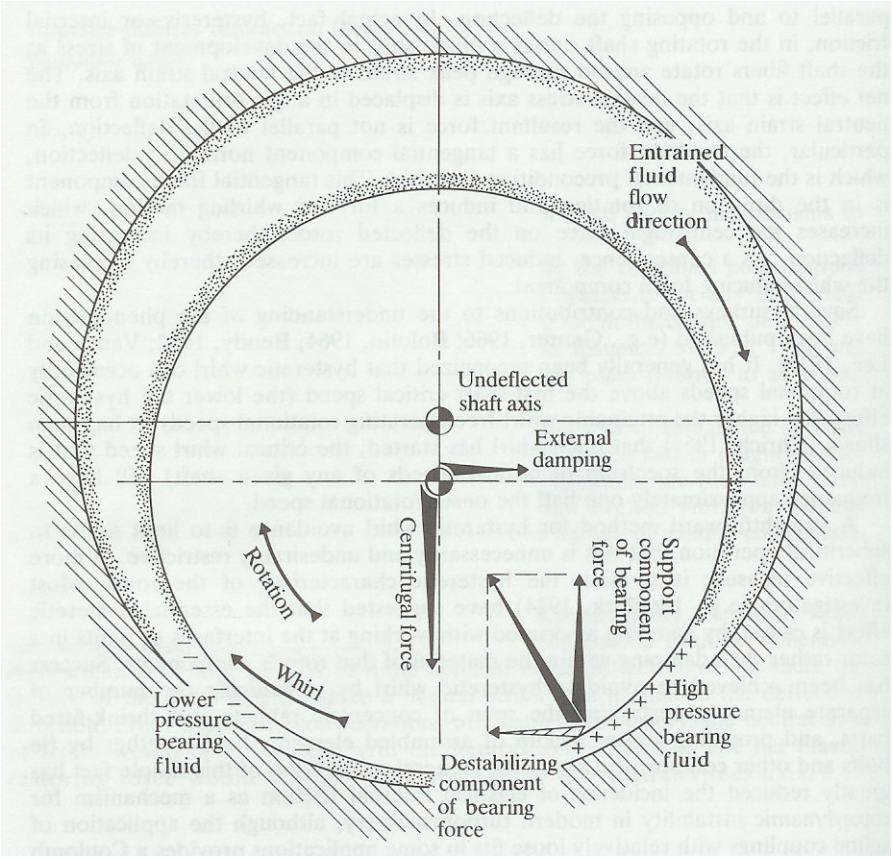

Figure 2.8 Fluid Bearing Whip [5]

Instabilities are expensive in business matters because of the operation delays they cause in addition to redesign and modification costs. These factors supply the need to design a stable turbocharger rotor-bearing system, which becomes a top priority for manufactures. In the past, there were not many research works presented for the rotordynamics of turbochargers because of the short of alternative –inexpensive- methods

of examining model design. However, in the recent years, developments in computational methods have made the design process much easier, faster, and reliable.

There are many approaches to improve the stability of automotive turbochargers. One way is to modify the bearing characteristics. Bearing type, shape or preloads can be altered. However, most automotive turbochargers are running in floating ring (bushing) bearings (Figure 2.9). These bearings show most reliable high-speed stability operation to manufacturing cost currently available in the market. However, most recent researches ([6], [8], and [15]) can show that subsynchronous vibrations still exist in these floating ring bearings with high amplitudes.

Figure 2.9 Floating Ring Bearings [6]

Certainly, improvement and upgrade of the rotor-bearing system for automotive turbochargers are fundamental needs to all vendors and users. With the use of advanced computational methods, evaluation of the rotordynamics of turbochargers becomes a vital part of the design process. This will be the main study in the following chapters.

Chapter 3

Nonlinear Dynamical Response

Nonlinearities are inherent in all automotive turbochargers running in fluid film bearings. Although they are vital in damping the destabilizing forces in the rotor-bearing system, instabilities will arise as these destabilizing forces exceed the nonlinearities effect. In this chapter an analytical approach using DyRoBeS© [7] code will be conducted to evaluate the nonlinear behavior of a turbocharger in floating ring bearings compared to former experimental investigations.

3.1 Turbochargers with Floating Ring Bearings

Floating ring bearings have become the standard type for small automotive turbochargers. They are likely preferred for the damping characteristics they provide to stabilize the rotor motion. In fact, fixed journal bearings (Figure 3.1) are known to have poor stable operations in high-speed rotors. Turbochargers normally run in speeds of 100,000 RPM and more, in most automotive types. In larger turbochargers like the diesel locomotive type, fixed journal bearings (e.g. 3 lobe or offset bearing) can be used with added external damping (e.g. squeeze-film damper) technique. This additional damping will reduce the destabilizing forces effects to have smoother running. However, in small automotive turbochargers, the aforementioned technique is difficult to maintain due to size and cost consideration [6]. Therefore, the design of floating ring bearings (Figure 3.2) introduces the external damping without the need of larger bearing housings.

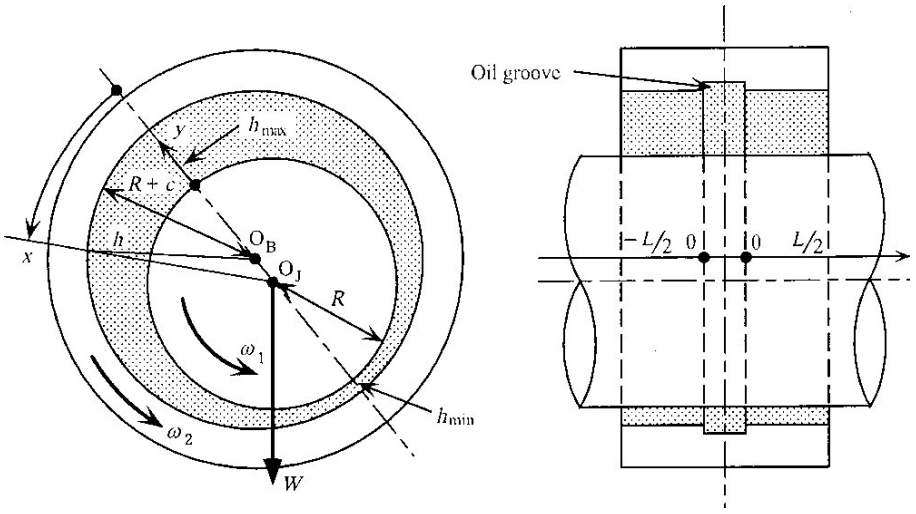

Figure 3.1 Plain Journal Bearing [15]

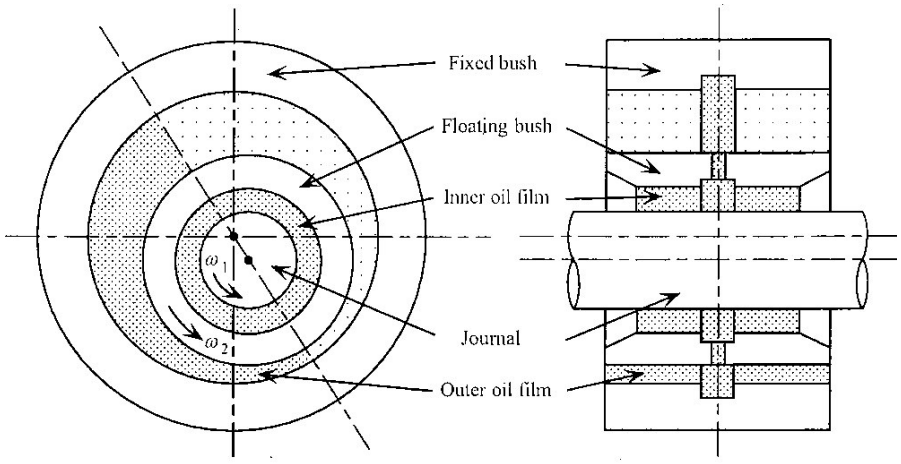

Figure 3.2 Floating Ring Bearing [15]

The floating ring bearing consist of a floating ring (bush) that rotates freely in an outer journal bearing with six-oil-groove feedings, in most designs. The ring also has six-oil groove (Figure 3.3) to supply oil between the outer film and inner film. The inner clearance is normally smaller that the outer clearance. Theoretically, the ring rotates in about one-half the speed of the shaft. However, experimental studies [6] shows that the floating ring rotational speed increases with the shaft speed but never reach one-half.

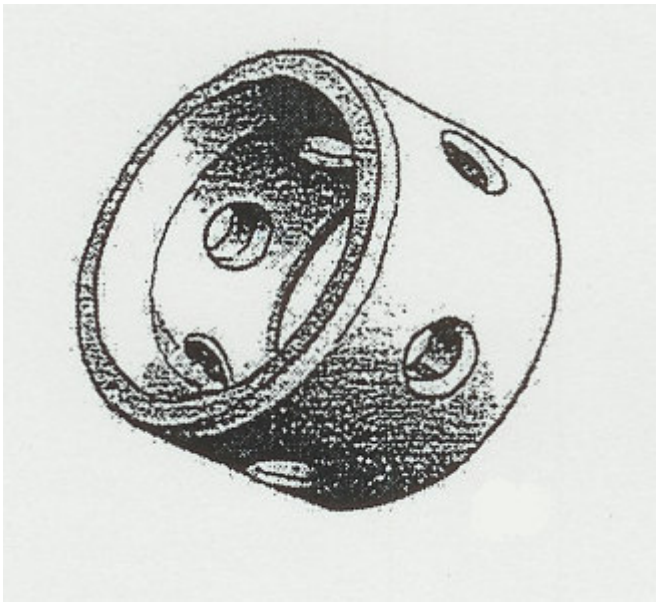

Figure 3.3 Floating Ring Bearing with Six-Oil Groove [8]

One significant reason why floating ring bearings are widely employed is that they are inexpensive to produce. Immediate alternative bearings that show better dynamic stability performance are possible to apply, but that would cost much more. Hence, designers are still trying to improve the floating ring bearing dynamical behavior and search for other reliable and inexpensive options.

3.2 Experimental Investigation of Whirl Instabilities

A former experimental work on the vibration of a typical turbocharger with floating ring bearings was presented by Holmes [8]. Figure 3.4 shows clearly the high subsynchronous vibrations amplitudes found on that turbocharger. Whirl instability starts at a very low speed. The first low frequency whirl mode is a rigid body mode of conical shape with the turbine and compressor wheels moving out of phase. This mode evidently dominates over a large speed range. At speeds above 40,000 RPM, a second whirling mode starts to build up. Both of the turbine and compressor wheels are whirling forward in phase at the second resonance frequency.

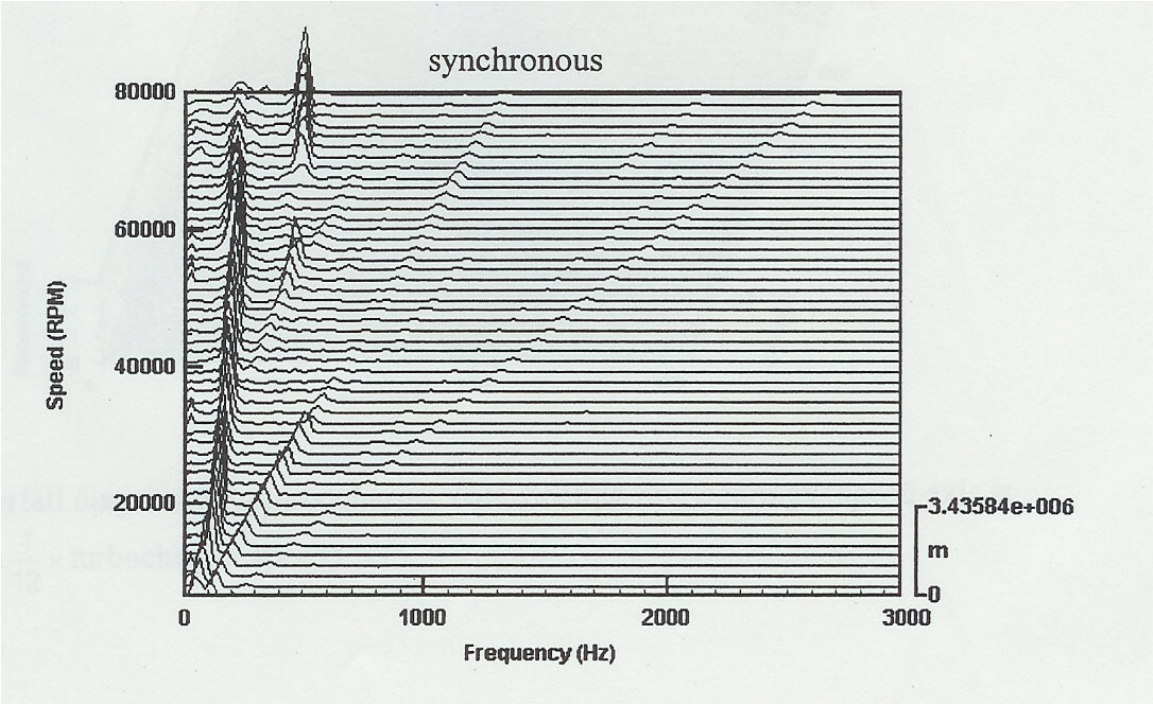

Figure 3.4 Typical Turbocharger Waterfall Diagram [8]

As can be observed from Figure 3.4, the second whirl mode restabilized at speeds around 55,000 RPM. A likely explanation of second whirl mode disappearance is the slight increase in bearing loading due to the possible presence of turbocharger third mode [6]. The second whirling mode shows up again at speeds above 70,000 RPM with higher amplitudes. The first conical whirling mode start to vanish as speed increased further. This may be due to the high limit cycle motion of the second mode that likely increases the bearing loading.

In fact, experimental investigation results show reliable information for the rotordynamics of turbochargers. Nevertheless, experimental work requires considerable expenses and time. Alternative methods for dynamical analysis became a critical necessity for designers.

3.3 Analytical Prediction of Whirl Motion

Computational advances in the recent years have made it possible to rely on Finite Element Analysis (FEA) in rotating machinery design and diagnosis. Several commercials codes are currently available with varying levels of sophistication. DyRoBeS©_Rotor is a powerful rotor dynamics program based on Finite Element Analysis (FEA). This program has been developed for the analysis of free and forced vibrations (Lateral, Torsional, and Axial) of multi-shaft and multi-branch flexible rotor-bearing-support systems. The acronym, DyRoBeS©, denotes "Dynamics of Rotor Bearing Systems". [7]

3.3.1 Model Assumption

In the current research, a Holset Turbocharger HX30 type (Figure 3.5) will be analyzed using DyRoBeS© code capabilities. A model of the rotor-bearing system is first developed as shown in Figure 3.6. The rotor shaft is made of carbon steel and the turbine is made from Inconel.

As can be seen from the model, the shaft and turbine are jointed as one body. The aluminum compressor weight will be assumed as added disks to the rotor. Two nonlinear floating ring bearings are placed between the turbine and compressor with the exact dimensions as provided by the vendor. The characteristics of the compressor end bearing and the turbine end bearing are shown in Figures 3.7 and 3.8, respectively.

There are inherent unbalance forces that act on the rotor-bearing system. The model employed values of 0.00095 kg-mm, 0.0011 kg-mm, 0.00063 kg-mm, and 0.00049 kg-mm, respectively from the compressor end. These imbalance loads were provided to Virginia Tech by Holset engineers and are typical of this class turbocharger.

Figure 3.5 Holset HX30 Turbocharger [16]

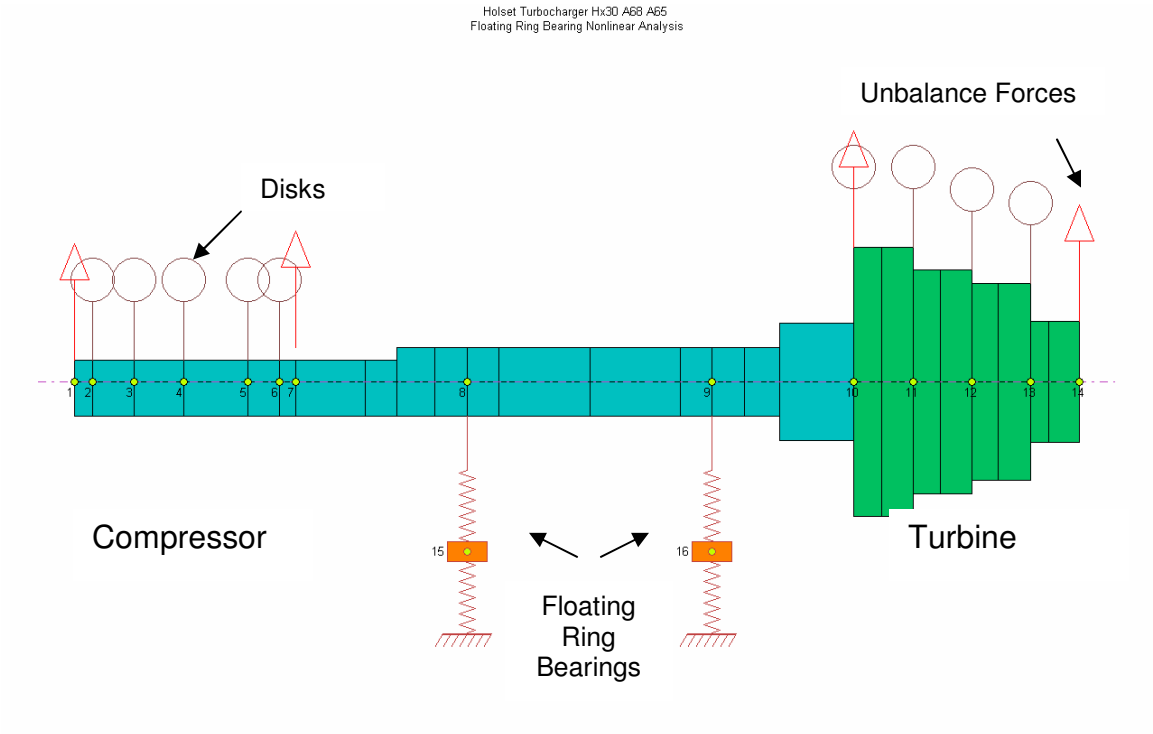

Figure 3.6 Holset HX30 Turbo with Floating Ring Bearings

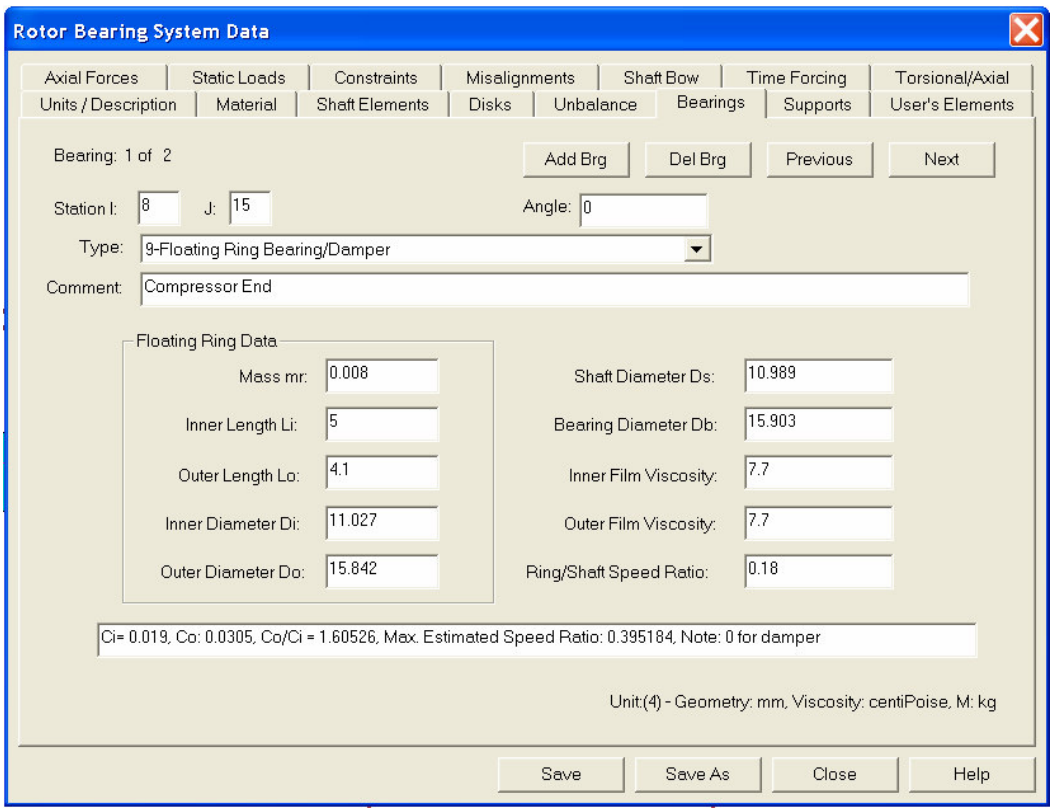

Figure 3.7 Characteristics of Compressor End Bearing

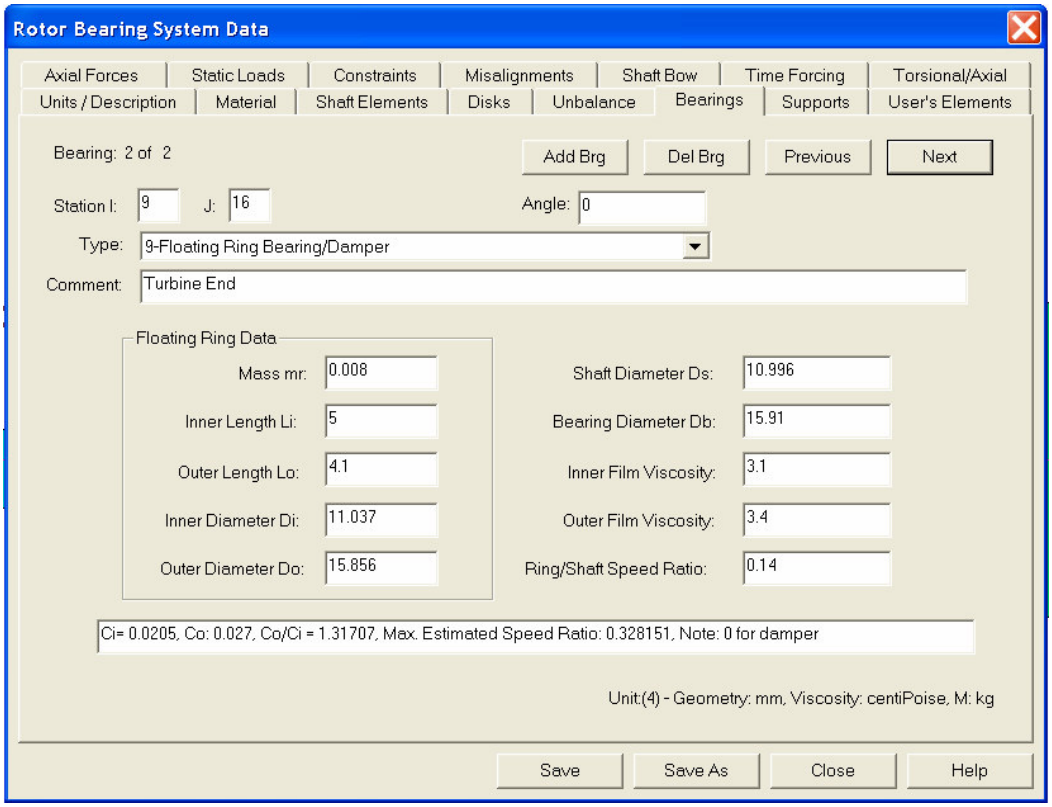

Figure 3.8 Characteristics of Turbine End Bearing

3.3.2 Time Transient Analysis

In order to examine the nonlinear behavior of the turbocharger with floating ring bearings, Time Transient Analysis was performed. The transient response for the rotor system was calculated for speeds from 10,000 RPM to 150,000 RPM with increment of 10,000 RPM. For comparison purposes between each speed response, the time interval and time step for computational integration were chosen in way to have approximately 166 shaft cycles in each running speed. Newmark solution method for integration was used in all calculations with a time step increment of 2e-6 s (Figure 3.9). The only effects considered in the analysis are the unbalance forces and gravity.

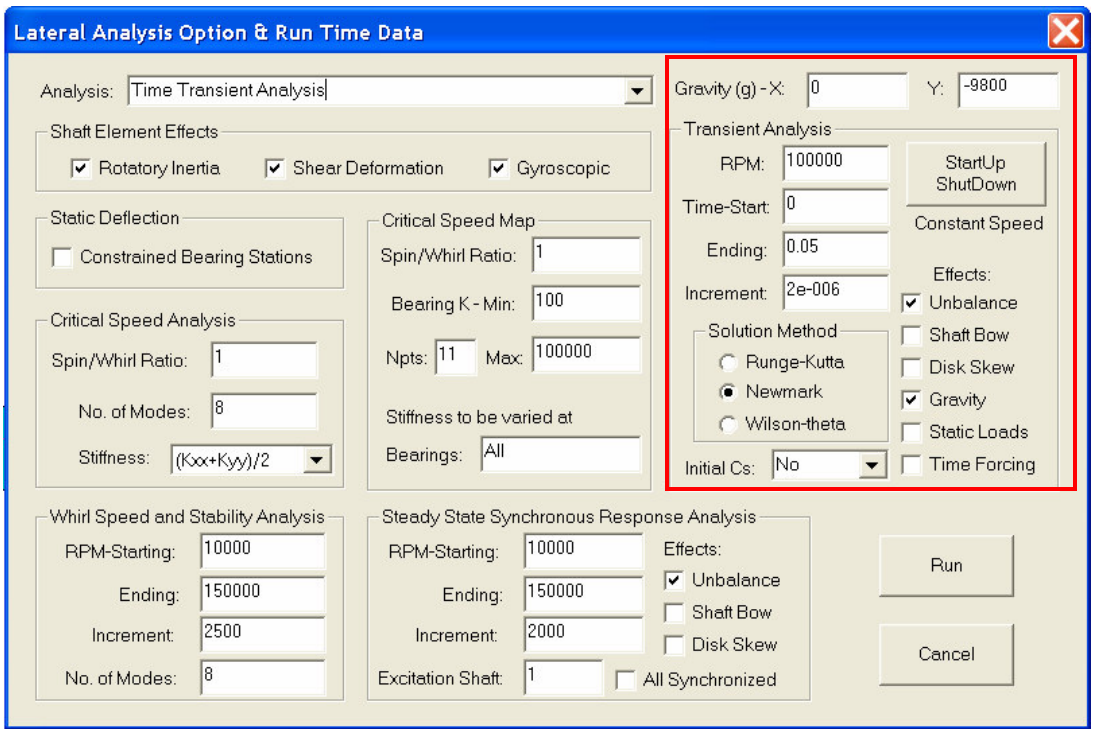

Figure 3.9 Time Transient Analysis at Speed of 100,000 RPM

The FFT spectrum data were collected for each speed then plotted accordingly using a specially developed Matlab code. Figures 3.10 and 3.11 display the waterfall diagram calculated from the time transient analysis of the Holset turbocharger for speeds from 10,000 RPM to 150,000 RPM. The first waterfall diagram data were picked from the compressor end tip and the second data were from the other opposite side, the turbine end tip.

One can notice the similarities between the experimental data (Figure 3.4) and the computed data (Figure 3.10). The waterfall diagram from the compressor end tip (Figure 3.10) clearly shows the subsynchronous vibrations found from the analysis. The low frequency whirling mode starts at speed 20,000 RPM. This first conical whirling mode then dominates with high amplitudes over the higher running speeds. The second in-phase whirling mode can be seen at speeds between 80,000 RPM and 100,000 RPM. Then a third whirl mode starts at 110,000 RPM and continues to 130,000 RPM then start to vanish over the speed range.

The unbalance synchronous vibrations found in the waterfall diagram (Figure 3.10) are significantly high. Excessive imbalance loads can be harmful to the bearings and the turbocharger casings.

Figure 3.12 displays the shaft transient response at 100,000 RPM. One can observe higher whirling motion of the compressor end (Figure 3.13), compared to the turbine rotor. This could be a result of the heavier weight of the turbine. That probably explains why vibration data at the compressor end (Figure 3.10) is richer than in the turbine end (Figure 3.11). In addition, nonlinear forces in the floating ring bearings make the shaft whirls in limit cycle in both ends (Figure 3.14). However, operation on high whirl motions could be harmful to the bearings and turbocharger casing.

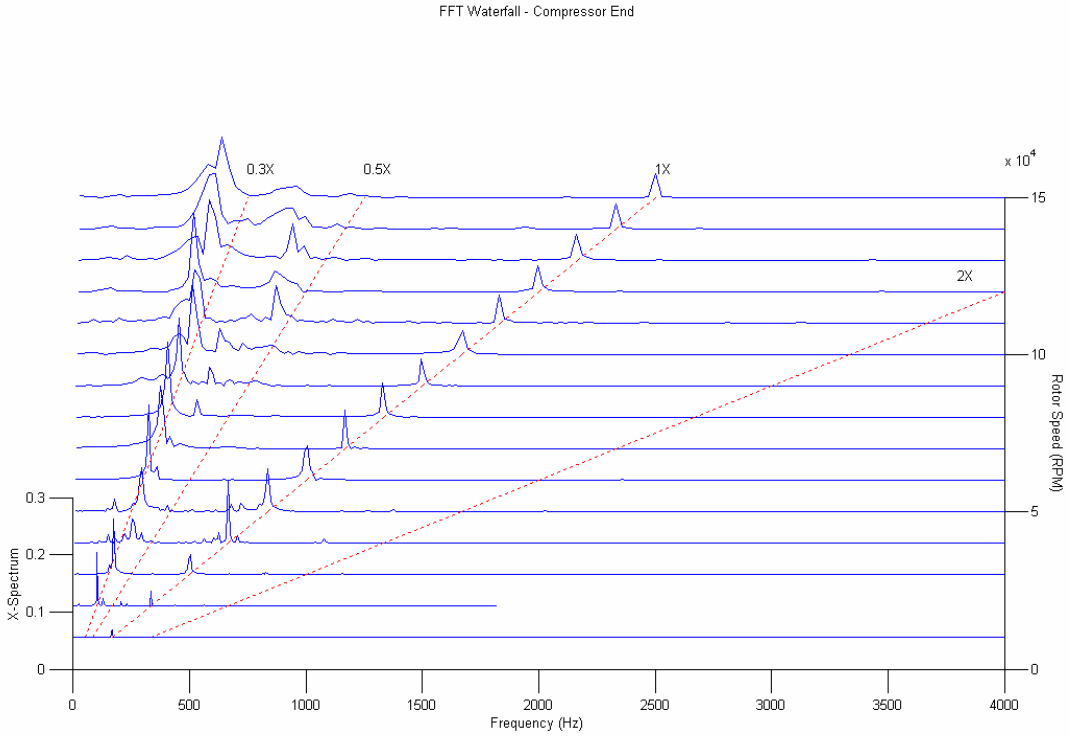

Figure 3.10 Holset Turbo Waterfall Diagram at Compressor End Tip

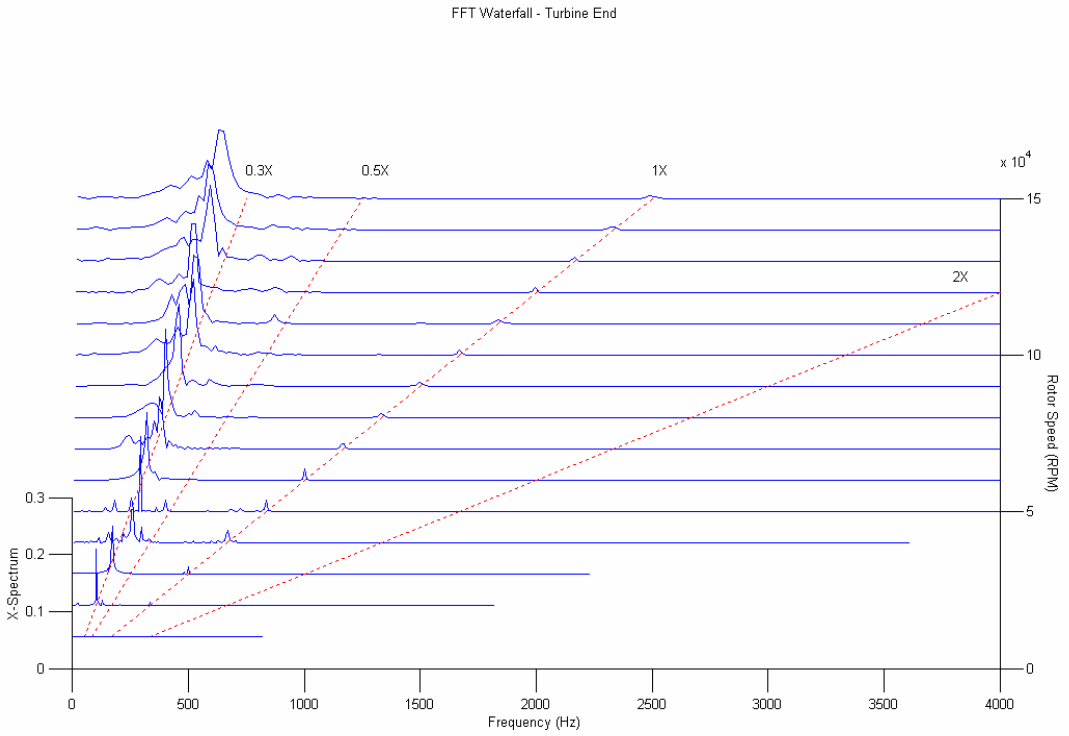

Figure 3.11 Holset Turbo Waterfall Diagram at Turbine End Tip

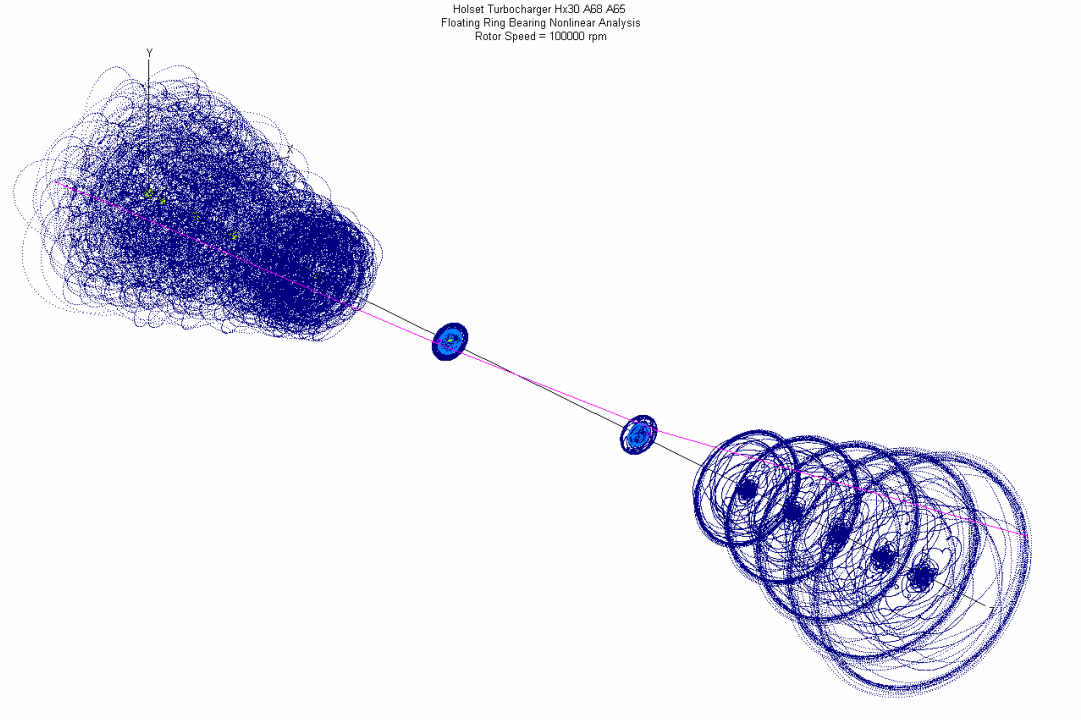

Figure 3.12 Shaft Transient Response

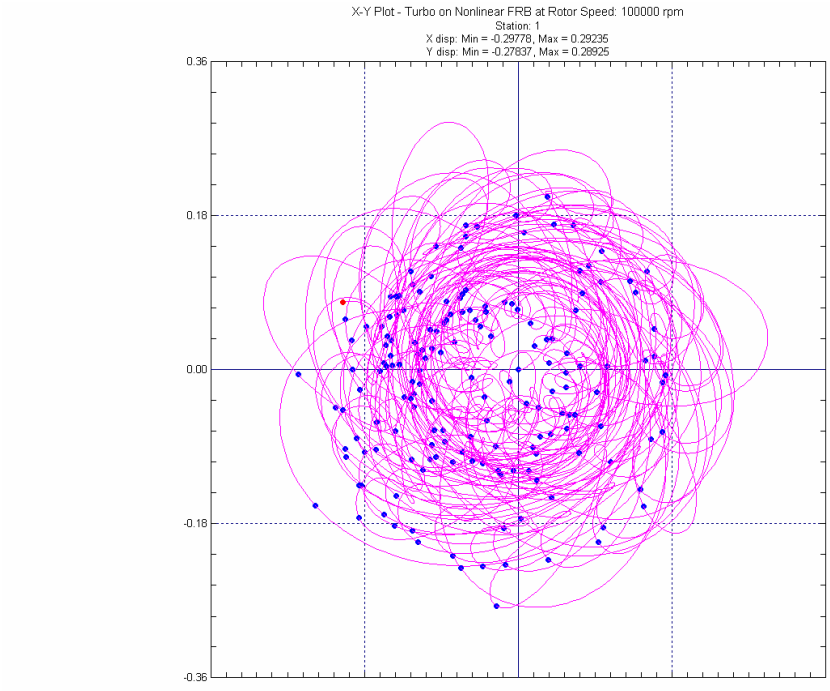

Figure 3.13 X-Y Orbit Plot of the Shaft at Compressor End

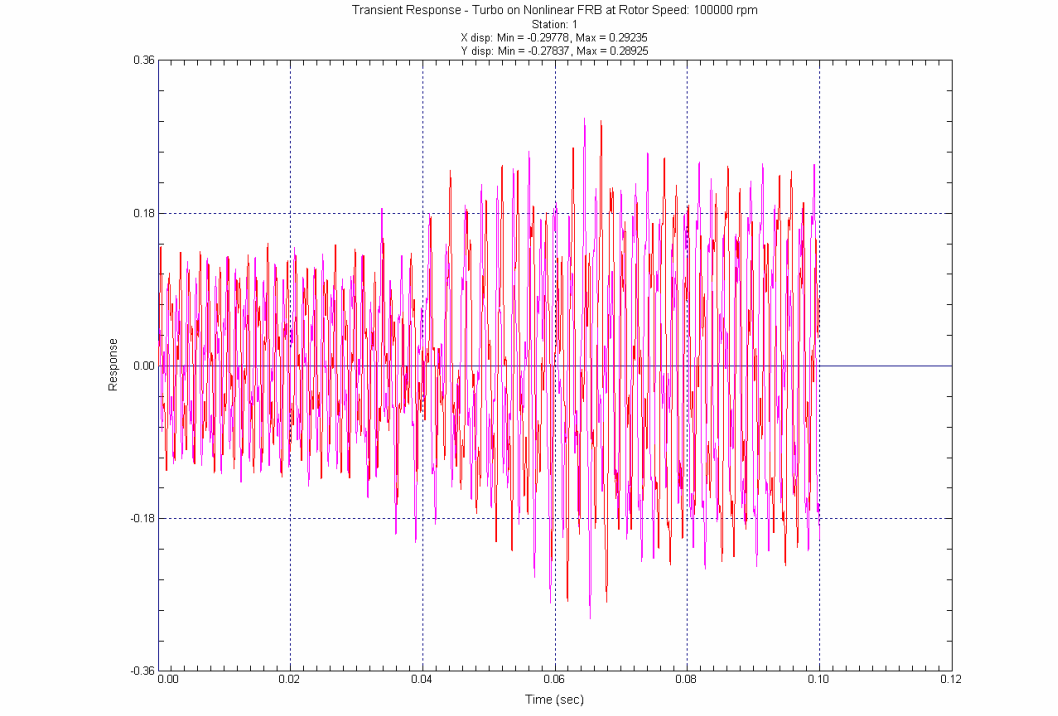

Figure 3.14 Transient Response at Compressor End

In order to further understand and detect the nonlinear dynamical performance of the turbocharger rotor-bearing system, it's always recommended to study the linear response. Therefore, the next part of the research will be essentially on linear analysis of the turbocharger.

Chapter 4

Dynamic Stability Linear Analysis

The rotordynamics characteristics of turbochargers are identical to larger high-speed turbomachinery. Large amplitude conditions are in nature. However, the linear performance of turbochargers is a dependable approach to evaluate the dynamic stability of turbocharger rotors operating under normal well balanced conditions.

The advances in computations have made it possible to develop codes that utilize the Finite Element Analysis (FEA) in rotordynamics of rotating machinery. The research will continue assessing the stability of the Holset HX30 turbocharger rotor-bearing system. DyRoBeS© was the main program used in this linear analysis. Several different hydrodynamic journal bearings will be employed in the study of the turbocharger linearized dynamic stability.

4.1 Turbocharger in Floating Ring Bearings

Floating ring bearings are still widely used in automotive turbochargers despite the fact that they exhibit high subsynchronous vibrations and instabilities. This study will show the behavior of the perfectly balanced turbocharger with linear floating ring bearings considering small amplitude motion about the static equilibrium positions.

Two floating ring bearings are modeled using the DyRoBeS©_BePerf. This computer code analyzes the bearing steady state and dynamic performance using the Finite Element Method (FEM). The governing equation for pressure distribution in a fluid film journal bearing is Reynolds equation which is derived from the Navier-Stokes equation. The fluid film forces acting on the journal are determined by application of boundary conditions and integration of pressure distribution. It is an iterative process until the convergence criterion is satisfied. Once the static equilibrium is found, the

bearing static performance, such as bearing eccentricity ratio, attitude angle, minimum film thickness, maximum film pressure, frictional power loss, and oil flow rate can be easily determined. Under dynamic conditions, the journal is oscillating with small amplitudes around the static equilibrium position. The eight bearing dynamic coefficients (stiffness and damping) are obtained by solving the perturbed pressure equations [7]:

$$\frac{\partial}{\partial x}\left(\frac{1}{G_x}\frac{h^3}{\mu}\frac{\partial P}{\partial x}\right)+\frac{\partial}{\partial y}\left(\frac{1}{G_y}\frac{h^3}{\mu}\frac{\partial P}{\partial y}\right)=\frac{U_x}{2}\frac{\partial h}{\partial x}+\frac{U_y}{2}\frac{\partial h}{\partial y}+\frac{\partial h}{\partial t}$$

where x is in the axial direction and y is in the circumferential direction. Gx and Gy called the turbulent flow coefficients are the correctional terms of viscosity caused by the turbulent diffusion:

$$G_x = 12 + 0.0043\,\mathrm{Re}^{0.96} \qquad \text{Axial direction}$$

$$G_y = 12 + 0.0136\,\mathrm{Re}^{0.90} \qquad \text{Circumferential direction}$$

$$\mathrm{Re} = \frac{\rho U h}{\mu} \qquad \text{Local Reynolds number}$$

For laminar flow, $Gx = Gy = 12$. A critical parameter affected by turbulence is the shear stress acting on the shaft.

$$\tau_s = C_f \frac{\mu U}{h} + \frac{h}{2}\frac{\partial P}{\partial y}$$

$$C_f = 12 + 0.0012\,\mathrm{Re}^{0.94}$$

where Cf is the turbulent Couette shear stress factor. For laminar flow, $Cf = 1$.

The boundary conditions in the axial coordinate are that the pressure is ambient at the edges of the bearing pad. The Swift-Stieber or Reynolds boundary conditions are applied in the circumferential coordinate. Film cavitation is considered and the transition boundary curve to the film rupture is determined by iteration. [7]

Figure 4.1 illustrates the linear floating ring bearing characteristics generated from DyRoBeS©_BePerf and all the bearings dimensions are identical to the Holset HX30 turbocharger. The eight bearing linear dynamic coefficients (k_{xx}, k_{xy}, k_{yx}, k_{yy}, c_{xx}, c_{xy}, c_{yx}, c_{yy}) were computed with running speeds from 10,000 RPM to 150,000 RPM with increment of 10,000 RPM. Bearing static loads were calculated from rotor static deflection where the values found to be +0.5311 N on the compressor end, and -4.506 N on the Turbine end, as shown in Figure 4.1. One can notice the higher static load on the turbine end due the heavier weight of the turbine. The bearing data are then transferred to the turbocharger DyRoBeS©_Rotor model. There are two options for employing the floating ring bearings data in the DyRoBeS©_Rotor. The first method is to assume that the inner and outer stiffness as two journal bearings connected in series (Figure 4.2(a)). The other method is taking the total impedance of the inner and outer stiffness and plug in the data to the rotor model acting as a single journal bearing (Figure 4.2(b)).

Steady State Synchronous Response

The turbocharger with floating ring bearings modeled as two journal bearings in series was evaluated for the steady state synchronous response. Figure 4.3 displays the linear synchronous unbalance response calculated from the rotor compressor end and turbine end, at running speeds from 10,000 RPM to 150,000 RPM with increment of 2,000 RPM. The turbocharger starts to exhibit high displacement response over the speed of 100,000 RPM. The system reaches the second critical speed at about 130,000 RPM. This would be the bending mode, where the displacement at the rotor both ends tend to be very large. The compressor end shows larger whirl than the turbine rotor which is about four times the displacement at the first critical speed.

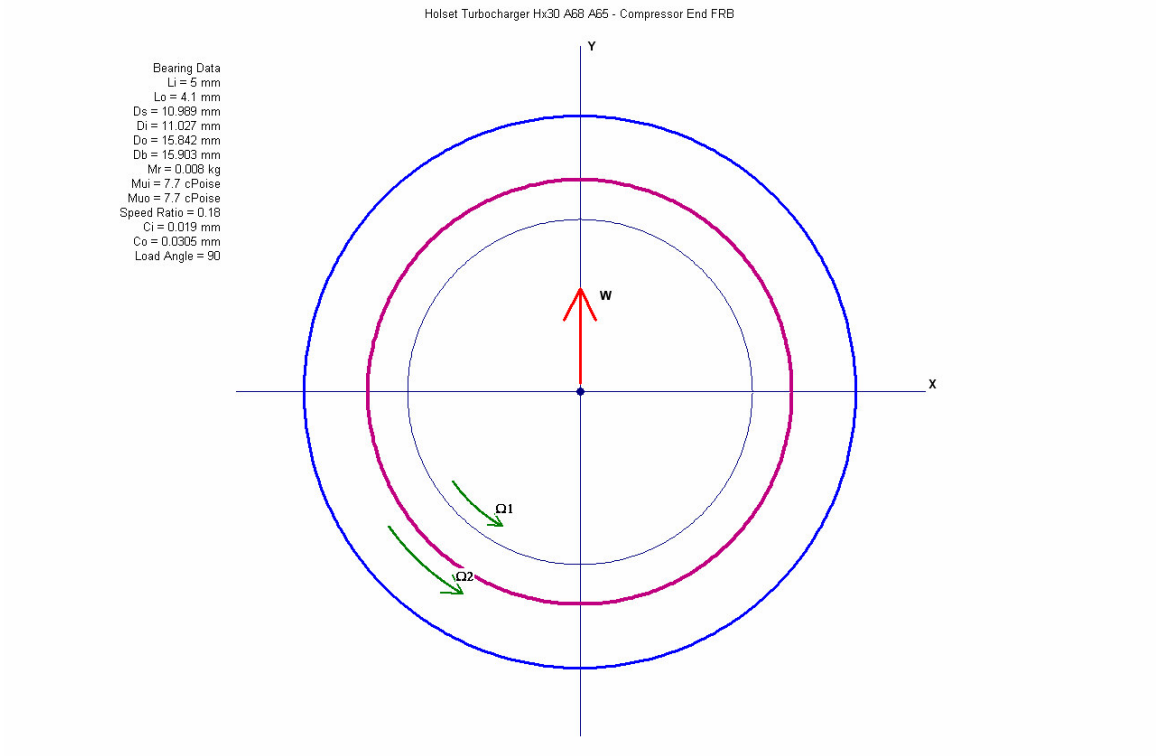

(a)

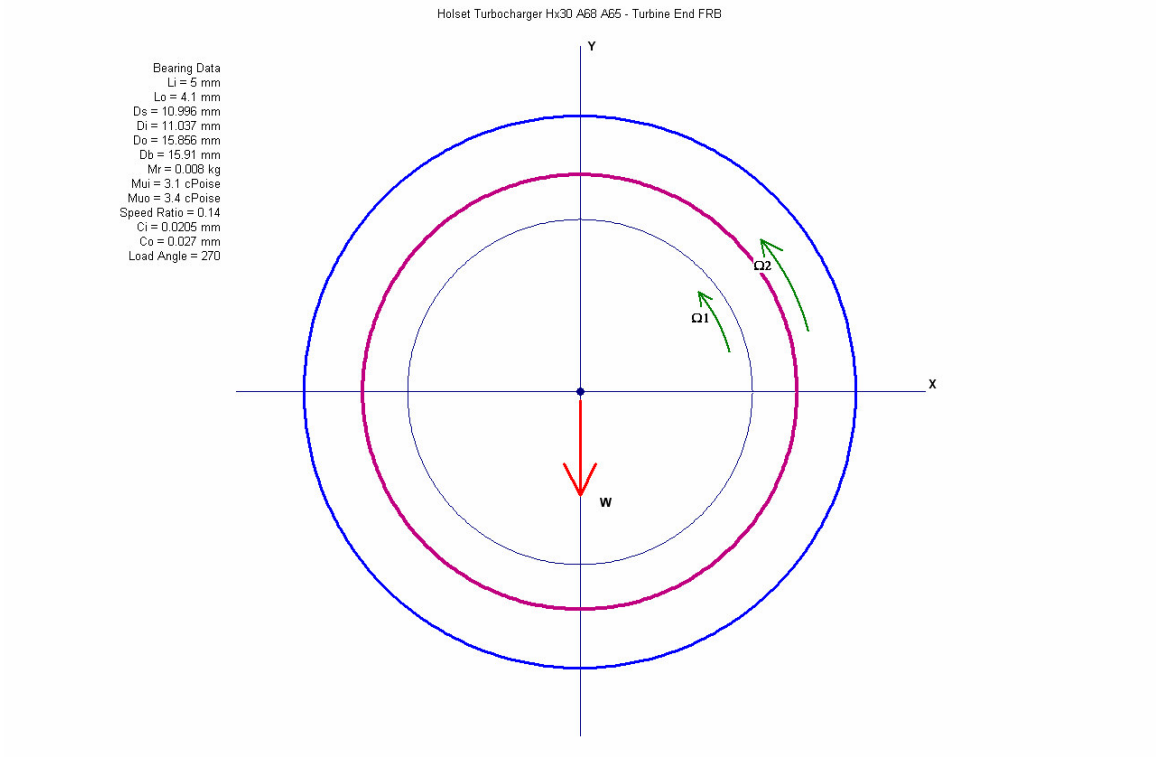

(b)

Figure 4.1 Floating Ring Bearings (a) at Compressor end (b) at Turbine end

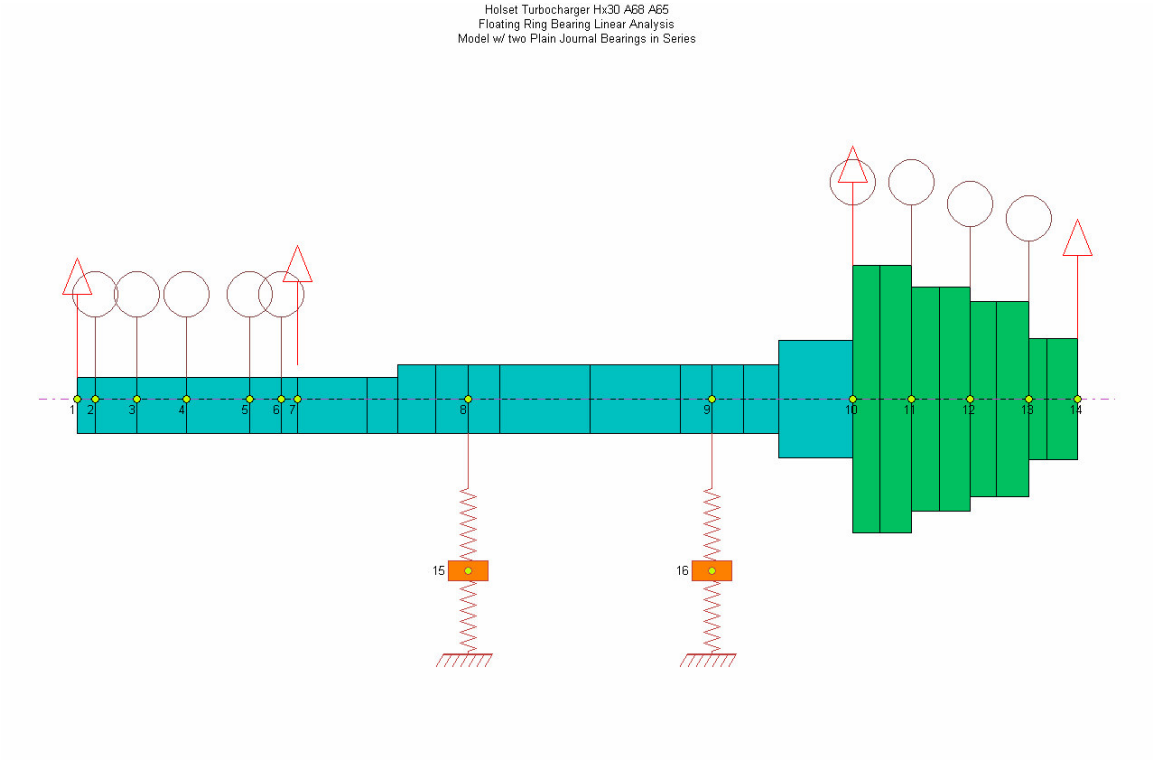

(a)

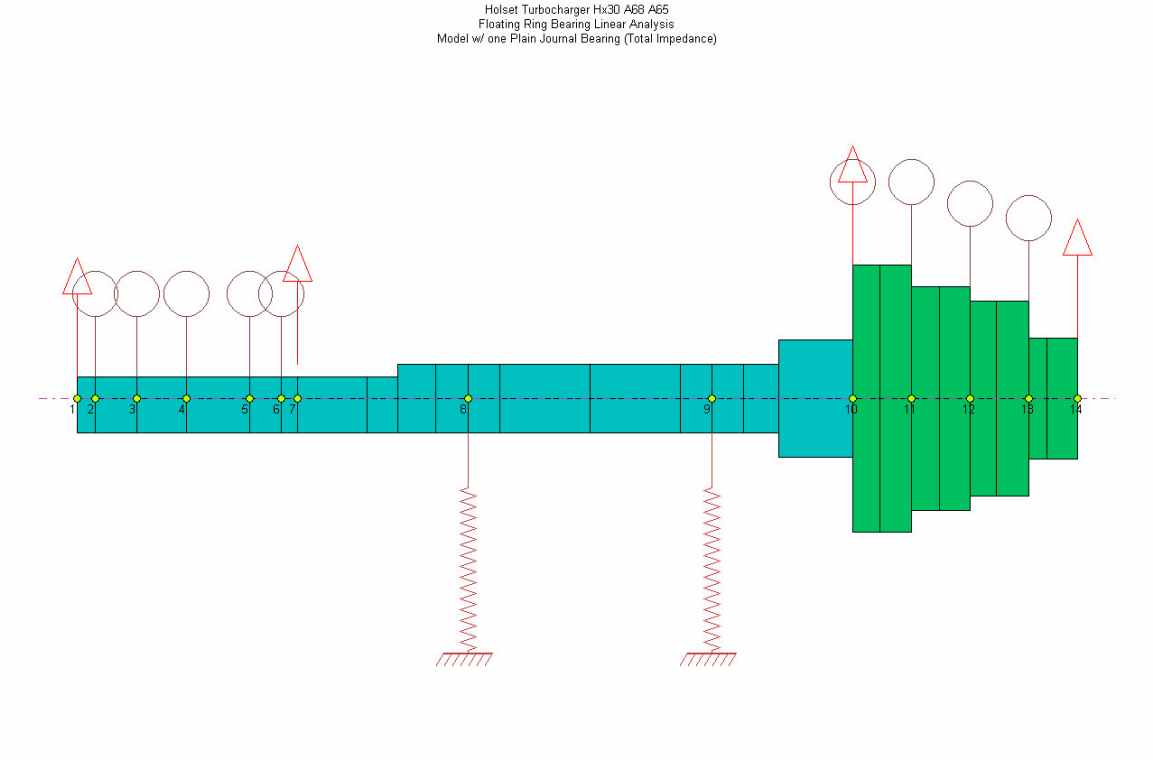

(b)

Figure 4.2 Turbo in Floating Ring Bearings (a) Inner and Outer Stiffness (b) Total Impedance

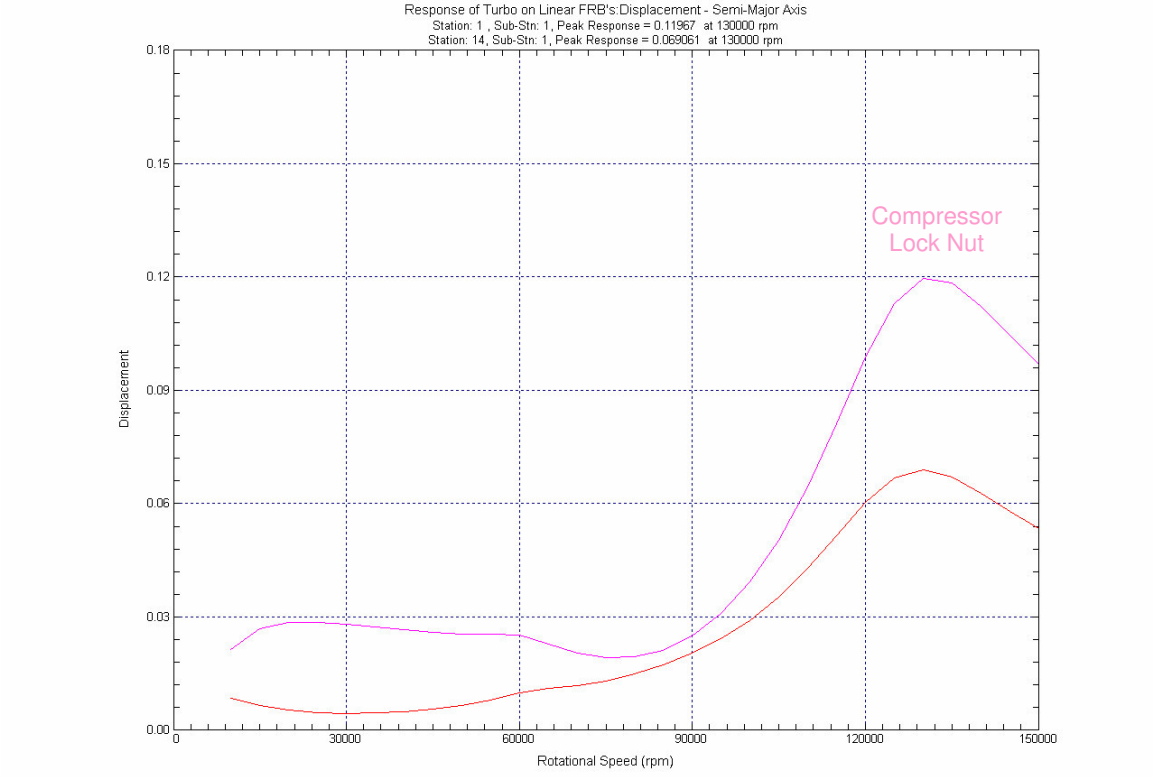

Figure 4.3 Turbo Synchronous Unbalance Response (Floating Ring Bearings).

Stability Analysis

The Stability Analysis calculates the damped natural frequencies (whirl speeds), damping coefficients, logarithmic decrements, and precessional mode shapes. The QR algorithm is utilized in the calculation of eigenvalues and eigenvectors of the system equation of motion. This algorithm has been well proven to be reliable and numerically stable. The imaginary parts of the eigenvalues are the system damped natural frequencies and they can be used to determine the damped critical speeds. The real parts of the eigenvalues are the system damping coefficients which can be used to determine the system stability. A positive damping coefficient indicates system instability. Very often, the logarithmic decrements are used to determine the system stability. A negative logarithmic decrement indicates system instability. When the value of a logarithmic decrement exceeds 1, that particular mode is considered to be well damped. [7]

A complex eigenvalue is given by [7]:

$$\lambda_i = \sigma_i \pm j\omega_{di}$$

where,

$$\sigma_i = -\xi_i \omega_{ni} \ , \ \text{and} \quad \omega_{di} = \omega_{ni}\sqrt{1-\xi^2}$$

The subscript "*i*" is the mode number. If the damped natural frequency is a non-zero value, this mode is a precessional mode with an oscillating frequency equals to the damped natural frequency. If the damped natural frequency equals to zero, this mode is a real mode or non-oscillating mode. The logarithmic decrement and damping factor for a precessional mode is defined to be [7]:

$$\delta = \frac{-2\pi\sigma}{\omega_d} = \frac{2\pi\xi}{\sqrt{1-\xi^2}}$$

and

$$\xi = \frac{\delta}{\sqrt{(2\pi)^2 + \delta^2}}$$

where

ξ	damping factor, or damping ratio
$\delta > 0$	stable or damped system
$\delta = 0$	threshold of instability
$\delta < 0$	unstable system

Figure 4.4 shows the stability map of the turbocharger with floating ring bearings models. The calculations where taken in running speeds between 10,000 RPM and 150,000 RPM with incremental speed of 2,500 RPM. The logarithmic decrement is plotted against the running speed as shown in the figures.

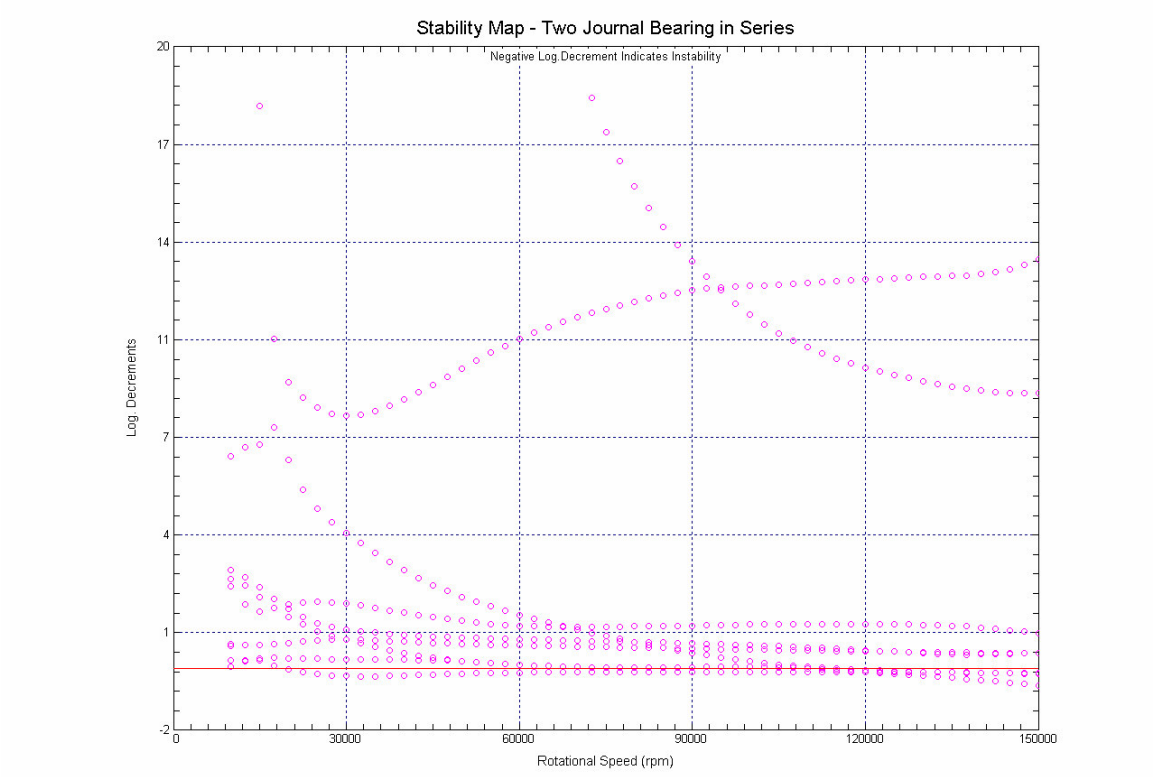

(a)

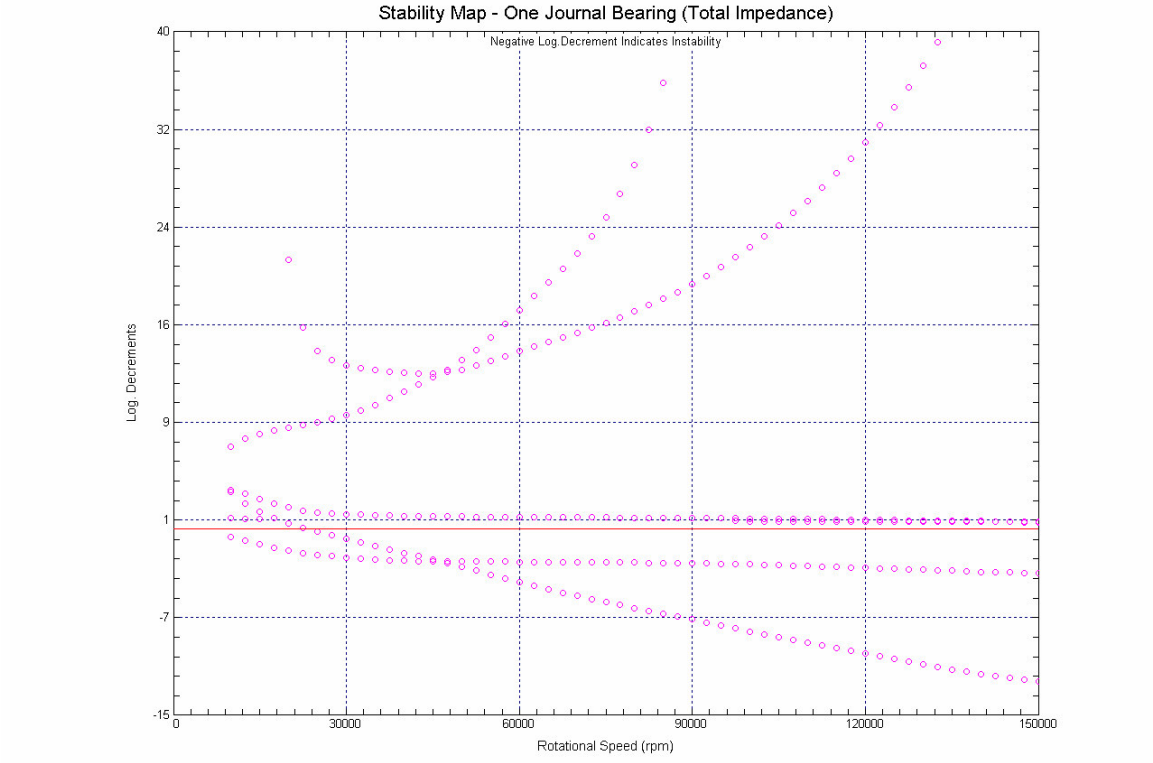

(b)

Figure 4.4 Turbo in Floating Ring Bearings Stability (a) First Modeling (b) Second Modeling

The modeling with two journal bearings in series proves a better estimation of the actual running (Figure 4.4 (a)). There are two main whirling modes that run instable. The first conical mode shows instabilities at low speeds and dominates for almost the whole running. The second in-phase whirl mode is marginally stable at low speeds (above 30,000 RPM) but it then goes unstable above 70,000 RPM.

The stability map for the model with total impedance stiffness (Figure 4.4 (b)) has a response similar to plain journal bearings, as we will see in the following section. The first and second whirling modes both go unstable at low speeds, though this is not the actual response of nonlinear floating ring bearings. The instabilities increase all the way with running speed. There is another mode that runs marginally stable above 100, 000 RPM. This is the third bending mode.

Linear analysis of the first model (Figure 4.2 (a)) would give good approximation of the turbocharger with nonlinear floating ring bearings. Hence it can be used for further improvement of the turbocharger rotordynamics and stability. In the following talk, more emphasize will be on the turbocharger dynamic stability investigations with different types of journal bearings. Ways of introducing new bearing designs will be discussed.

4.2 Performance with Fluid-Film Journal Bearings

In the continuation of the goal to evaluate the dynamic stability of the automotive turbocharger, this section will examine the rotordynamic response of Holset HX30 turbocharger with different types of fluid film journal bearings. The first condition considers a journal bearing that is similar to the outer journal characteristics of the standard floating ring bearings. After that, different bearing types will be studied seeking better stability.

4.2.1 Six-Oil-Groove Journal Bearings

Since the outer journal of the floating ring bearings has six oil-feeding grooves, we will design two bearings with the same characteristics of the outer journal. The model has the same dimensions, clearance and oil viscosity of the outer journal. The computations of stiffness and damping will be from 10,000 RPM to 150,000 RPM with incremental speed 10,000 RPM. The static loads are the same as applied for the floating ring bearing in the previous section. The loading will be applied between the oil-feed holes. Figure 4.5 illustrates the bearing models used on the compressor and turbine end.

Critical Speeds and Strain Energy Distribution

The undamped natural frequency calculations were generated to provide insight into the fundamental turbocharger mode shapes and also evaluate the relative potential energy distribution for the shaft and bearings for a given mode. Figure 4.6 represents the first calculated mode which is essentially a rigid body conical mode where the compressor and turbine wheels are moving out of phase. The first undamped critical speed is 2,759 RPM. The potential energy is greatest in the compressor bearing for the first mode (Figure 4.7). Attention should be given for this bearing in stabilizing the first mode.

The second mode shape (Figure 4.8) exhibit a slight bending where the potential energy in the shaft arises to 4.4 % (Figure 4.9). The second critical speed is 10,505 RPM, which is still at low running speed. Both of the turbine and compressor wheels move in-phase. For the second mode, the potential energy is highest at the turbine bearing with 89.98% of the total system potential energy. This may be because of the heavier weight of the turbine rotor. The turbine bearing characteristics are therefore critical in controlling the second mode.

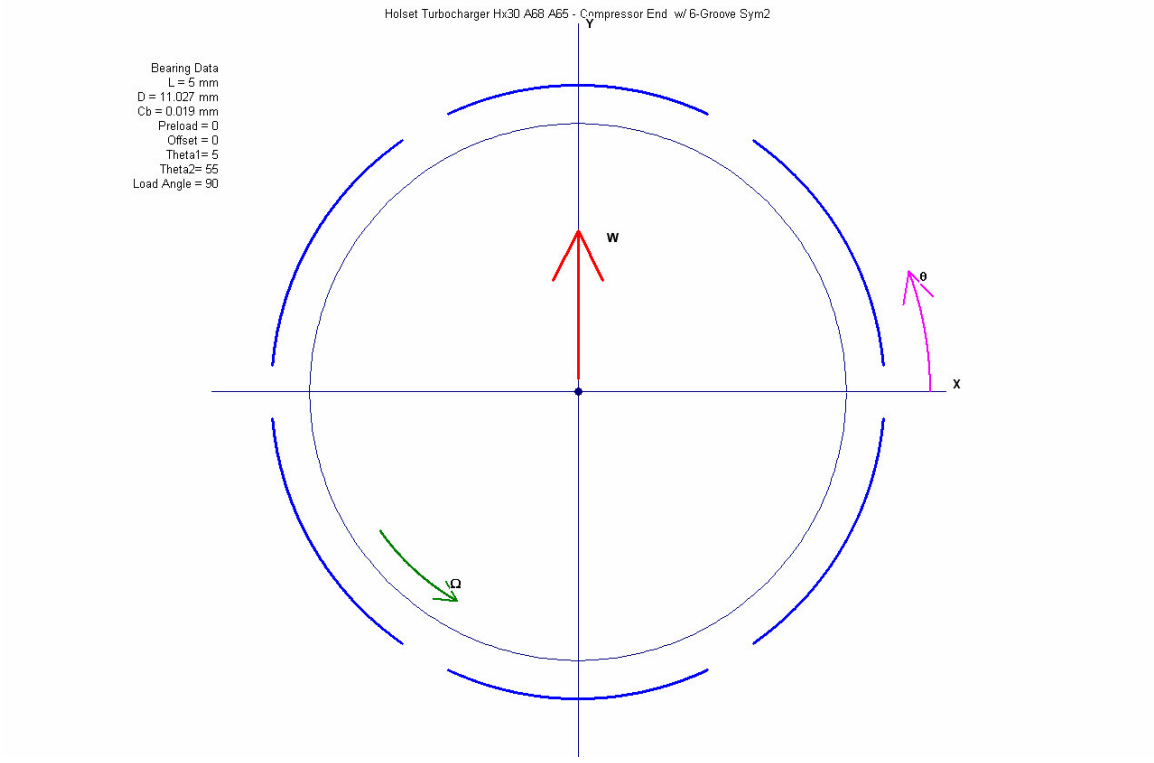

(a)

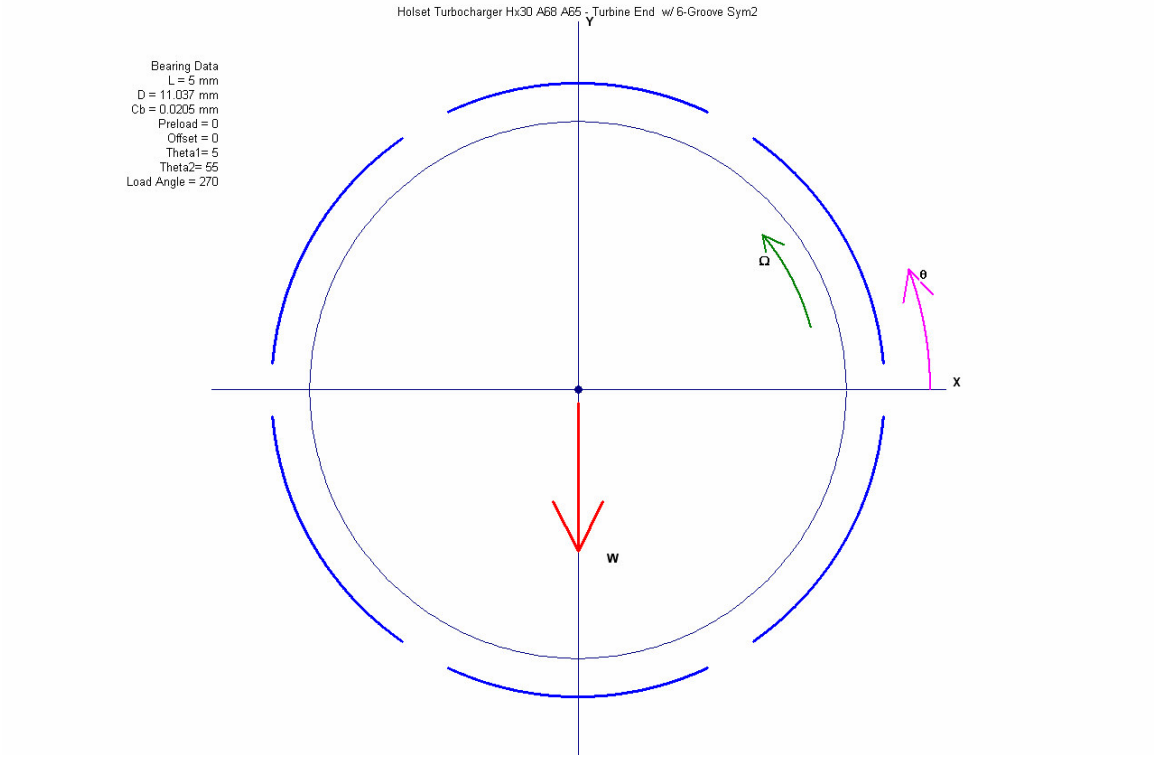

(b)

Figure 4.5 Six-Oil-Groove Bearings (load between holes) (a) at Compressor end (b) at Turbine end

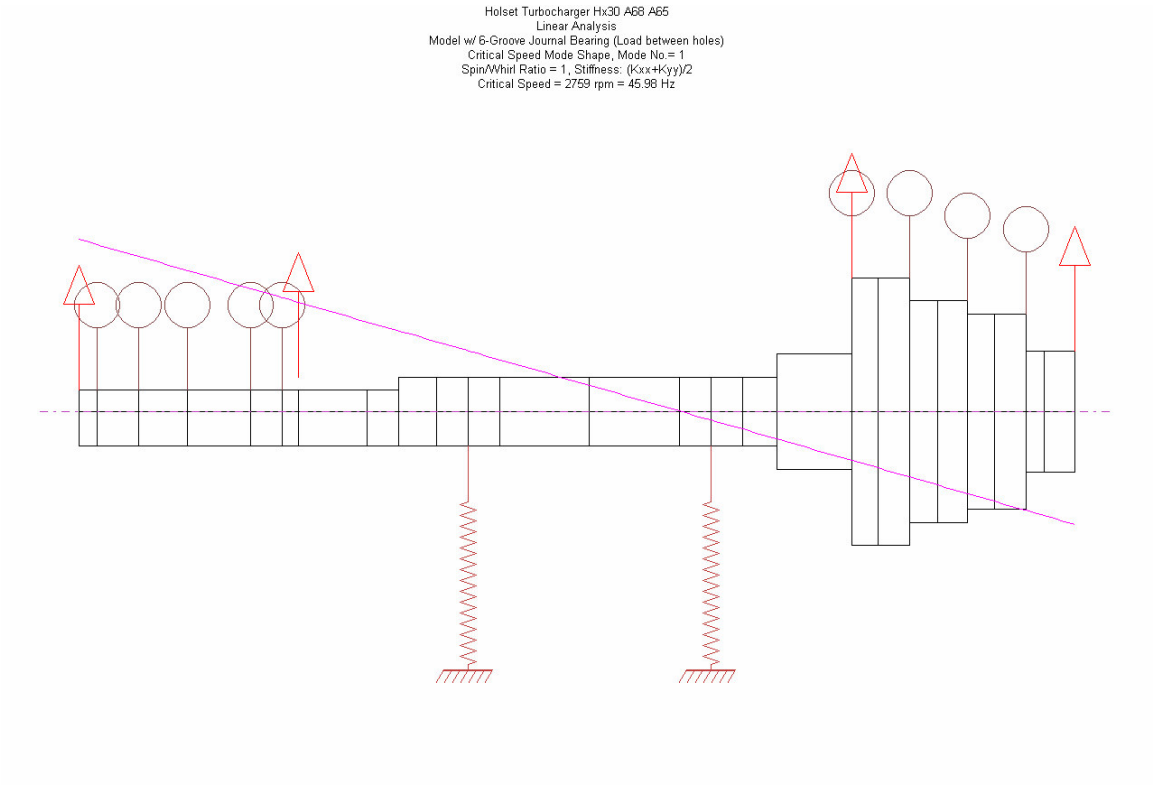

Figure 4.6 Turbo with 6-Groove Bearings – Mode Shape No. 1 at 2,759 RPM

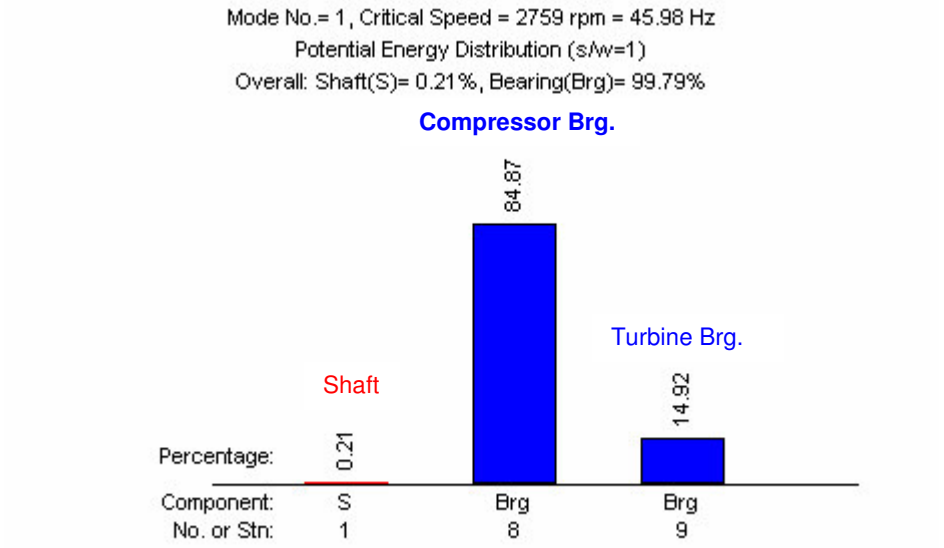

Figure 4.7 Turbo with 6-Groove Bearings –
Potential Energy Distribution for 1st Critical Speed

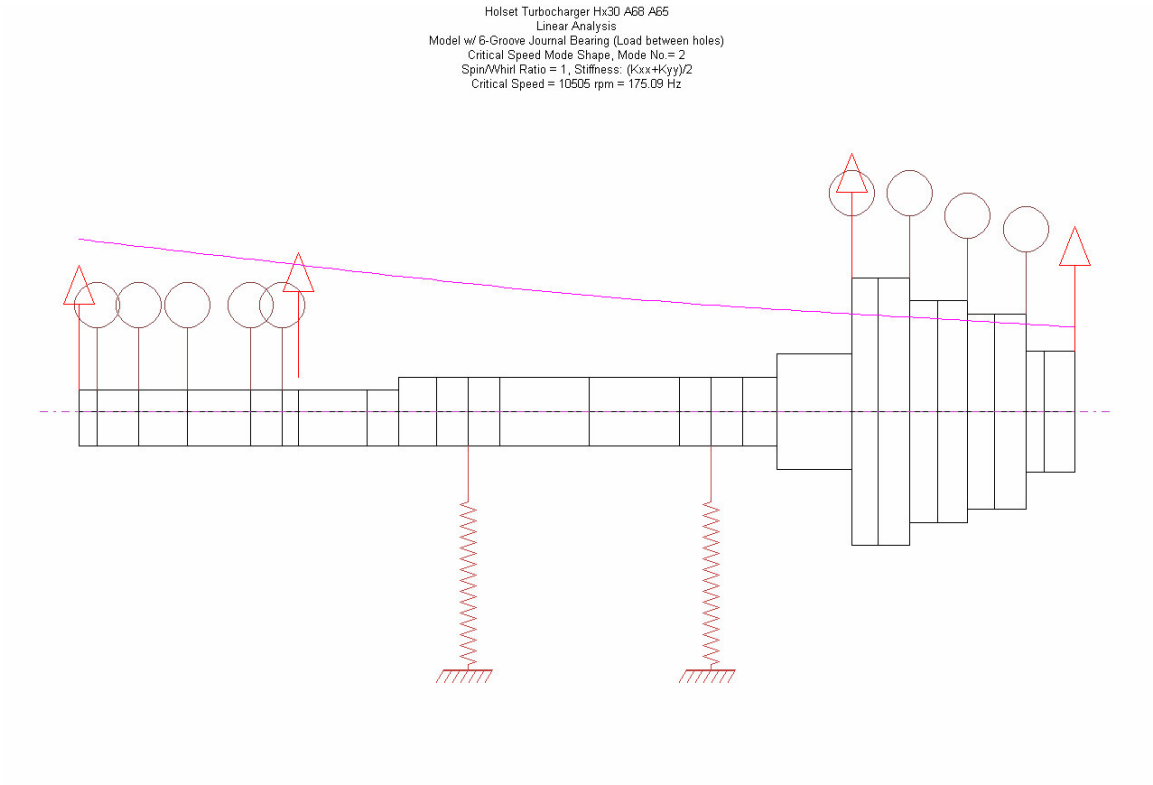

Figure 4.8 Turbo with 6-Groove Bearings – Mode Shape No. 2 at 10,505 RPM

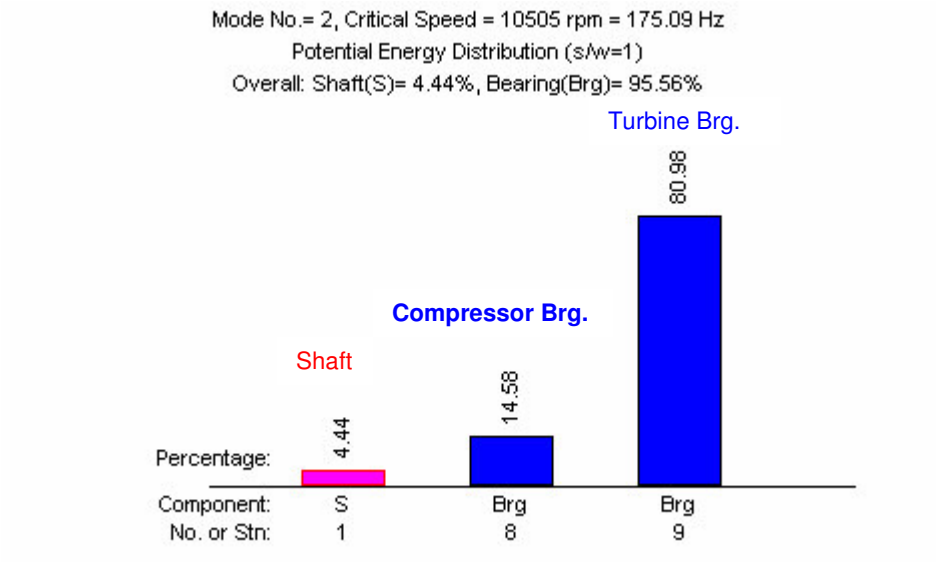

Figure 4.9 Turbo with 6-Groove Bearings –
Potential Energy Distribution for 2nd Critical Speed

The third mode shape is a pure bending mode at speed 134,412 RPM (Figure 4.10). Almost all the system potential energy is in the shaft bending which is 95.79% (Figure 4.11). The bearings have little effect on stabilizing this mode. The shaft stiffness will play the major role in controlling the third bending mode.

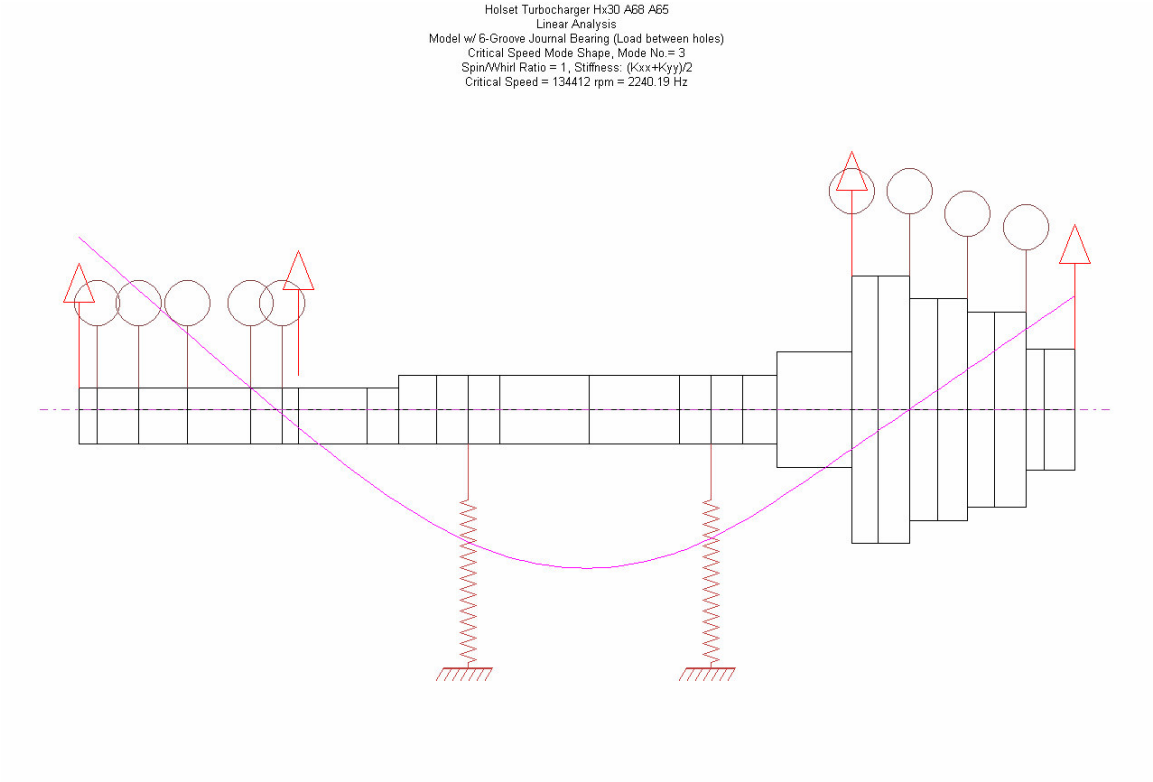

Figure 4.10 Turbo with 6-Groove Bearings – Mode Shape No. 3 at 134,412 RPM

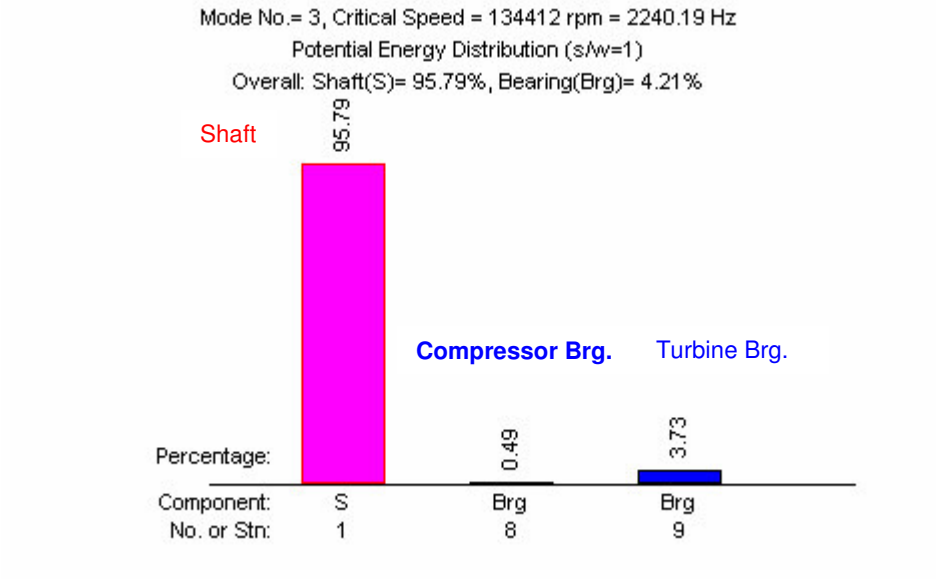

Figure 4.11 Turbo with 6-Groove Bearings –
Potential Energy Distribution for 3rd Critical Speed

Steady State Synchronous Response

Figure 4.12 represents the synchronous unbalance response of the turbo with six-oil-groves bearings. The system starts to have high displacement response over 100,000 RPM, which is in the normal operating range. In this critical speed the rotor begins to whirl in bending mode. The greatest synchronous response is about 140,000 RPM. At this speed, the rotor will have very high displacements and loading on the bearing. Turbochargers operation should not reach such critical response to avoid permanent damage to bearings and turbocharger housing.

Whirl Speed and Stability Analysis

The stability map for the system was calculated for speeds from 10,000 RPM to 150,000 RPM with increment of 2,500 RPM. In Figure 4.13, there are two unstable modes all over the running speed. There are also another two modes considered marginally stable over 120,000 RPM.

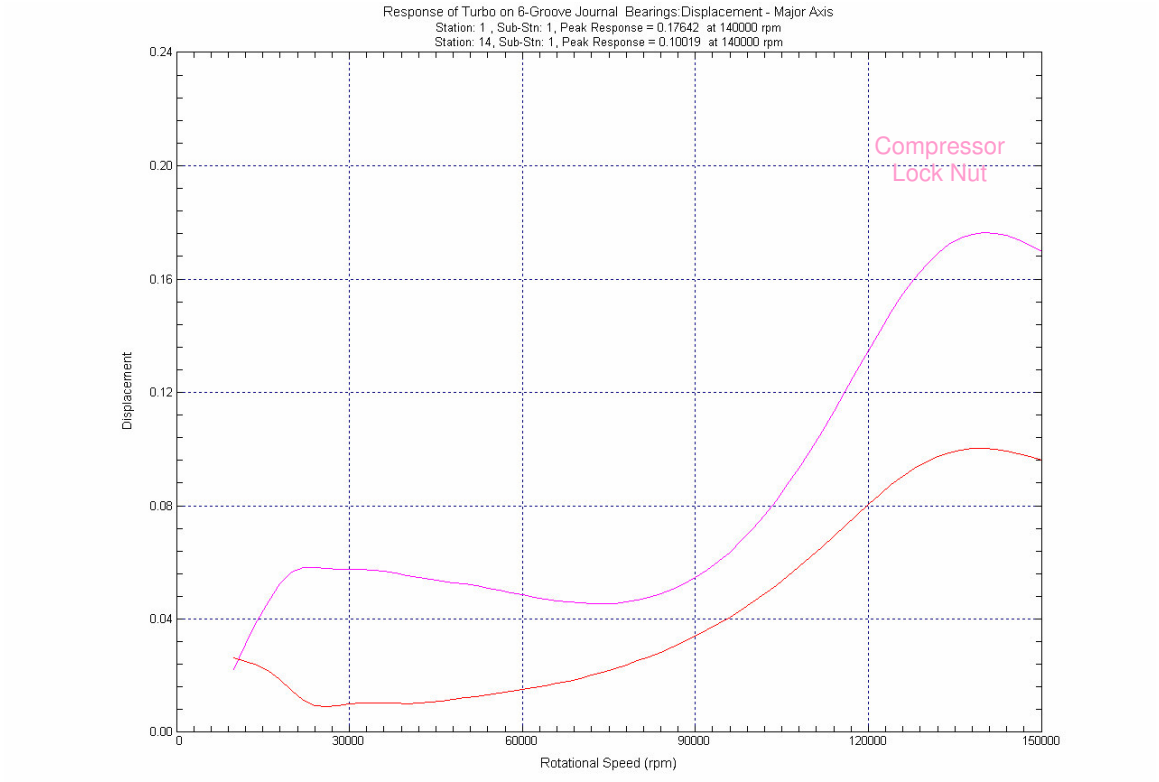

Figure 4.12 Turbo with 6-Groove Bearings - Synchronous Unbalance Response

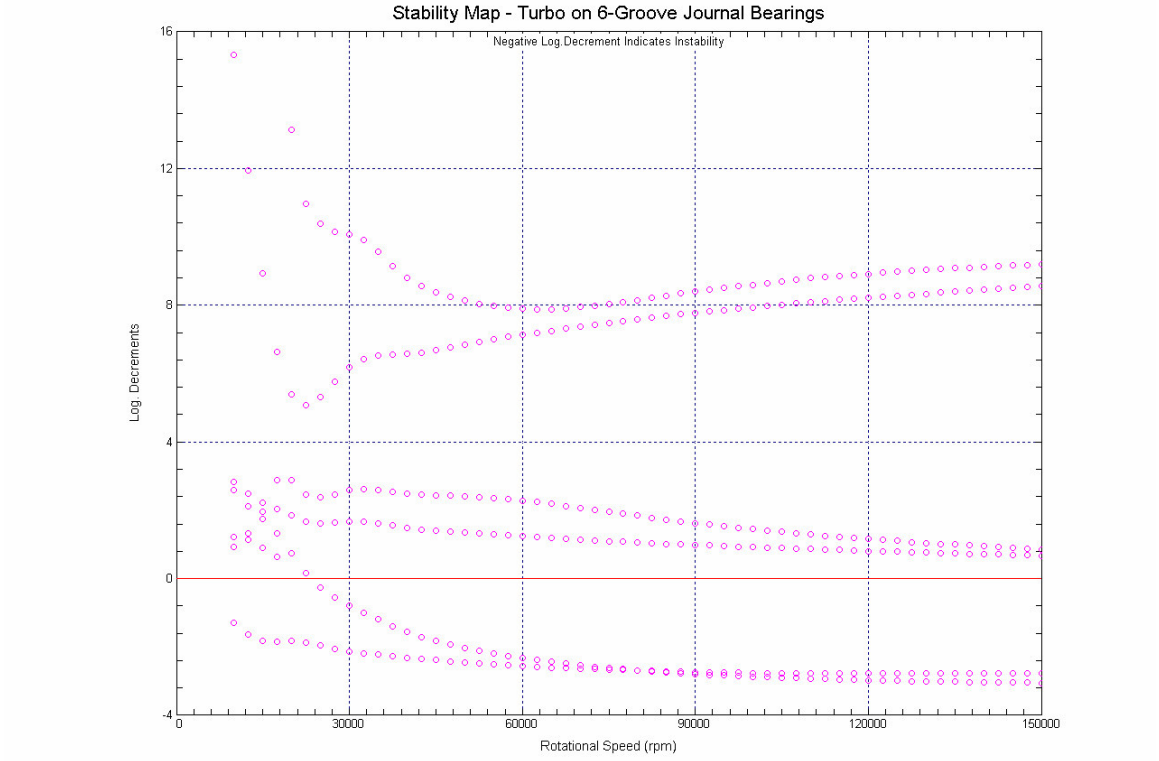

Figure 4.13 Turbo with 6-Groove Bearings – Stability Map

The precessional mode shapes (whirling mode shapes) were calculated for the system at speeds from 10,000 RPM to 150,000 RPM. Figures 4.14 through 4.19 display the first six mode shapes, which are most significant for the turbocharger dynamical analysis, with the associated whirl speeds (damped natural frequencies) computed at a constant speed of 100,000 RPM. The reason of studying the mode shapes at this specific speed is that the turbocharger normally functions at 100,000 RPM or to some extent higher. The logarithmic decrement for each mode was also presented to determine whether the mode is stable or unstable.

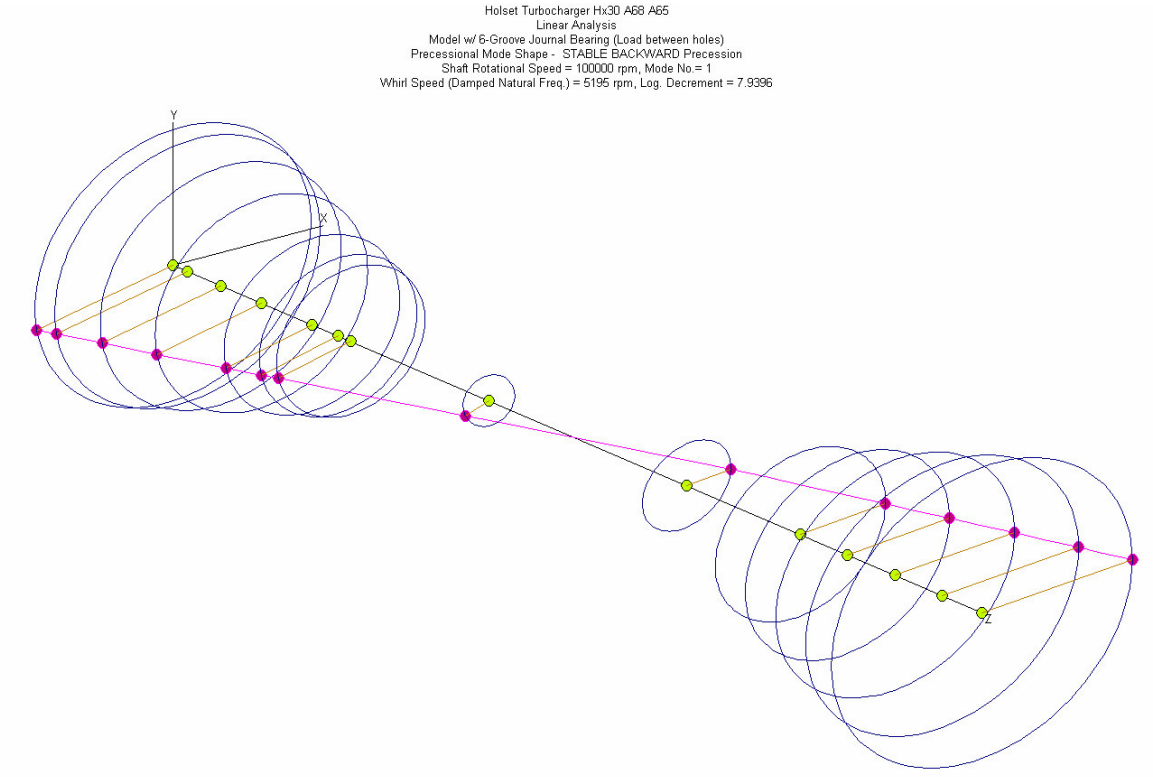

Figure 4.14 Stable Backward Precession at Whirl Speed 5,195 rpm

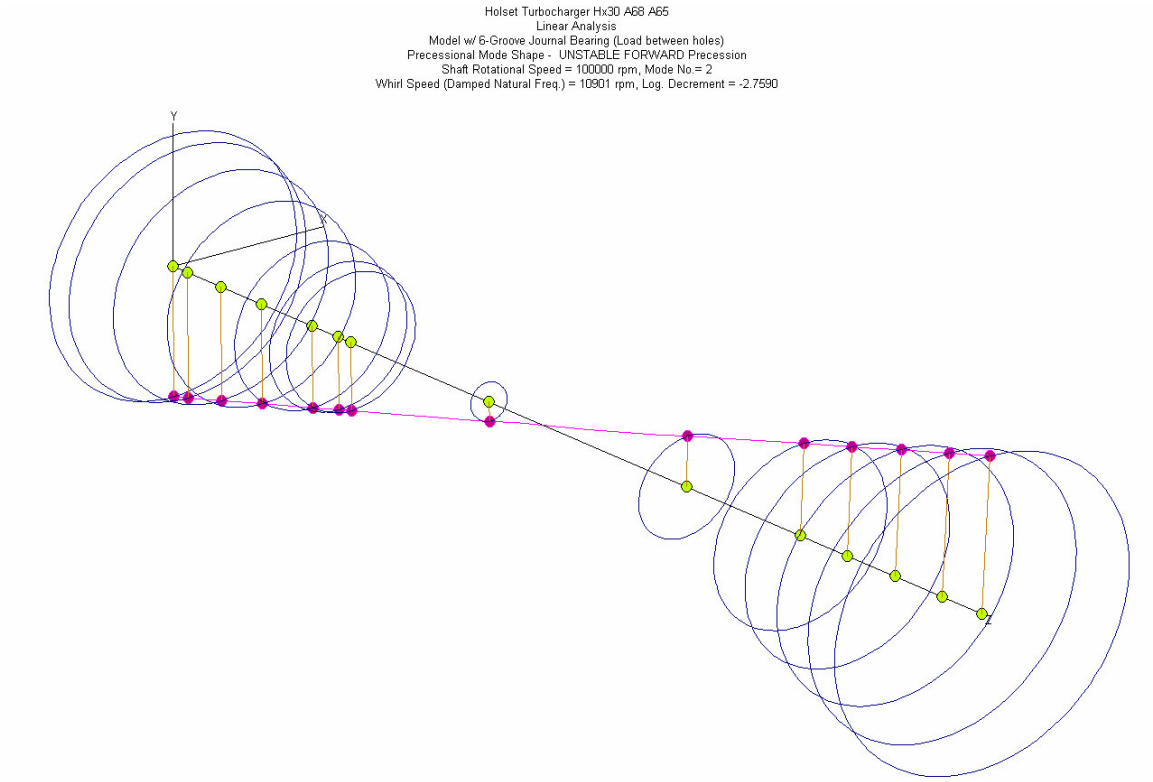

Figure 4.15 Unstable Forward Precession at Whirl Speed 10,901 rpm

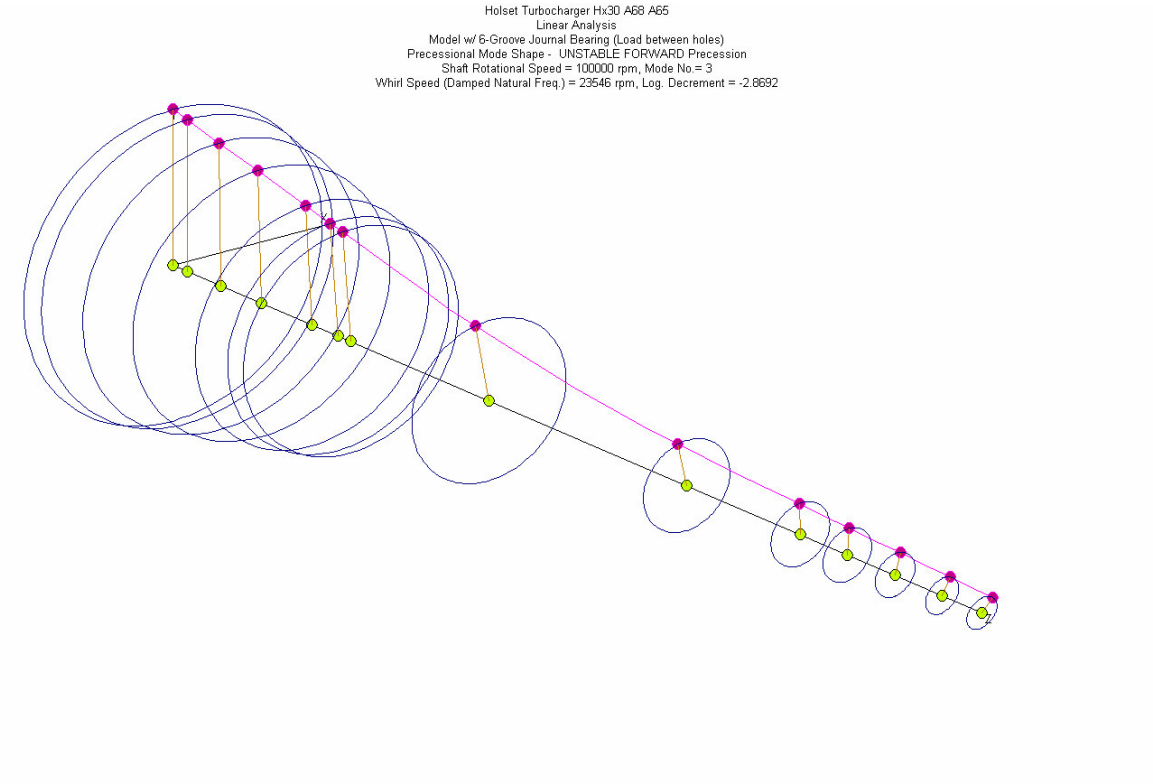

Figure 4.16 Unstable Forward Precession at Whirl Speed 23,546 rpm

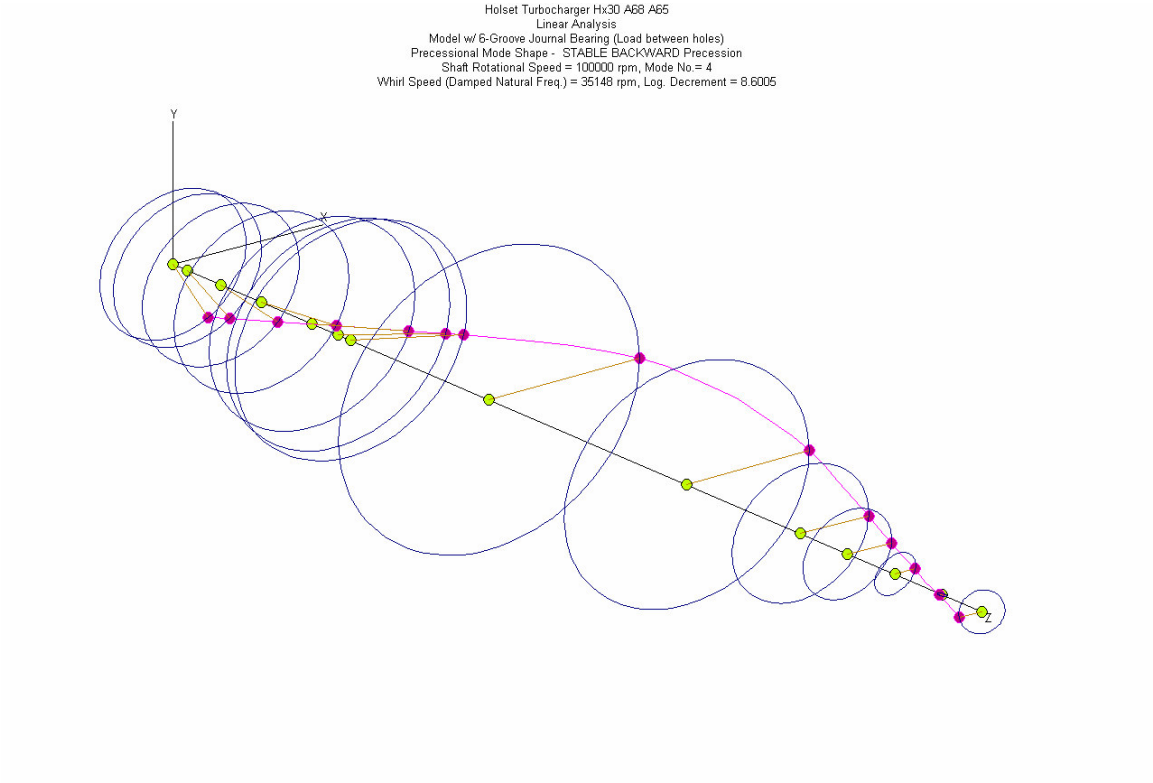

Figure 4.17 Stable Backward Precession at Whirl Speed 35,148 rpm

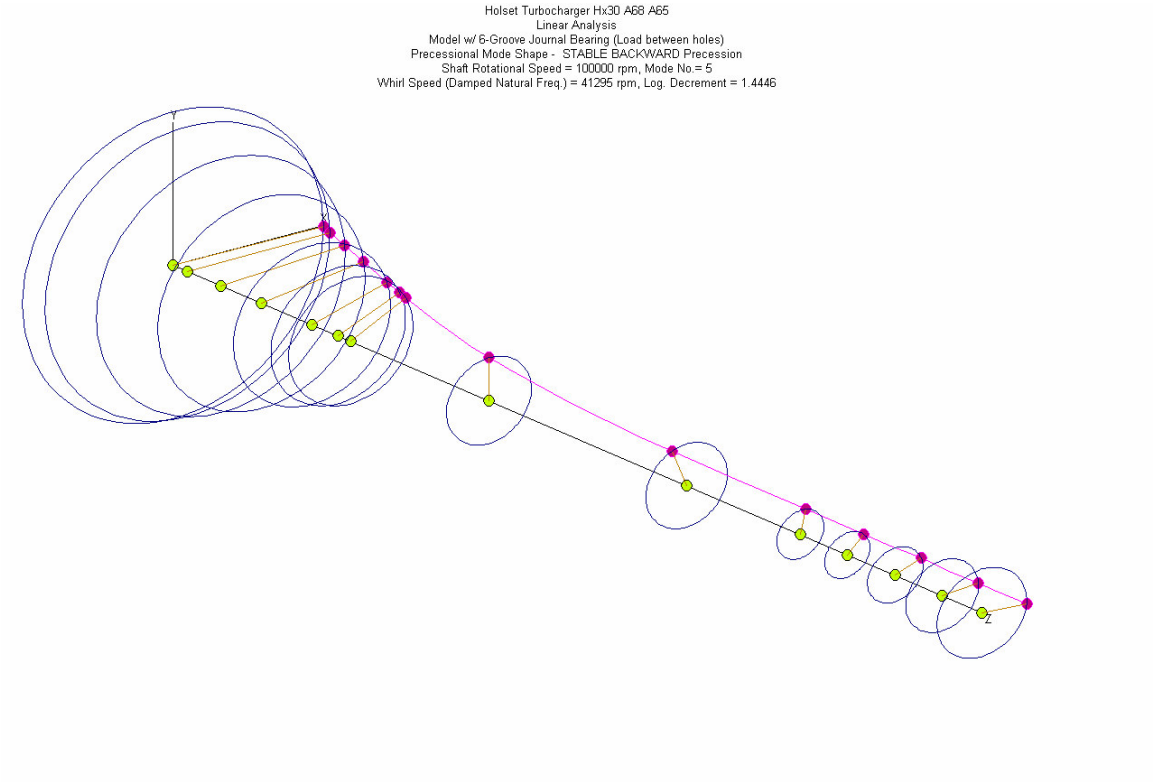

Figure 4.18 Stable Backward Precession at Whirl Speed 41,295 rpm

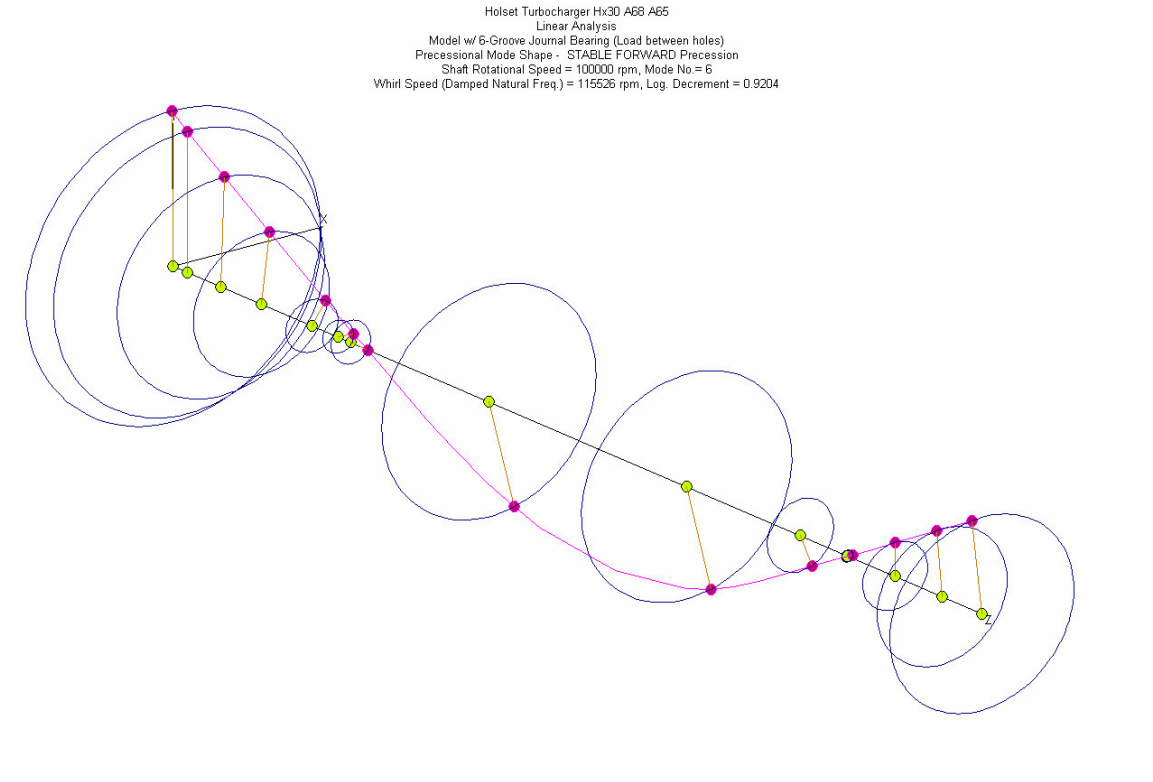

Figure 4.19 Stable Forward Precession at Whirl Speed 115,526 rpm

Figures 4.15 and 4.16 represents the two unstable whirling mode shapes predicted from the stability map (Figure 4.13). The whirl speeds of the first unstable mode and the second unstable mode are 10,901 RPM and 23,546 RPM, respectively. It can be seen clearly from Figure 4.15 that the whirling mode is a rigid body mode where both ends of the rotor (compressor and turbine wheels) whirl forward out of phase. From Figure 4.16, both ends in the second unstable mode whirl forward in-phase with small bending in the shaft.

The forward whirling bending mode shape (Figure 4.19) is marginally stable at the running speed of 100,000 RPM. The logarithmic decrement for this mode is 0.92. As predicted from Figure 4.13, the logarithmic decrement values for the bending mode decrease slightly as the running speed increases.

As a point of interest, one can observe a backward whirling bending mode at a low whirl speed of 35,148 RPM. Though the backward whirling bending mode is stable, it could mislead the whirl instabilities analysis from the nonlinear time transient response. One can also see that all the unstable modes are forward whirling, whereas the backward whirling coupled modes are all well damped (stable).

Figures 4.20 and 4.21 represent the first forward whirling modes at speeds 10,000 RPM and 150,000 RPM, respectively. In both speeds the mode is unstable. At lower speed the compressor wheel exhibit higher whirl, whereas at higher speeds the turbine rotor whirls in larger orbits. On the other hand, the second forward whirl runs stable at lowest speed (Figure 2.22) but it rapidly goes unstable at higher speeds (Figure 2.23). As speed increase, the compressor wheel whirls in higher orbits and the shaft bends slightly.

The above investigations confirm that there are two main whirling modes that need to be stabilized in order to have an acceptable design. A frequent technique to stabilize the rotor-bearing system is by adding external damping. The current research will attempt to introduce a method of optimizing the stability of the turbocharger rotor-bearing system but before that, it is worth presenting the dynamic response of the turbocharger with other types of journal bearings.

4.2.2 Other Types of Journal Bearings

FEM codes such as DyRoBeS© can save researchers large amount of money and time in evaluating the performance of their design, instead of unnecessary experimental costs. In this part of the research, different linear bearings models with various characteristics will be designed in order to test the dynamical performance of the Holset HX30 turbocharger.

Preload and offset are two common terms used in improving the characteristics and geometry of fixed lobe (or groove) bearings. For a positive preloaded bearing

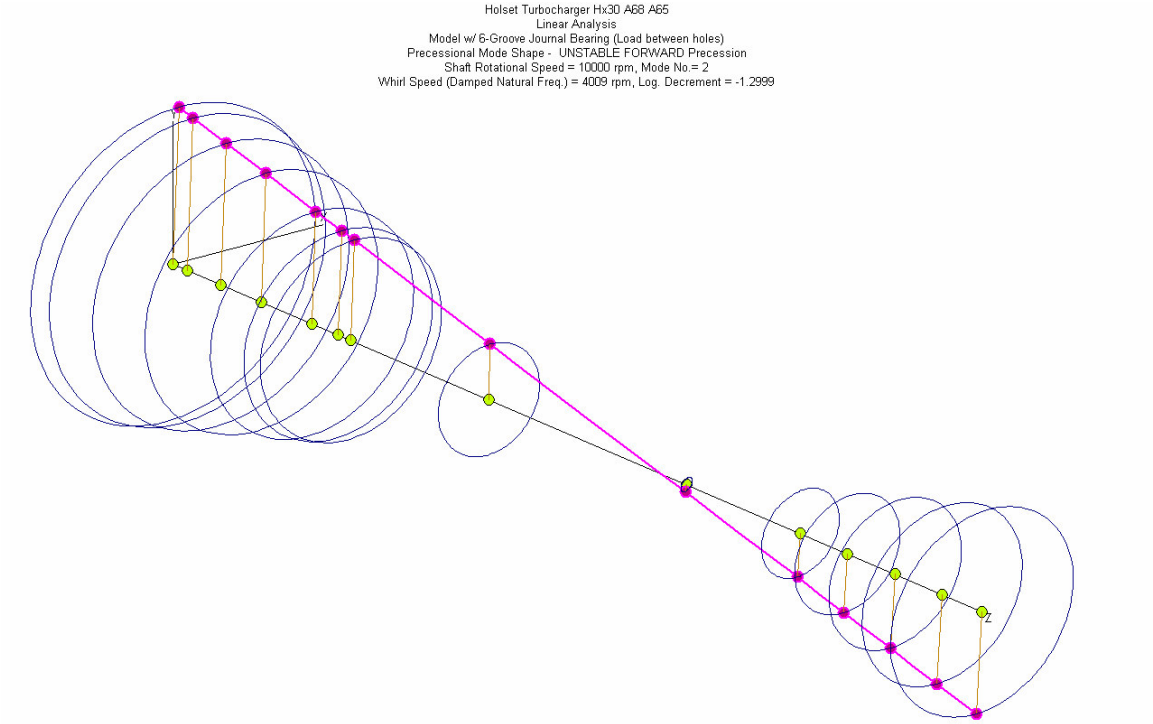

Figure 4.20 1st Forward Precession:

Shaft Running Speed 10,000 rpm, Whirl Speed 4,009 rpm

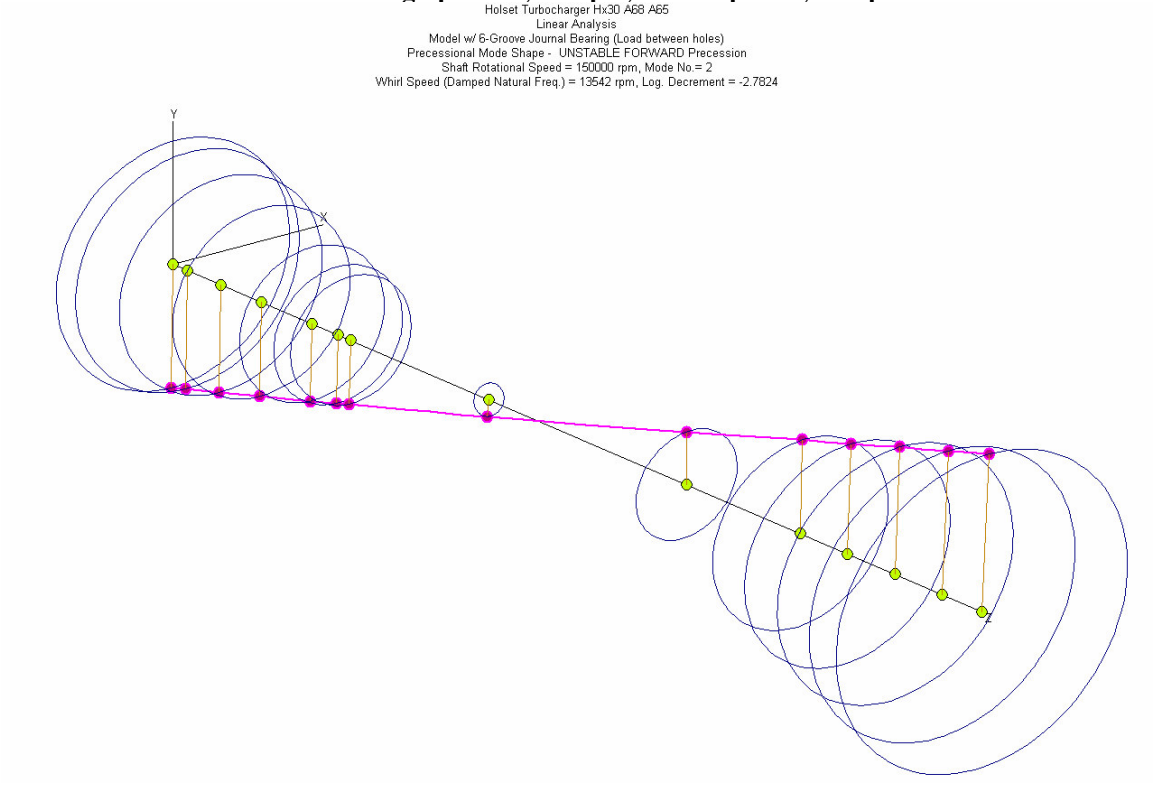

Figure 4.21 1st Forward Precession:

Shaft Running Speed 150,000 rpm, Whirl Speed 13,542 rpm

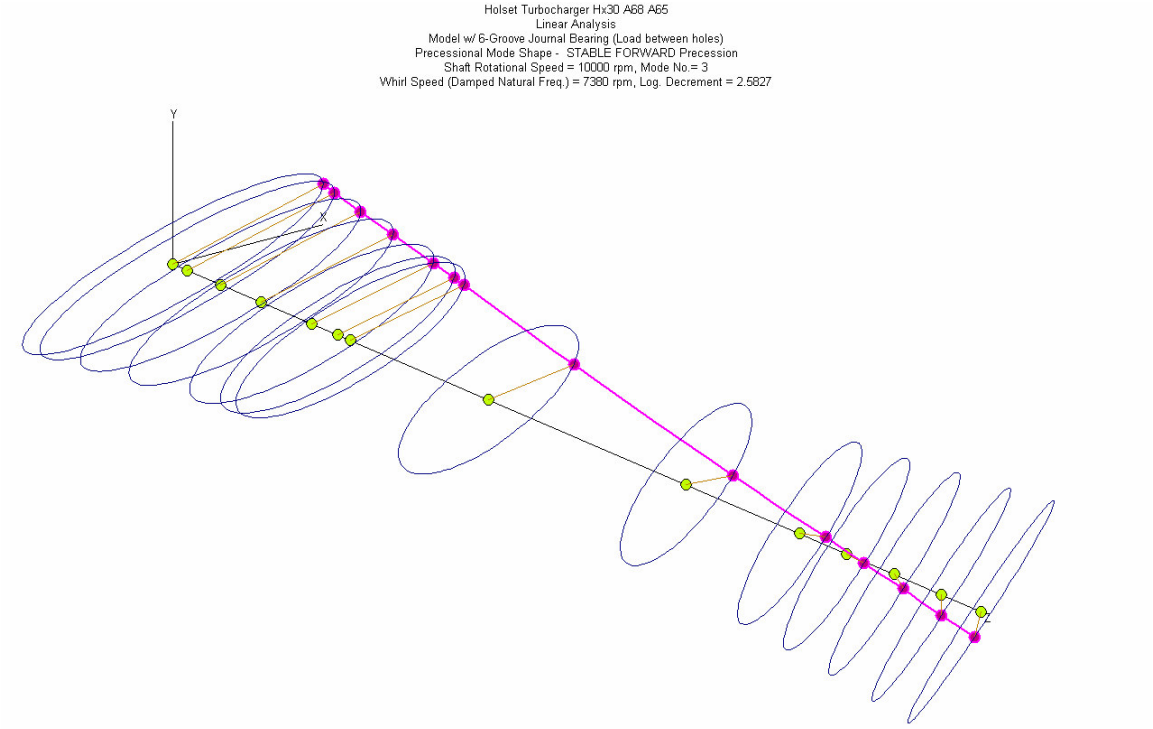

Figure 4.22 2nd Forward Precession:

Shaft Running Speed 10,000 rpm, Whirl Speed 7,380 rpm

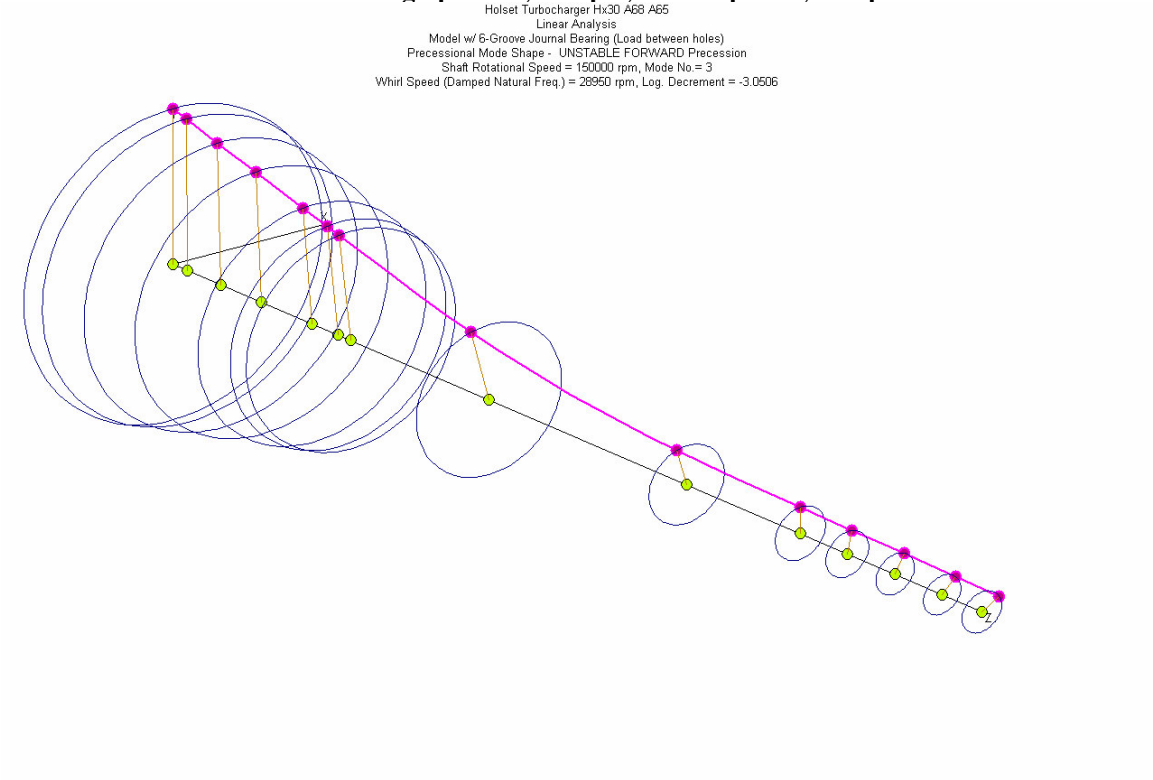

Figure 4.23 2nd Forward Precession:

Shaft Running Speed 150,000 rpm, Whirl Speed 28,950 rpm

(Figure 4.24), pad radius (*Rp*) is greater than bearing radius (*Rb*) and the circular pads are moved inward the bearing center. Thus, when the journal is centered in the bearing, the pads are loaded by geometry effect. The fraction of the distance between pad center of curvature and bearing center to pad radial clearance is called "Preload" [7]:

$$m = \frac{(C_p - C_b)}{C_p} = 1 - \frac{C_b}{C_p}$$

When the preload is zero, the pad centers of curvature coincide with the bearing center and the bearing is cylindrical. When the preload has a value of 1, the shaft touches all the pads and the bearing minimum radial clearance is zero. Typical preload value for a fixed lobe bearing ranges from 0.4 to 0.75. [7]

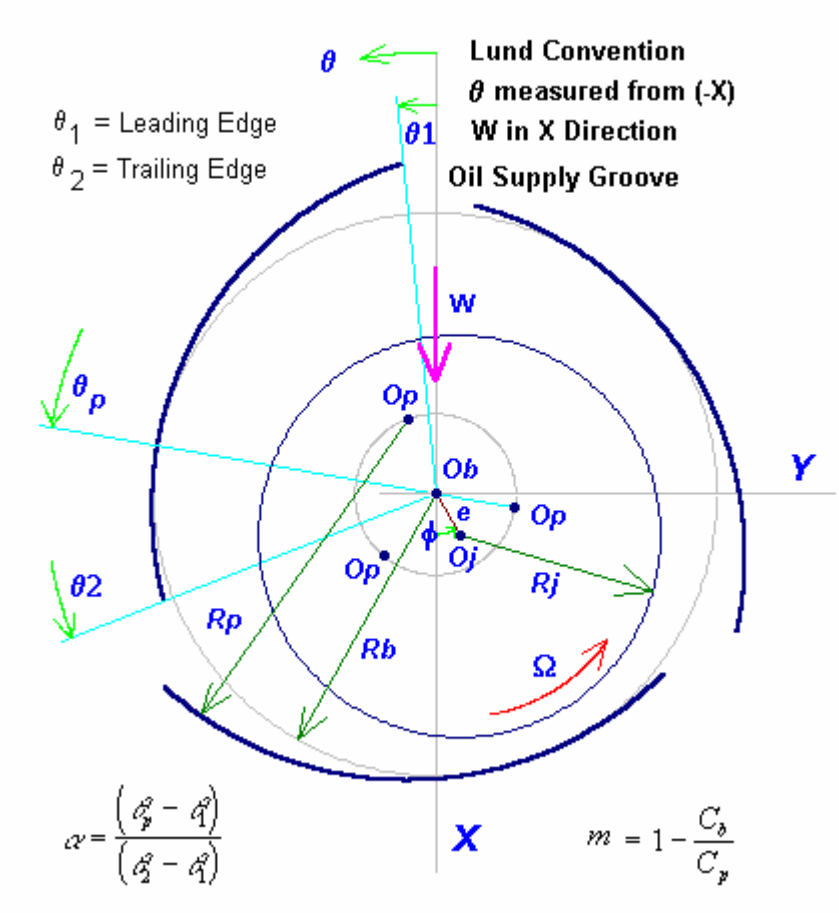

Figure 4.24 Fixed Lobe Bearing Geometry [7]

The other key parameter used to describe the preloaded bearing geometry is the fraction of converging pad length to the full arc length. This parameter is called "Offset" and is given by the following expression [7]:

$$\alpha = \frac{(\theta_p - \theta_1)}{(\theta_2 - \theta_1)} = \frac{\chi_b}{\chi}$$

The value of offset is meaningful only when the bearing is preloaded. At θ_p, the bearing has a minimum clearance for a centered shaft and the lobe arc intersects with bearing base circle. Typical offset ranges from 0.5 to 1.0. [7]

The bearings static loads in the previous six-oil-groove bearings were acting between the oil feeding grooves (holes). Therefore, in the next step of the analysis the bearings will be fitted in the turbocharger in a way where the rotor loading is acting on the hole. Figure 4.25 represents the model of six-oil-groove bearing at the turbine end, where the loading acting directly on the hole. The stability map for the turbocharger with this type of bearings (Figure 4.26) clearly shows that there are two whirling modes running unstable for the whole speed range. These modes are the first and second forward whirling modes. There is also a third forward whirling mode that runs marginally stable over speed 100,000 RPM.

Another design for the six-groove bearing can be achieved by changing the preloading. In Figures 4.27 and 4.29, six-groove bearings have 50% preload and 90% offset where loadings acting between the holes, and in the hole, respectively. Both of the bearings give similar response in the turbocharger. Figures 4.28 and 4.30 can show the similarities in the dynamic behavior of the turbocharger, with slight improvement in the stability. The first whirl mode is unstable at low speeds and over the whole speed range for both bearings geometries. The second whirl mode is stable at low speeds but over speed 50,000 RPM it goes unstable.

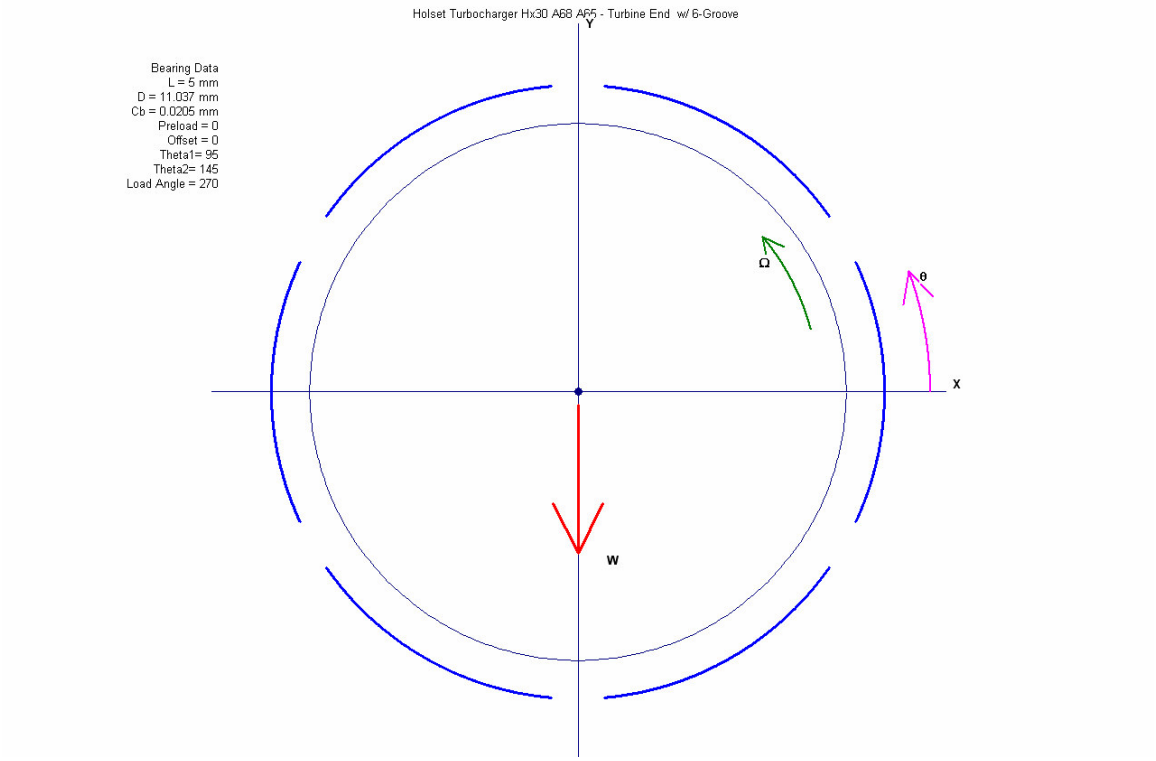

Figure 4.25 6-Groove Bearing (Load on Hole) at Turbine End

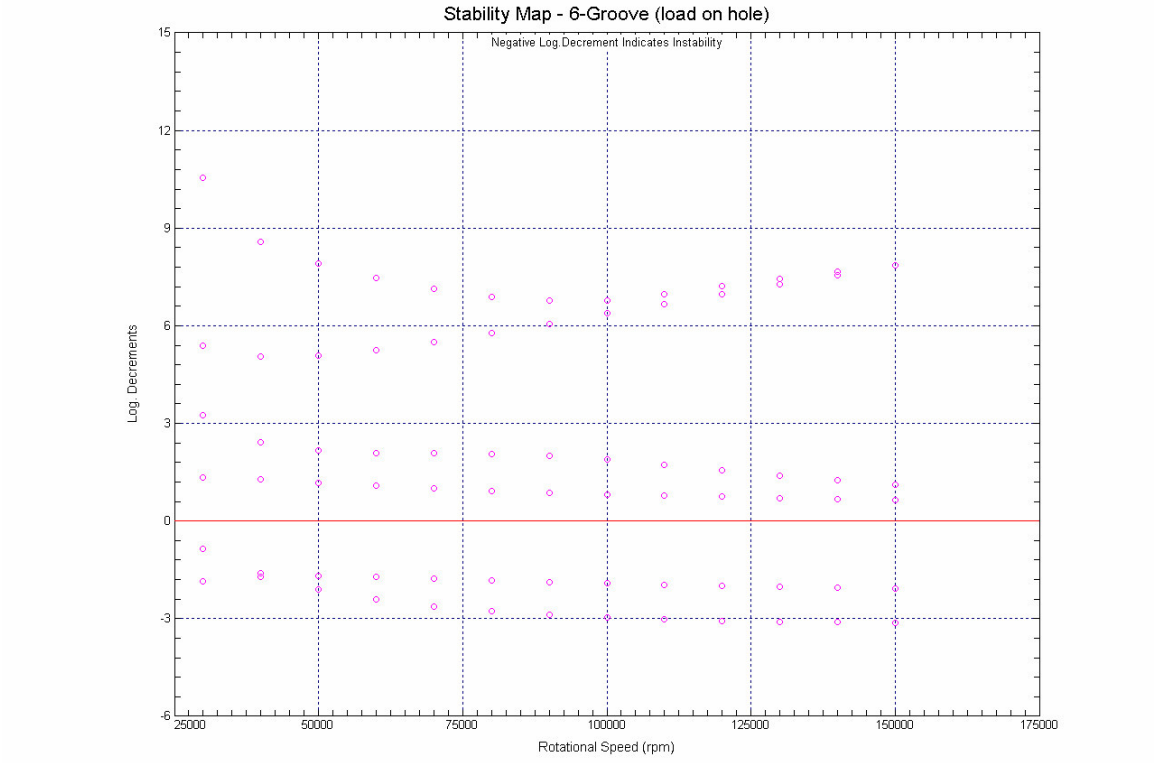

Figure 4.26 Turbo with 6-Groove Bearings (Load on Hole) - Stability Map

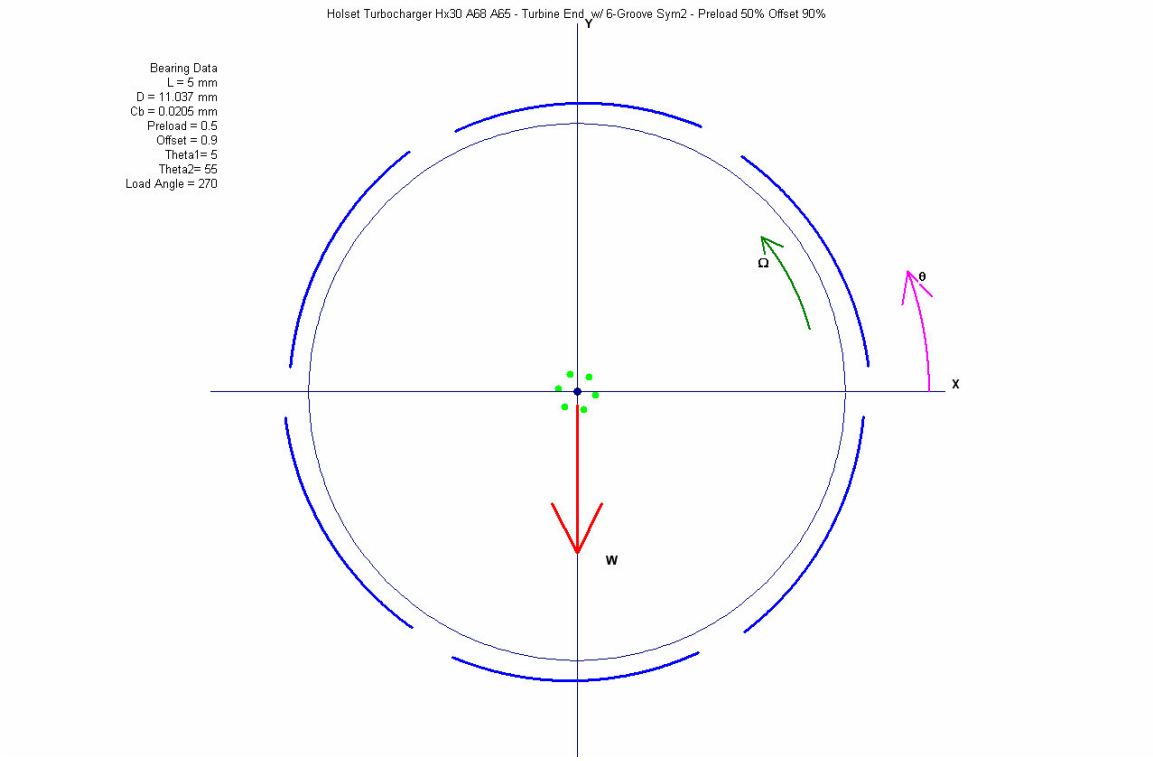

Figure 4.27 6-Groove Bearing (Load between Holes) – Preload 50%, Offset 90% - at Turbine End

Figure 4.28 Turbo with 6-Groove Bearings (Load between Holes) – Preload 50%, Offset 90% - Stability Map

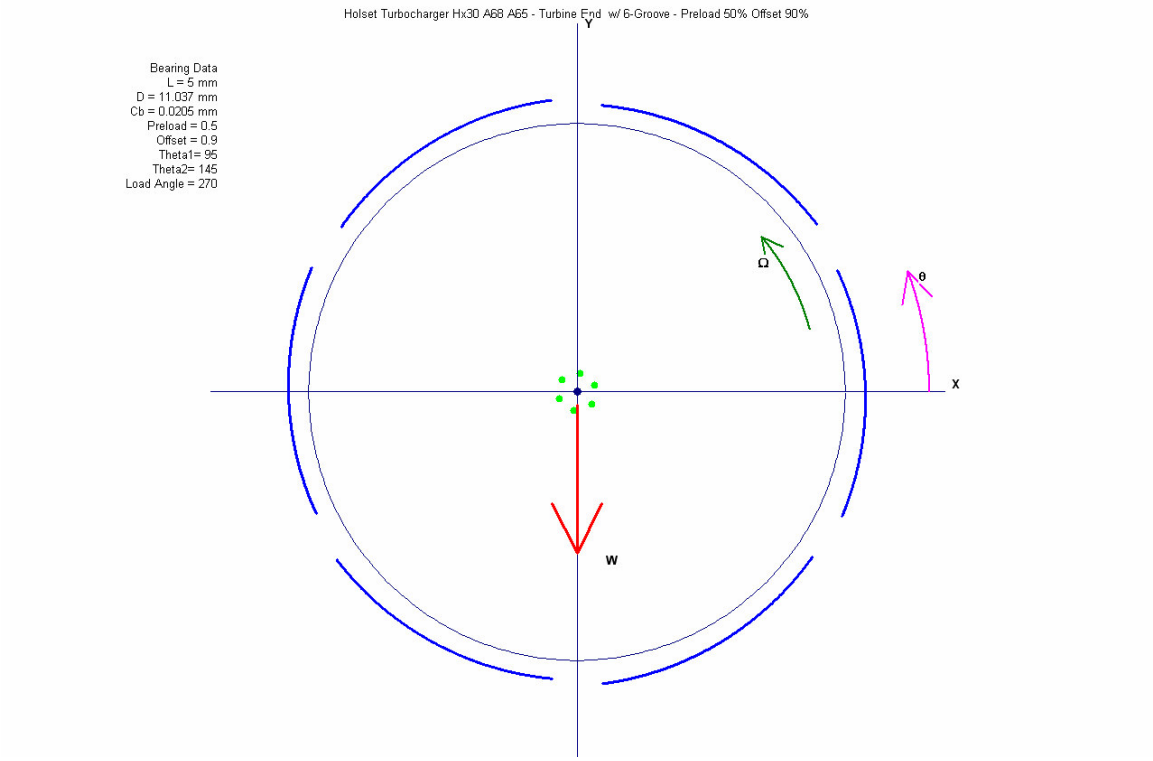

Figure 4.29 6-Groove Bearing (Load on Hole) – Preload 50%, Offset 90% - at Turbine End

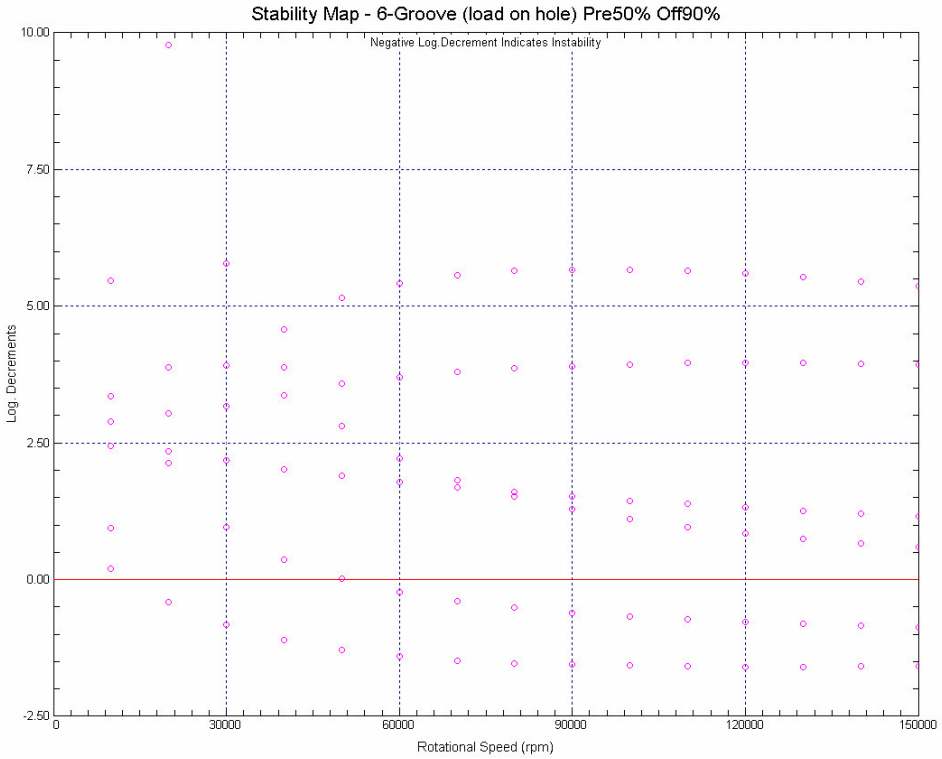

Figure 4.30 Turbo with 6-Groove Bearings (Load on Hole) – Preload 50%, Offset 90% - Stability Map

When the preloading increased as in Figures 4.31 and 4.33 to 75% preload and 100% offset, the stability map for the turbocharger model did not change solely rather it's like tuning the mode shapes. In other words, the first and second whirling modes had the same logarithmic decrements values (Figures 4.32 and 4.34) but with a phase lag in the speed of about 30,000 RPM. The first and second whirling modes run unstable over speeds 25,000 RPM and 75,000 RPM, respectively.

Six-Pocket bearings were also employed in the analysis. Figures 4.35 and 4.36 represent six-pocket bearings with loading is between the holes and on the hole, respectively. The pocket depth is 3 times the bearing clearance *Cb*. The arc length of the pocket is 60% of the pad and the axial length is 60% of the bearing width. The stability maps for both modeling (Figures 4.36 and 4.38) do not show any critical change in the behavior of the turbocharger rotor. Both of the first and second whirling modes are unstable for almost the entire speed range.

Increasing the pocket depth did not show any improvement to the dynamic stability of the turbocharger. The pocket depth was increased to 4 times the bearing clearance *Cb* (Figures 4.39 and 4.41), though no critical distinction is observed in the dynamic stability (Figures 4.40 and 4.42).

Another type of journal bearings are the elliptical or lemon bore bearings. The bearings were installed in the turbocharger model with three different settings: horizontal, vertical and cross-tilted (Figures 4.43, 4.45 and 4.47). The horizontal and vertical installations have almost the same stability response as represented in Figures 4.44 and 4.46, respectively. Instabilities still show up at low speed (first and second whirl modes) and dominate for higher speeds. At very high speeds, a third whirling mode switch with the second whirling mode over 135,000 RPM, where the second mode stabilizes again. This new unstable mode could be the bending mode. Installing the lemon bore bearings as cross-tilted (Figure 4.47) does not add any enhancement to the stability of the Holset turbocharger. From Figure 4.48, the first whirling mode is unstable for the entire speed range, whereas the second mode whirls unstable over 45,000 RPM.

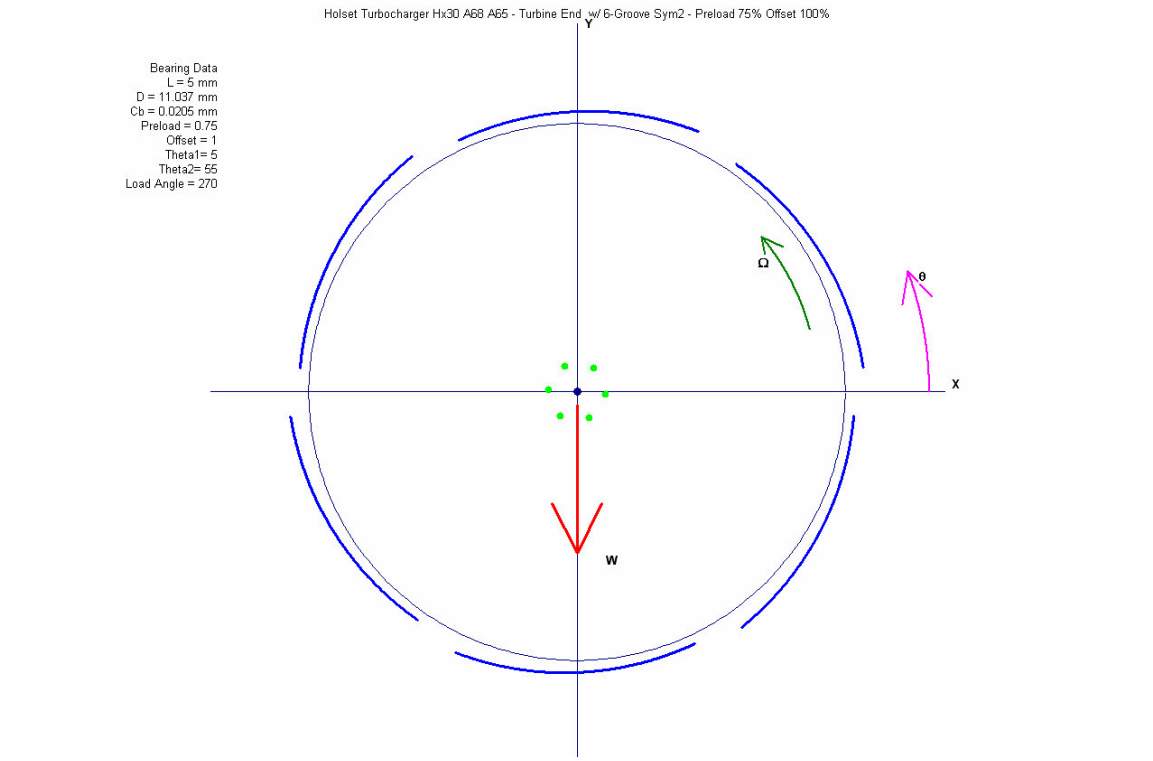

Figure 4.31 6-Groove Bearing (Load between Holes) – Preload 75%, Offset 100% - at Turbine End

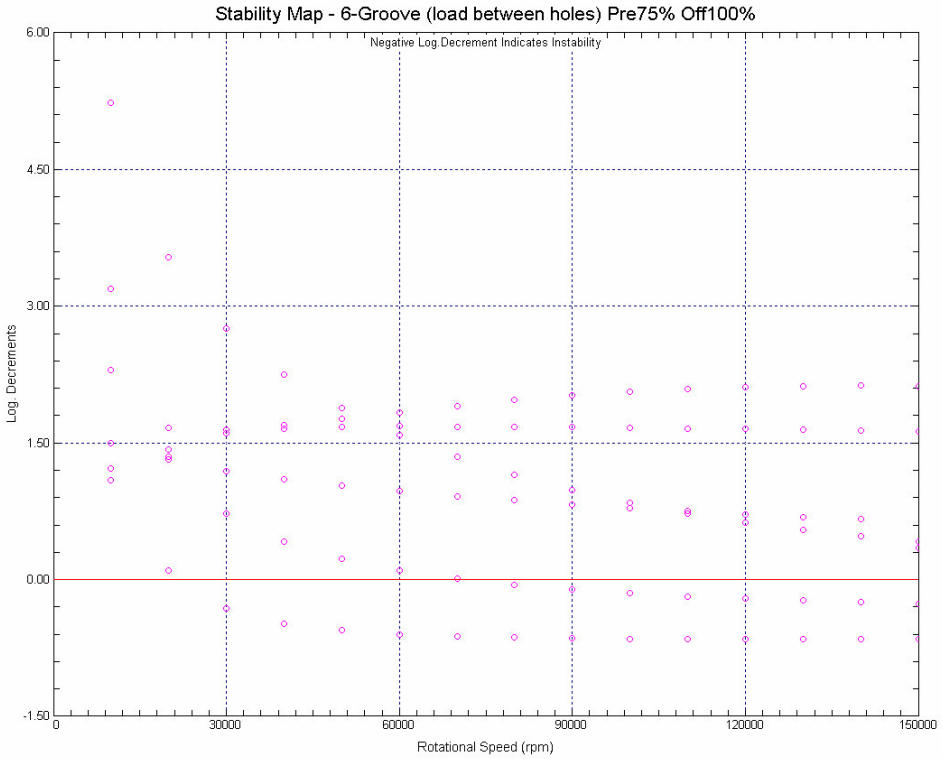

Figure 4.32 Turbo with 6-Groove Bearings (Load between Holes) – Preload 75%, Offset 100% - Stability Map

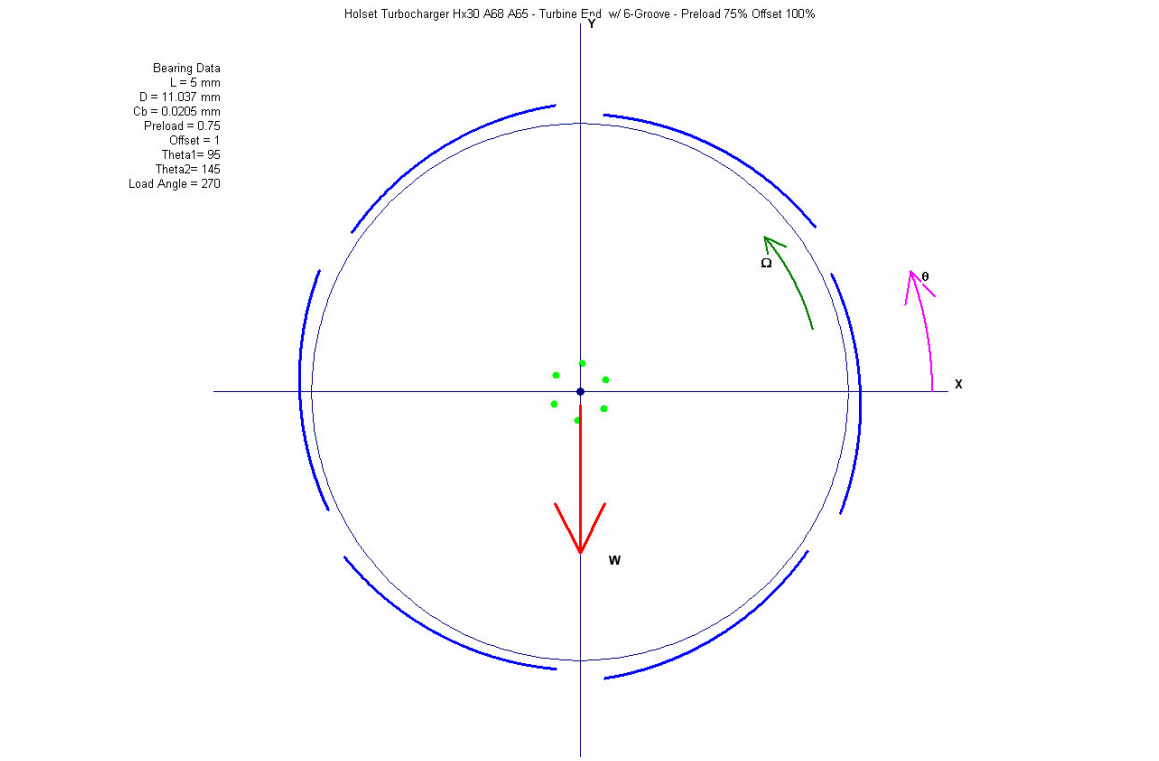

Figure 4.33 6-Groove Bearing (Load on Hole) – Preload 75%, Offset 100% - at Turbine End

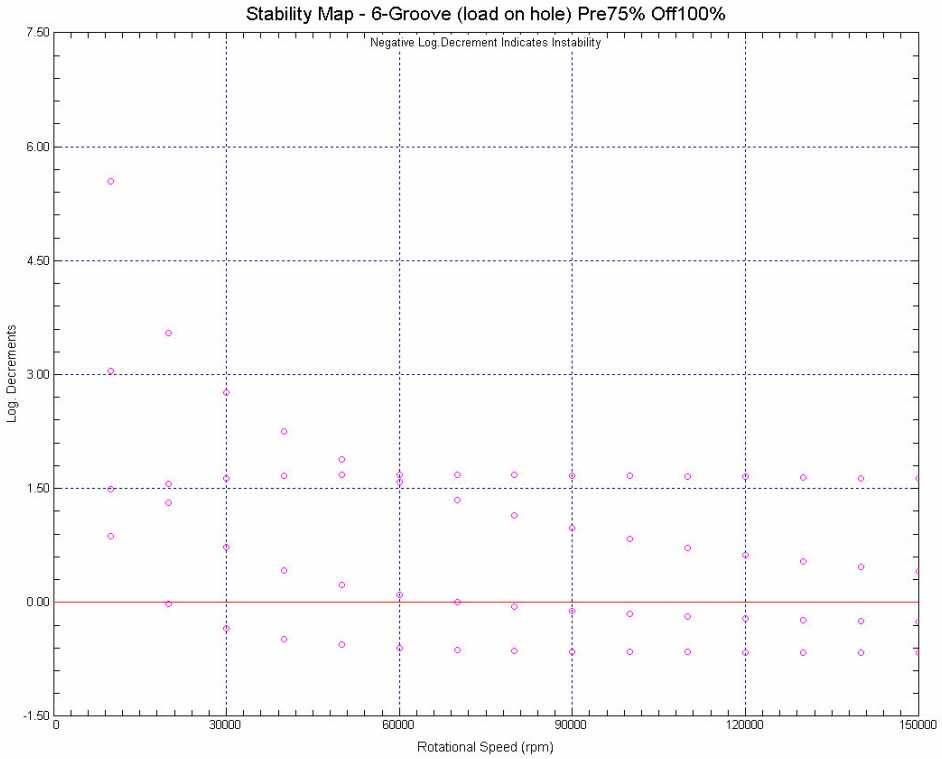

Figure 4.34 Turbo with 6-Groove Bearings (Load on Hole) – Preload 75%, Offset 100% - Stability Map

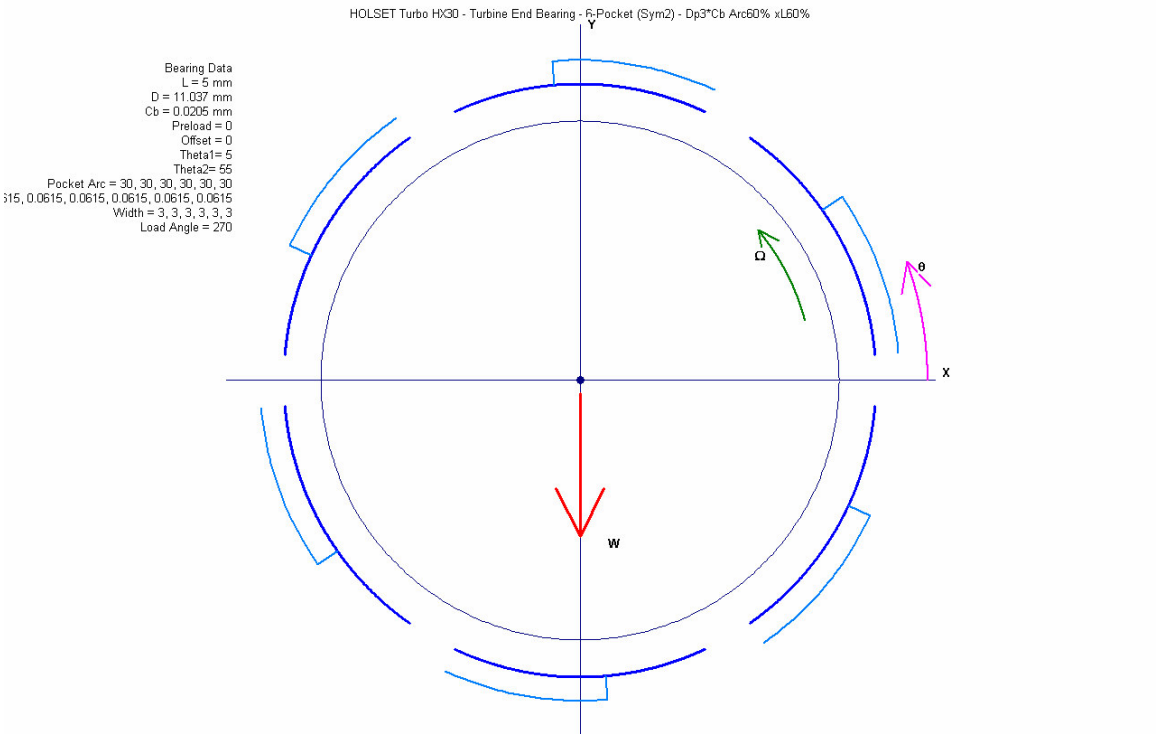

Figure 4.35 6-Pocket Bearing (Load between Holes) – Pocket Depth 3xCb, Arc 60%, xL 60% - at Turbine End

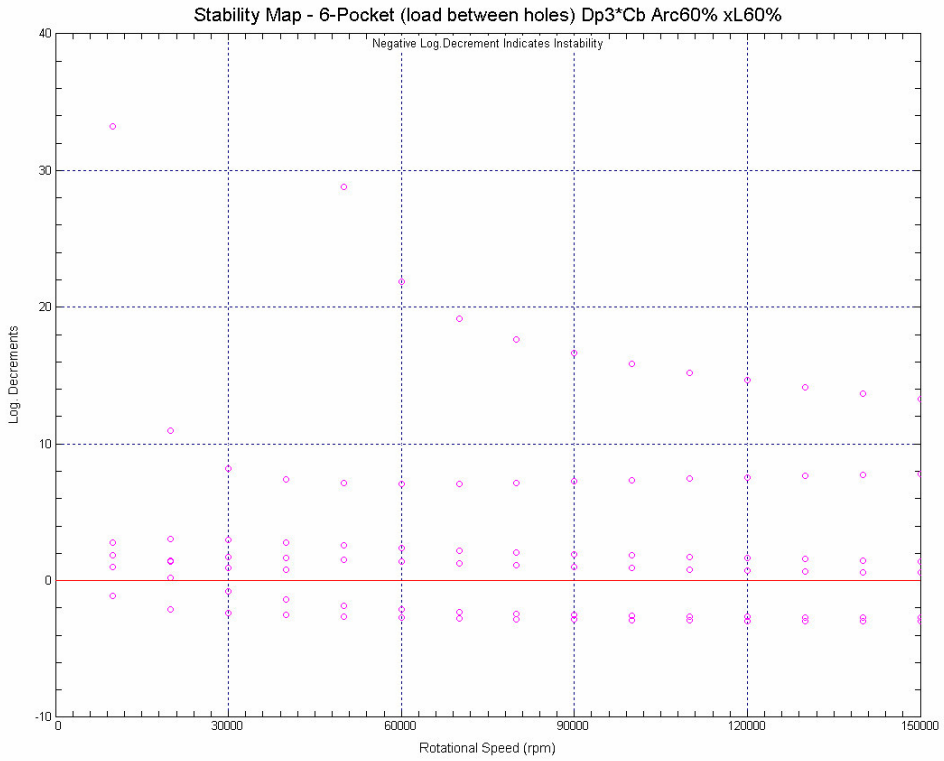

Figure 4.36 Turbo with 6-Pocket Bearings (Load between Holes) – Pocket Depth 3xCb, Arc 60%, xL 60% - Stability Map

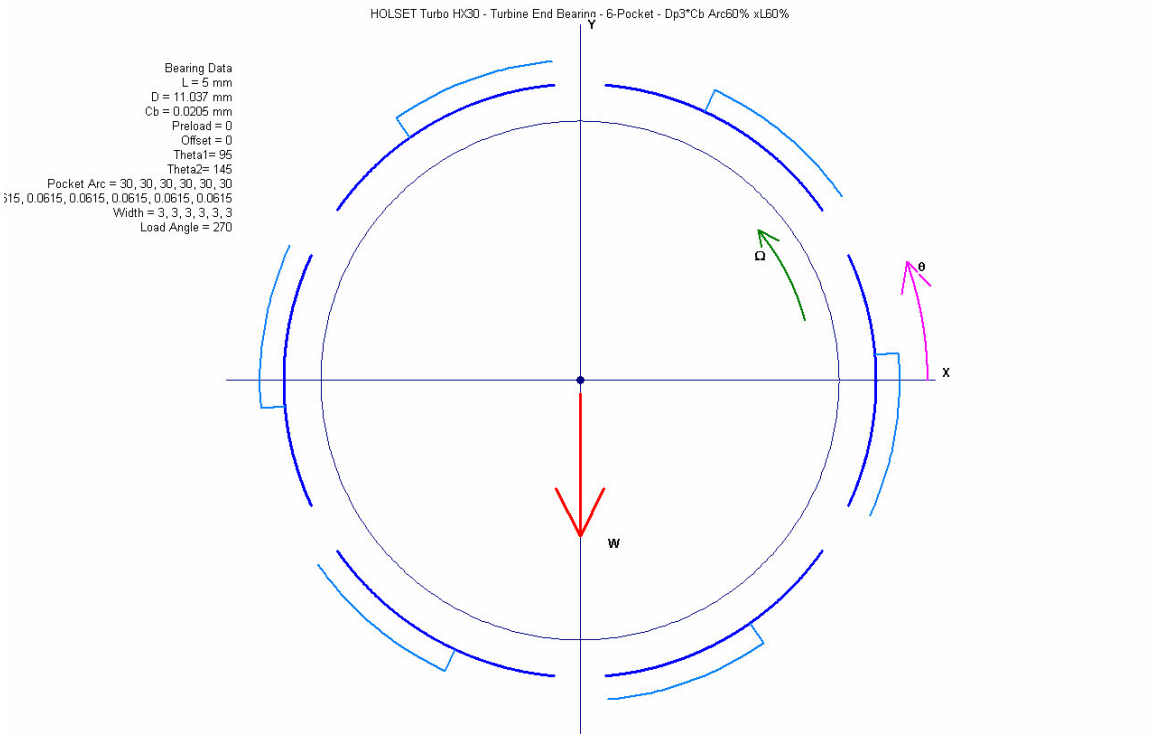

Figure 4.37 6-Pocket Bearing (Load on Hole) – Pocket Depth 3xCb, Arc 60%, xL 60% - at Turbine End

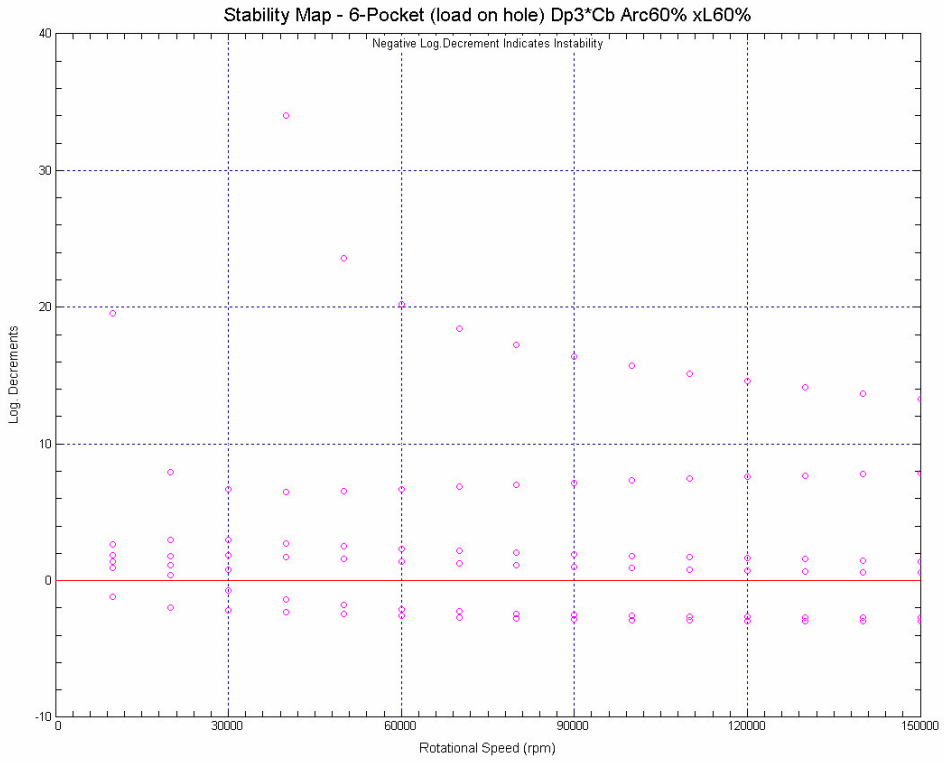

Figure 4.38 Turbo with 6-Pocket Bearings (Load on Hole) – Pocket Depth 3xCb, Arc 60%, xL 60%- Stability Map

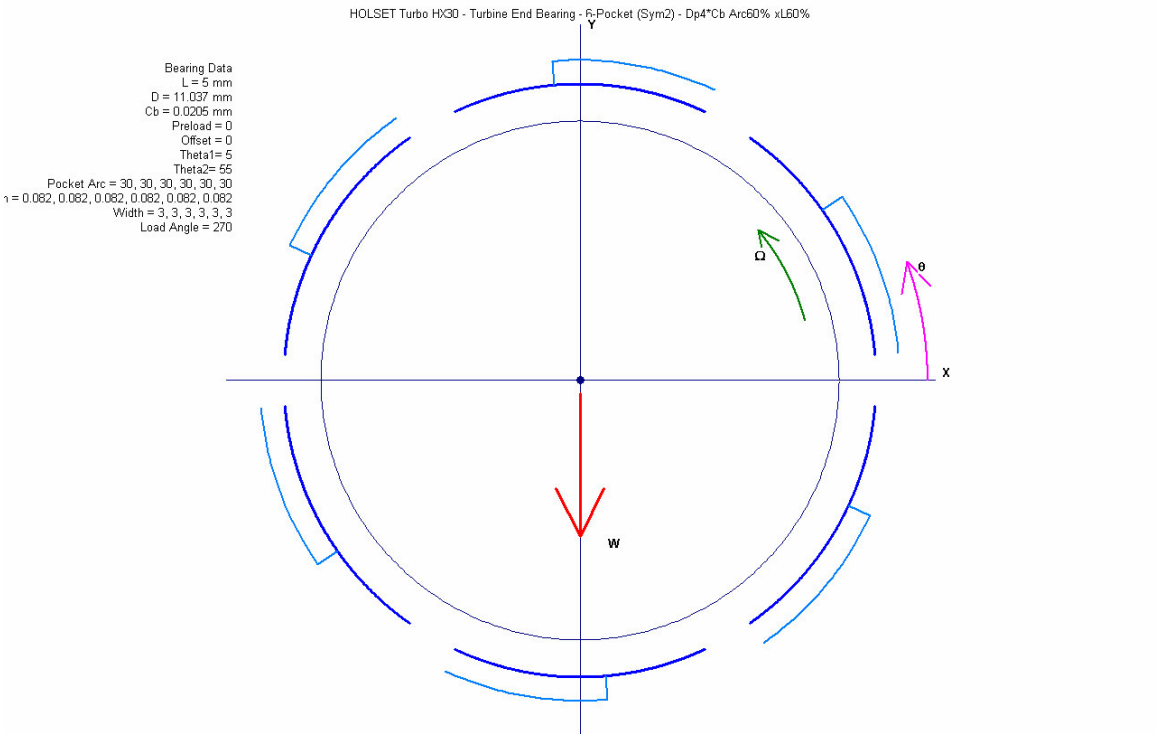

Figure 4.39 6-Pocket Bearing (Load between Holes) – Pocket Depth 4xCb, Arc 60%, xL 60% - at Turbine End

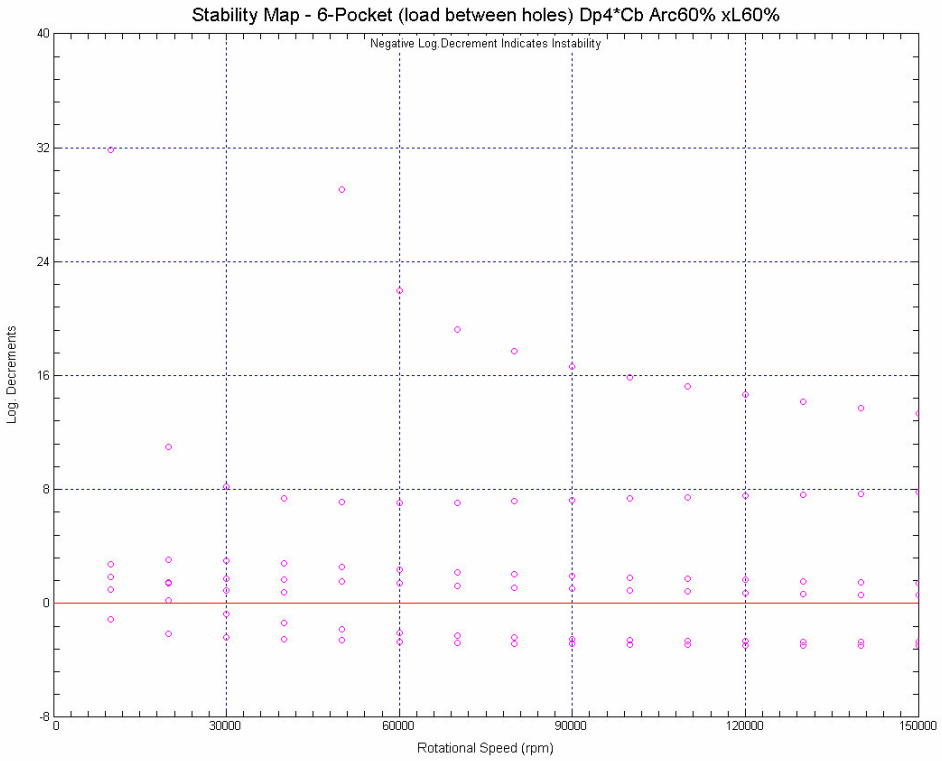

Figure 4.40 Turbo with 6-Pocket Bearings (Load between Holes) – Pocket Depth 4xCb, Arc 60%, xL 60% - Stability Map

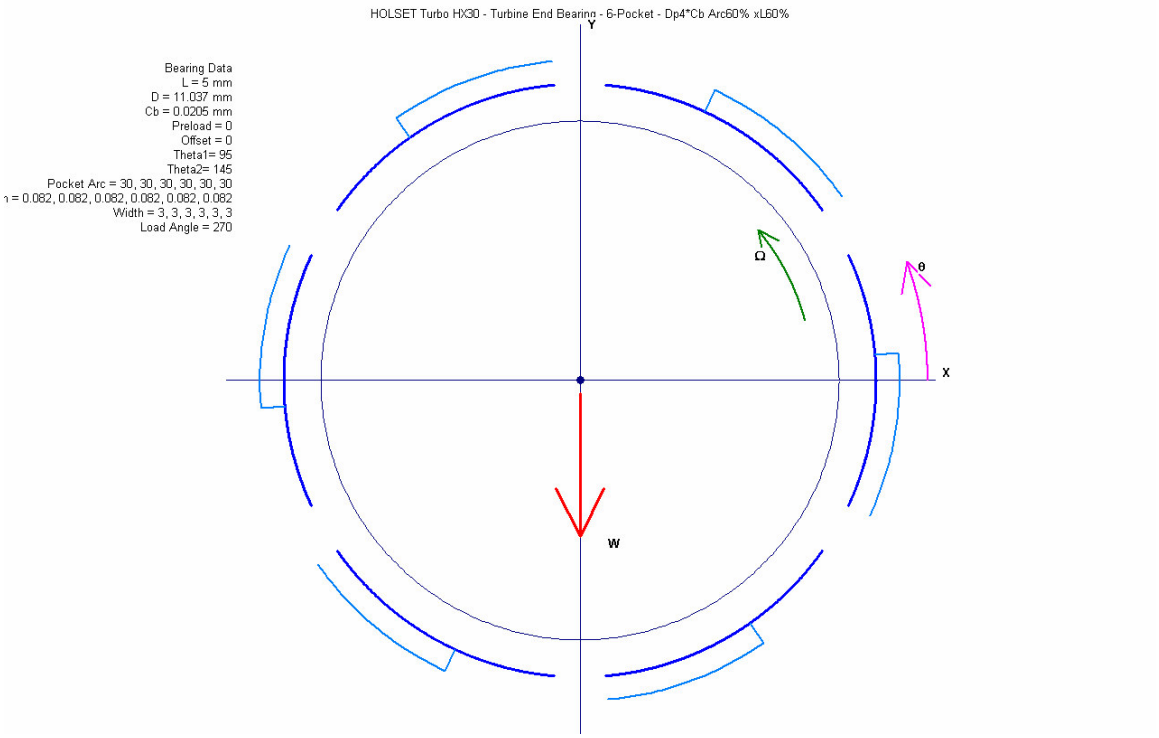

Figure 4.41 6-Pocket Bearing (Load on Hole) – Pocket Depth 4xCb, Arc 60%, xL 60%- at Turbine End

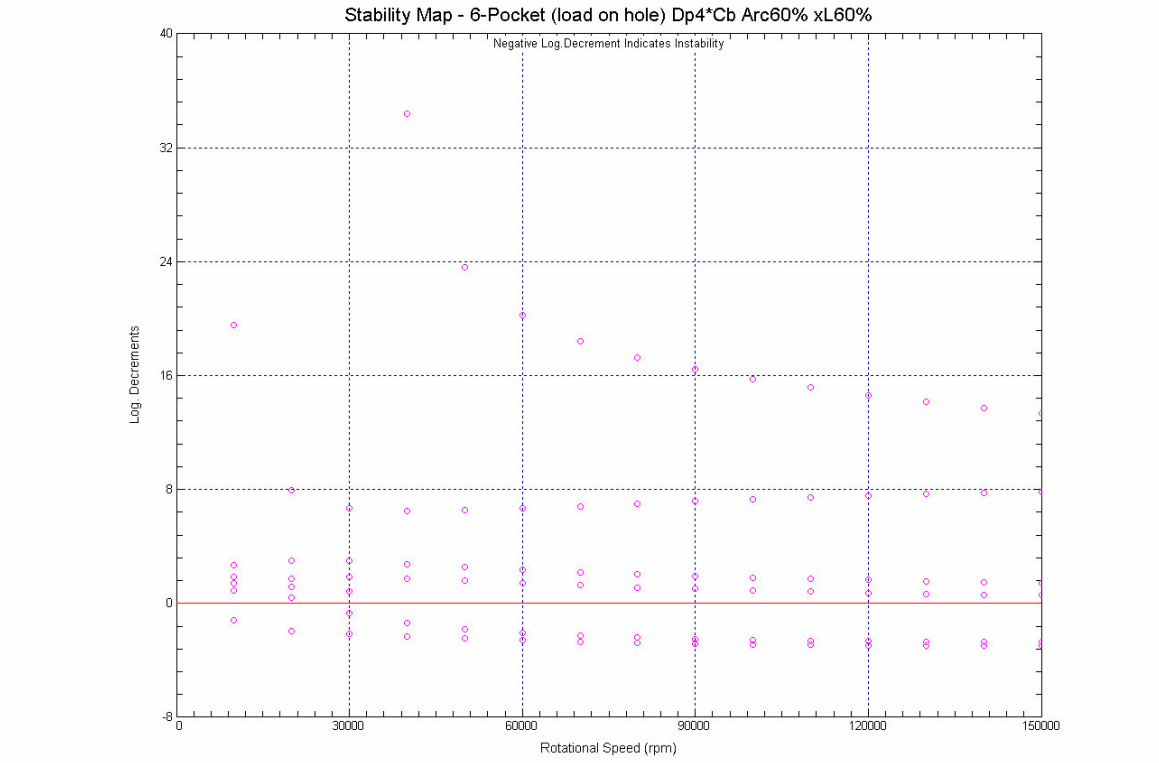

Figure 4.42 Turbo with 6-Pocket Bearings (Load on Hole) – Pocket Depth 4xCb, Arc 60%, xL 60%- Stability Map

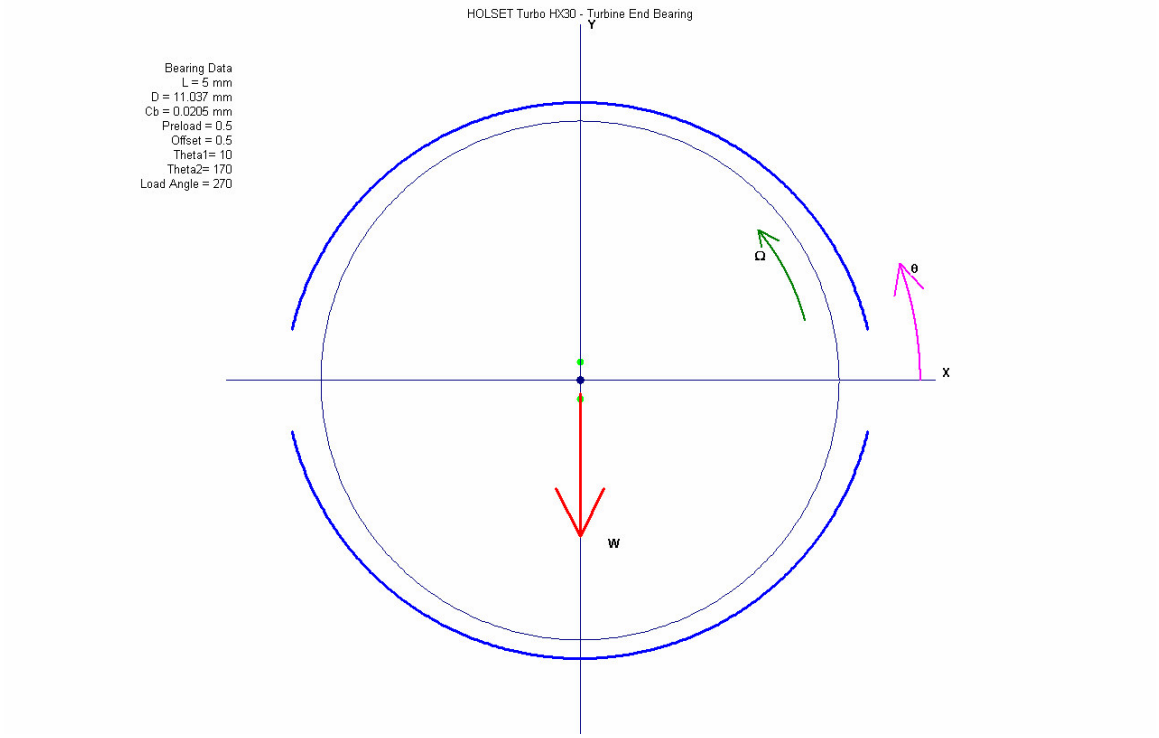

Figure 4.43 Elliptical (Lemon Bore) Bearing – Horizontal Fitting – at Turbine End

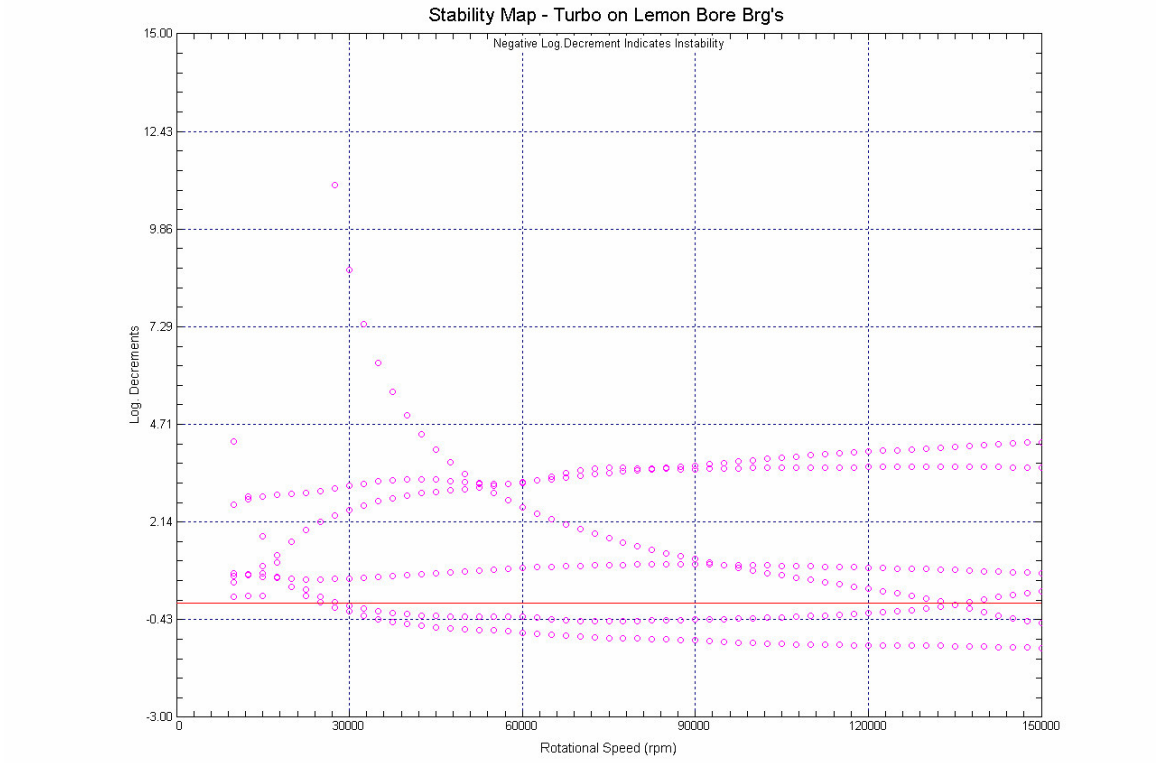

Figure 4.44 Turbo with Elliptical (Lemon Bore) Bearings – Horizontal Fitting - Stability Map

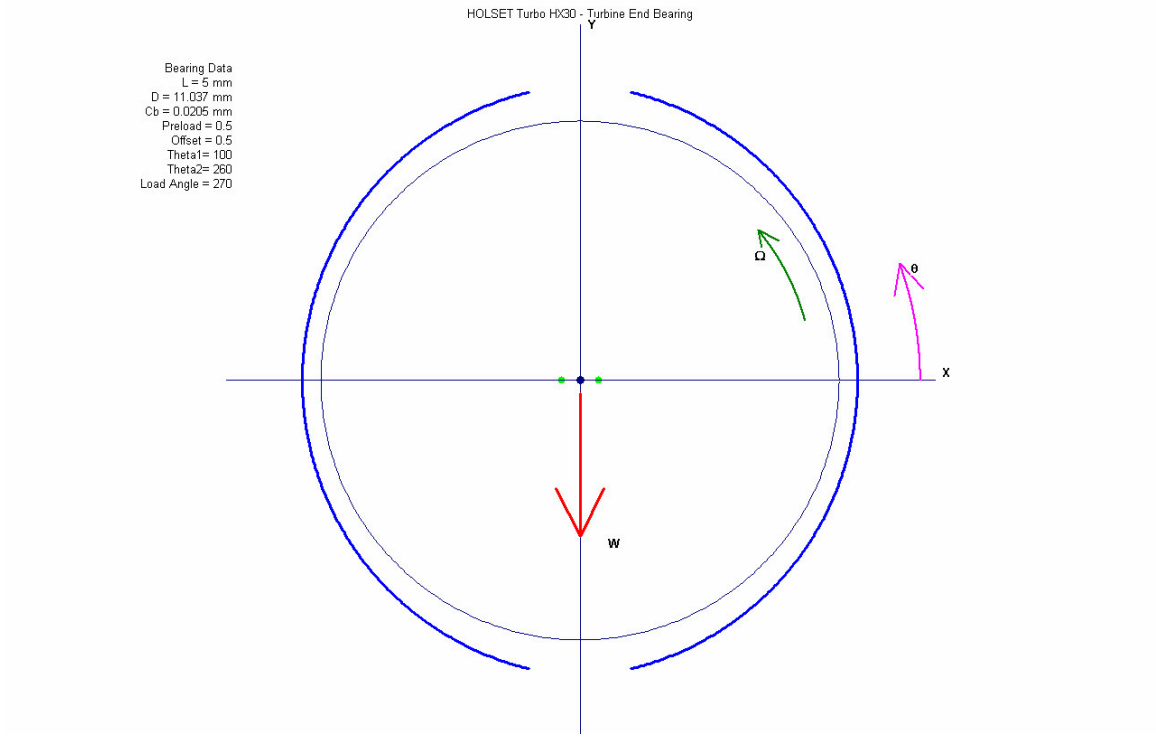

Figure 4.45 Elliptical (Lemon Bore) Bearing – Vertical Fitting – at Turbine End

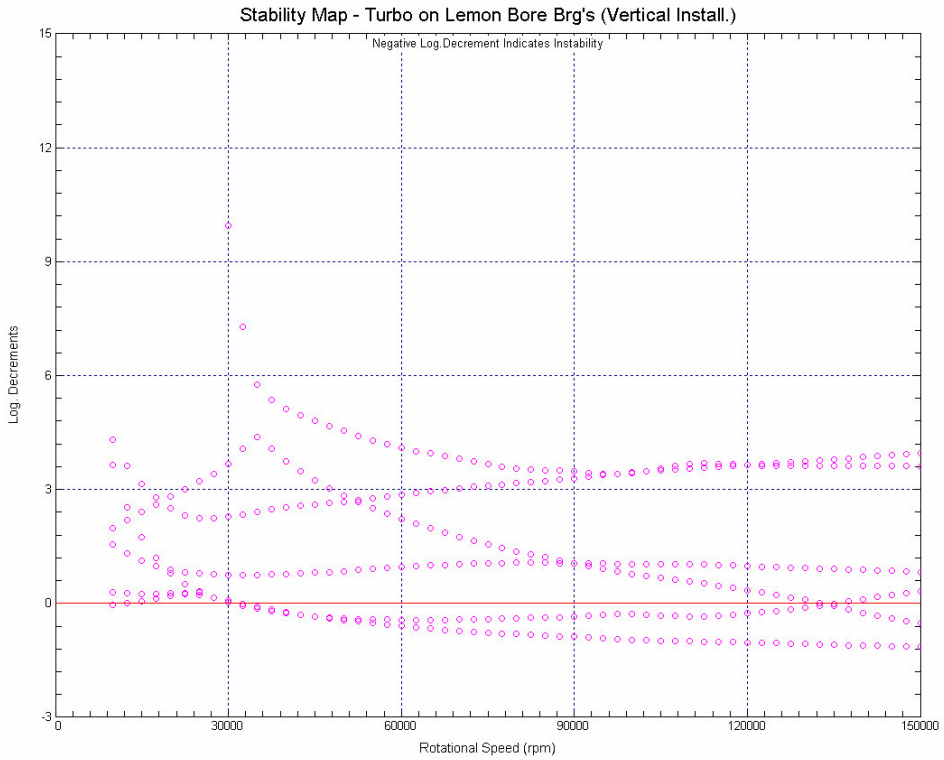

Figure 4.46 Turbo with Elliptical (Lemon Bore) Bearings – Vertical Fitting -Stability Map

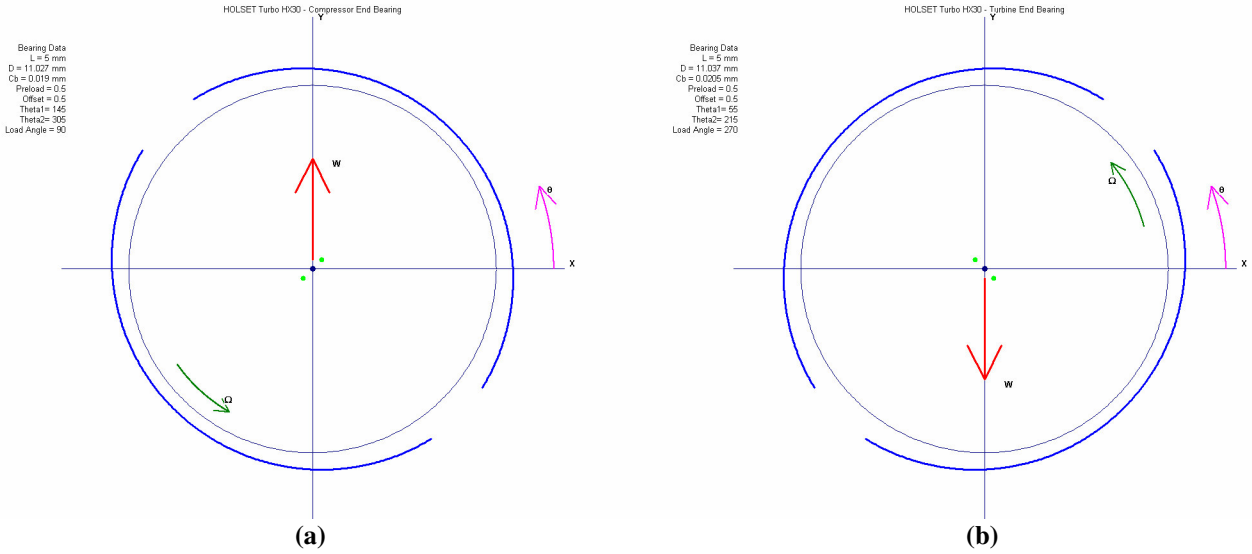

Figure 4.47 Elliptical (Lemon Bore) Bearings – Cross Fitting (a) Compressor Brg. (b) Turbine Brg.

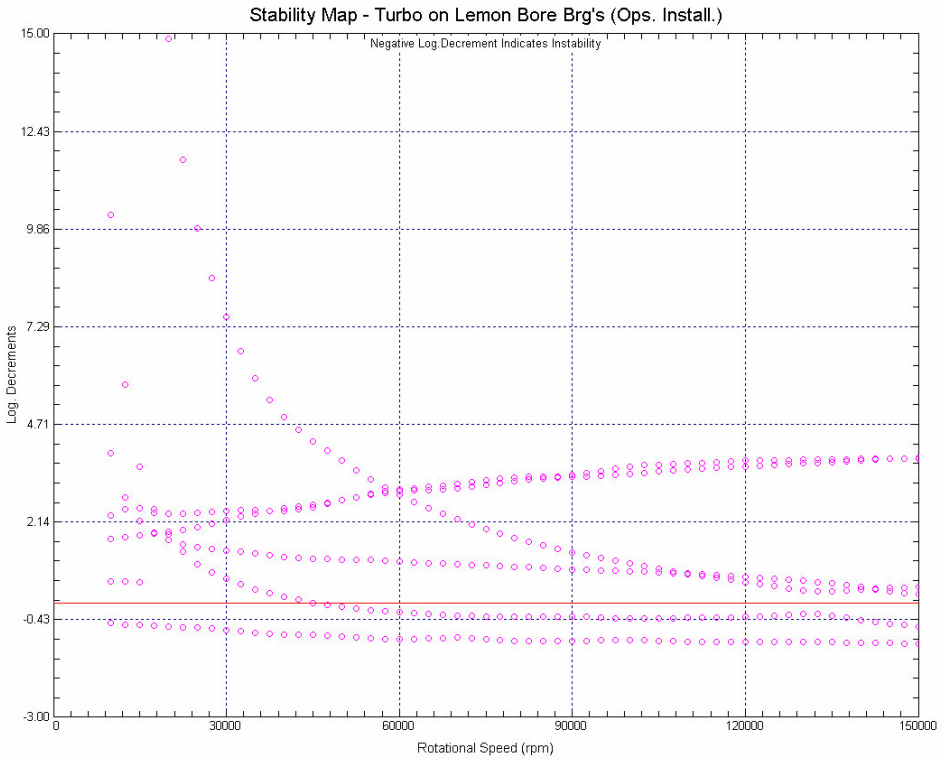

Figure 4.48 Turbo with Elliptical (Lemon Bore) Bearings – Cross Fitting - Stability Map

Tilting-pad bearings are very common in large sized turbomachinery. Figures 4.49 and 4.51 represents two tilting-pad bearings installations where the bearing load is between the pivots and on the pivot, respectively. In the linear whirling and stability analysis, both bearings set present a superior dynamic stability for the rotor-bearings system. In the tilting-pad bearings where the loading is between the pivots, all the modes are stable throughout the speed range (Figure 4.50). Though the modes are stable, two modes are marginally stable over 60,000 RPM. These modes are backward and forward whirling modes of conical shape where the turbine and compressor wheels moving out of phase.

The second model of the tilting-pad bearings, where the loading acts on the pivot (Figure 4.49), provides the most stable system as predicted from the stability map in Figure 4.52. All the modes are clearly well damped for the whole speed range. The absence of cross-coupled coefficients is definitely the reason of achieving the good stability.

Since the rotor-bearing system is linearly stable, one can examine the rotor time transient response. Figures 4.53 and 4.55 represent the shaft transient response with tilting-pad bearings at 100,000 RPM, where the loading in between the pivots and on the pivot, respectively. The rotor whirls with little higher amplitudes at the compressor end. This could be a result of the lighter weight of the compressor. Both designs exhibit limit whirl cycle motion (Figures 4.54 and 4.56).

Although the tilting-pad bearings are known to be reliable and widely used in high-speed turbomachinery, they are not yet usual in automotive turbochargers manufacturing. Most important factor in not implementing such bearings is the high costs of production. Engineers are trying to lower the costs of turbochargers for further distribution, and hence thinking of tilting-pad bearings as a substitute would be the last option to be taken for the current time.

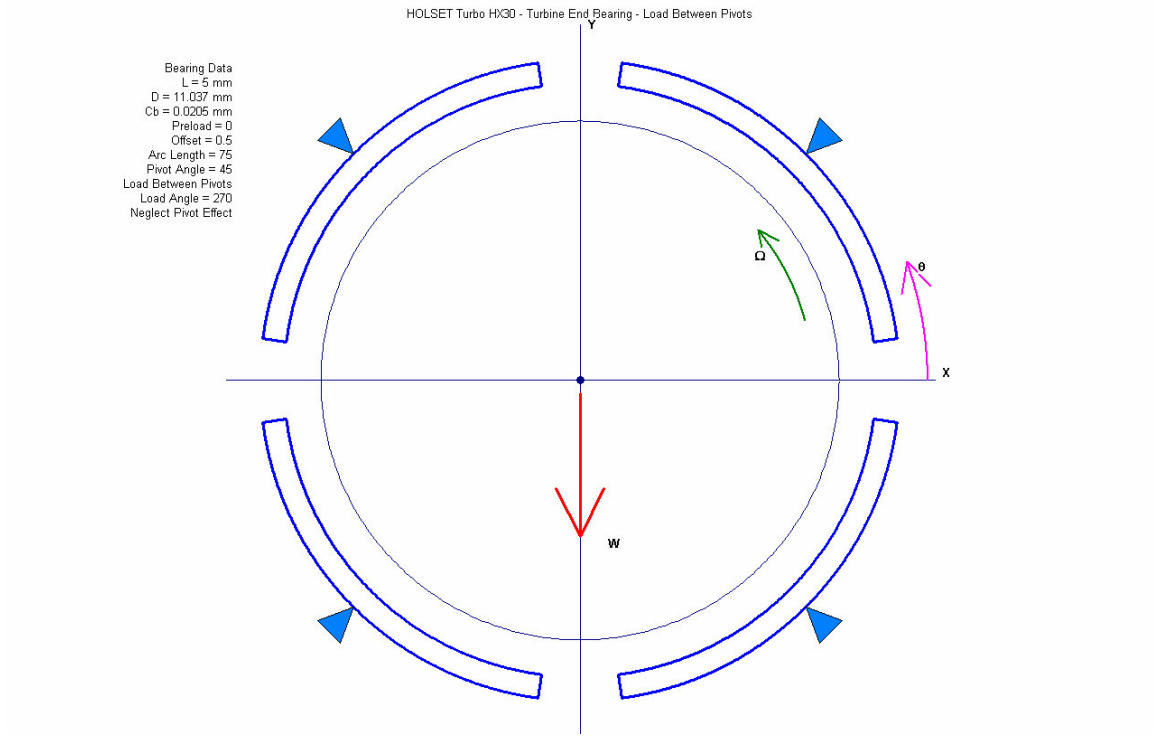

Figure 4.49 Tilting-Pad Bearing (Load between Pivots) at Turbine End

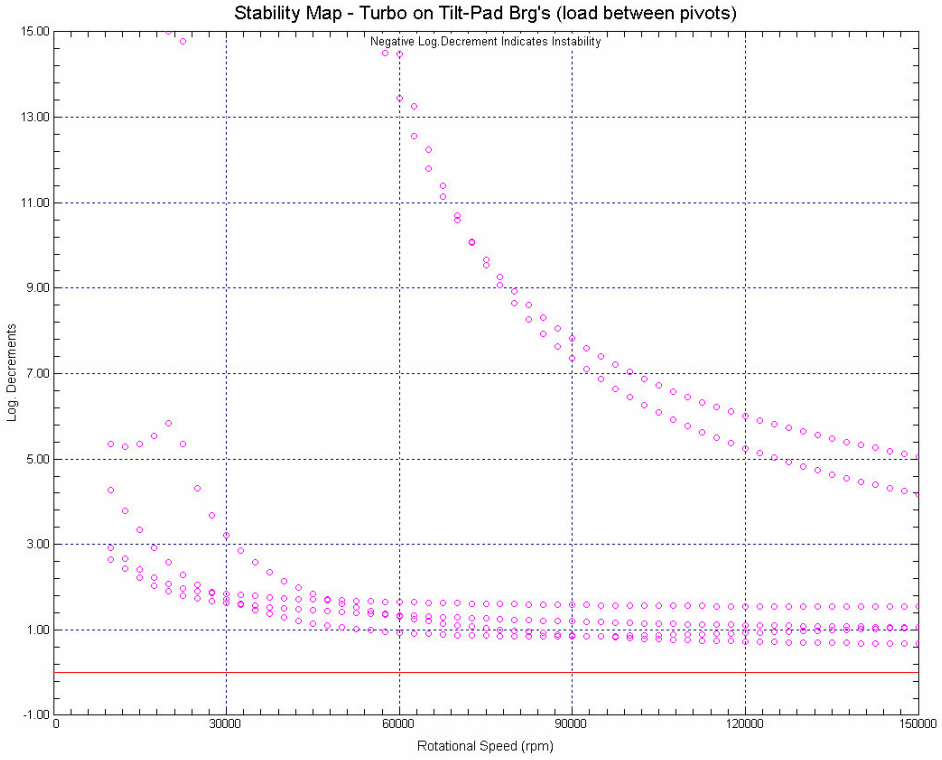

Figure 4.50 Turbo with Tilting-Pad Bearings (Load between Pivots) – Stability Map

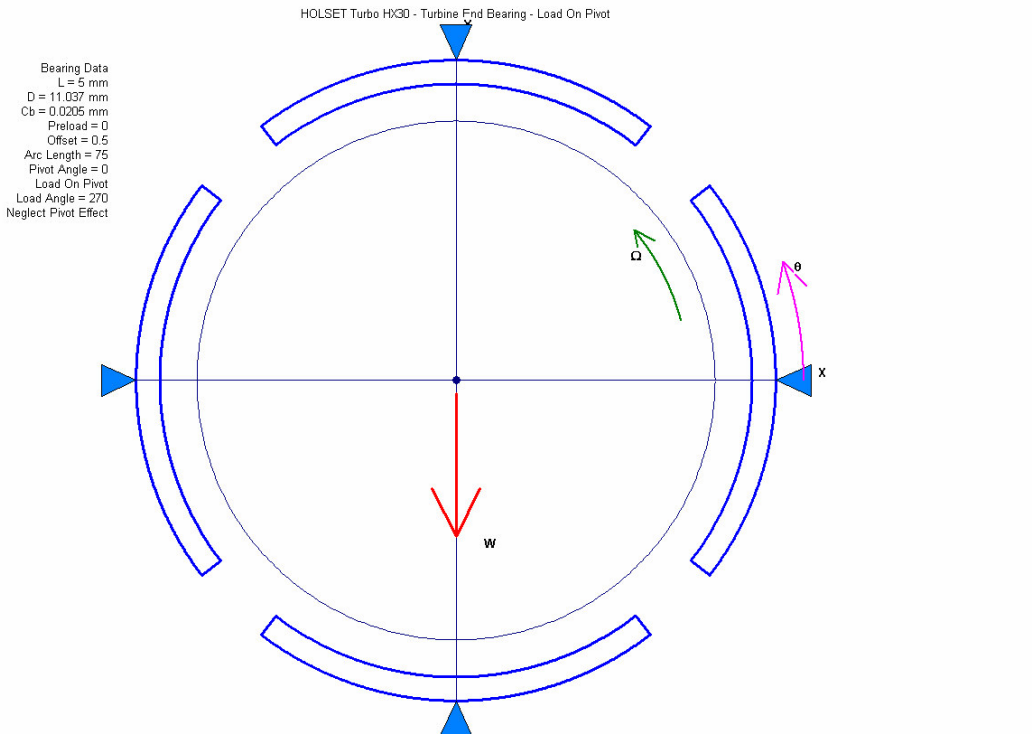

Figure 4.51 Tilting-Pad Bearing (Load on Pivot) at Turbine End

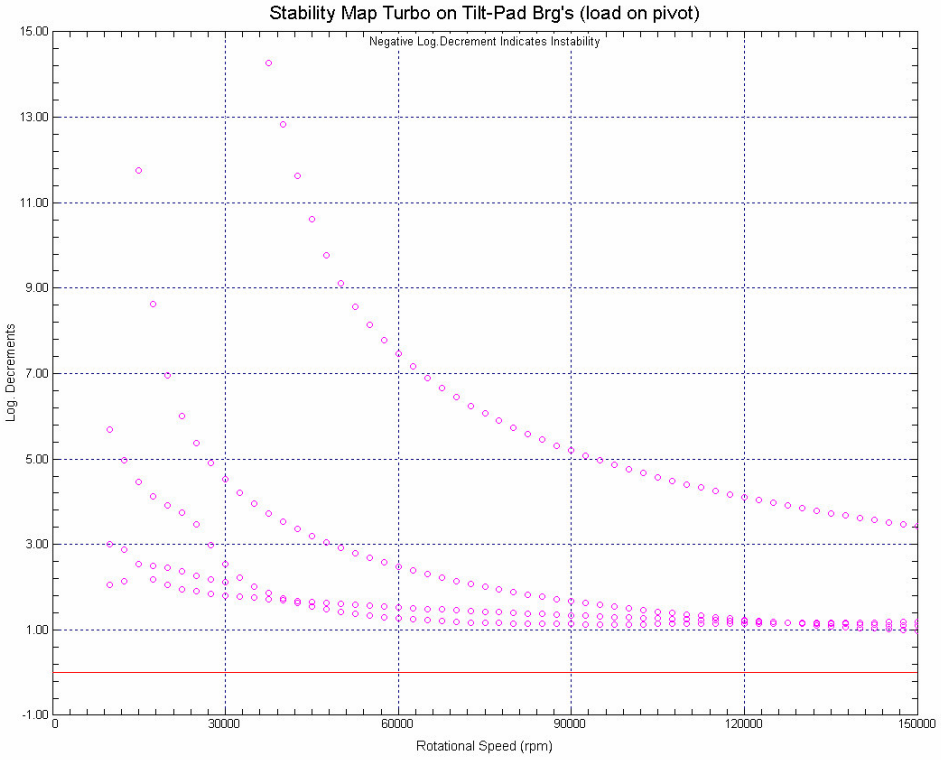

Figure 4.52 Turbo with Tilting-Pad Bearings (Load on Pivot) – Stability Map

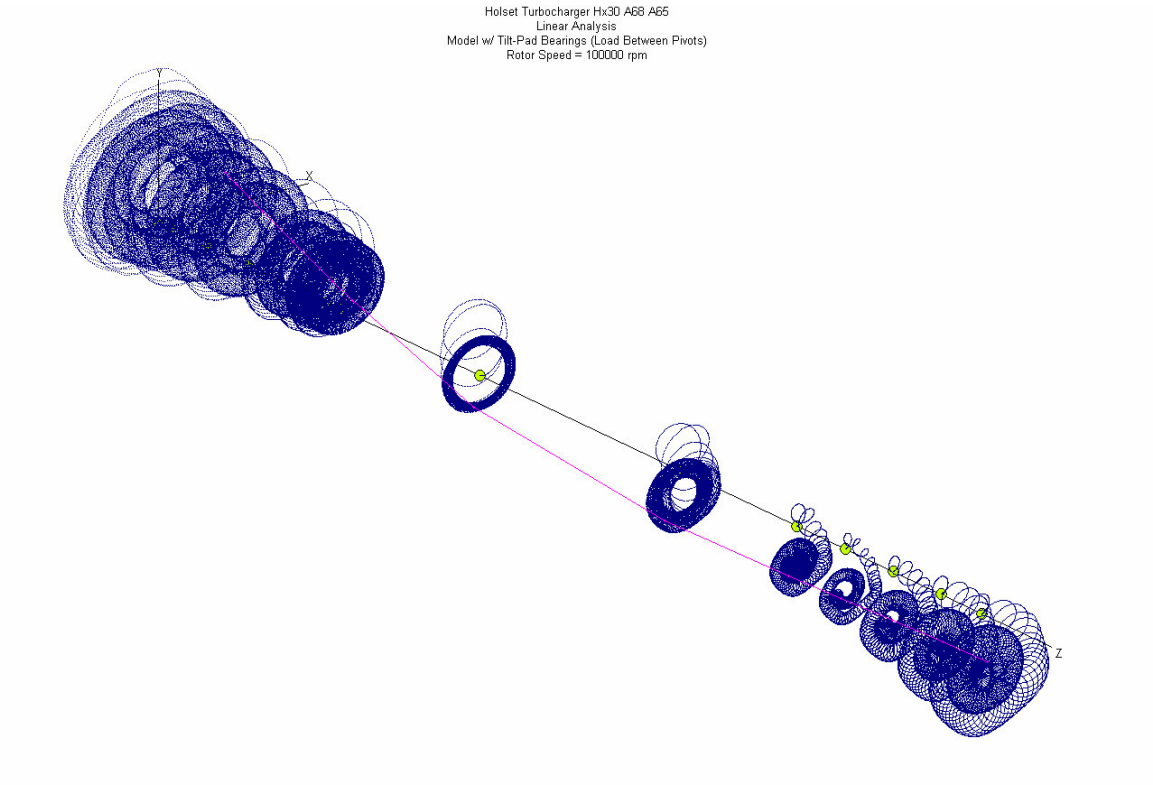

Figure 4.53 Turbo with Tilting-Pad Bearings (Load between Pivots) – Shaft Transient Response

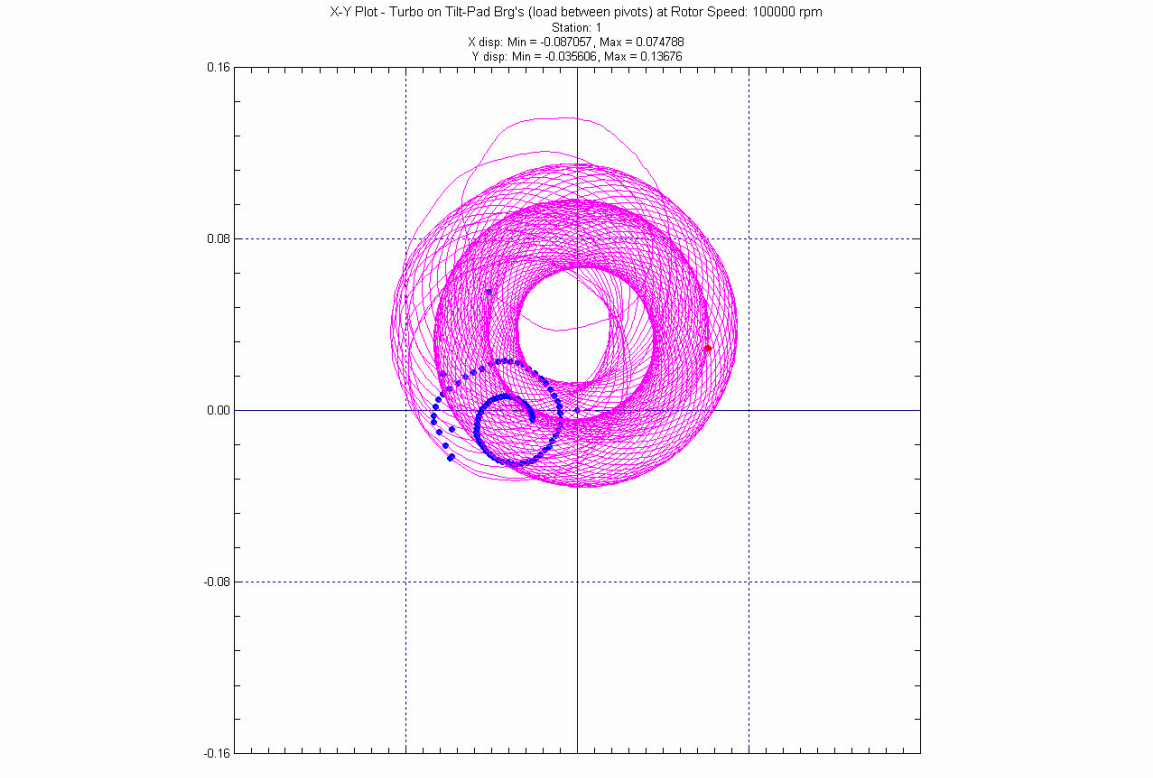

Figure 4.54 Turbo in Tilt-Pad Bearings (Load between Pivots) – X-Y Orbit at St1 (Compressor)

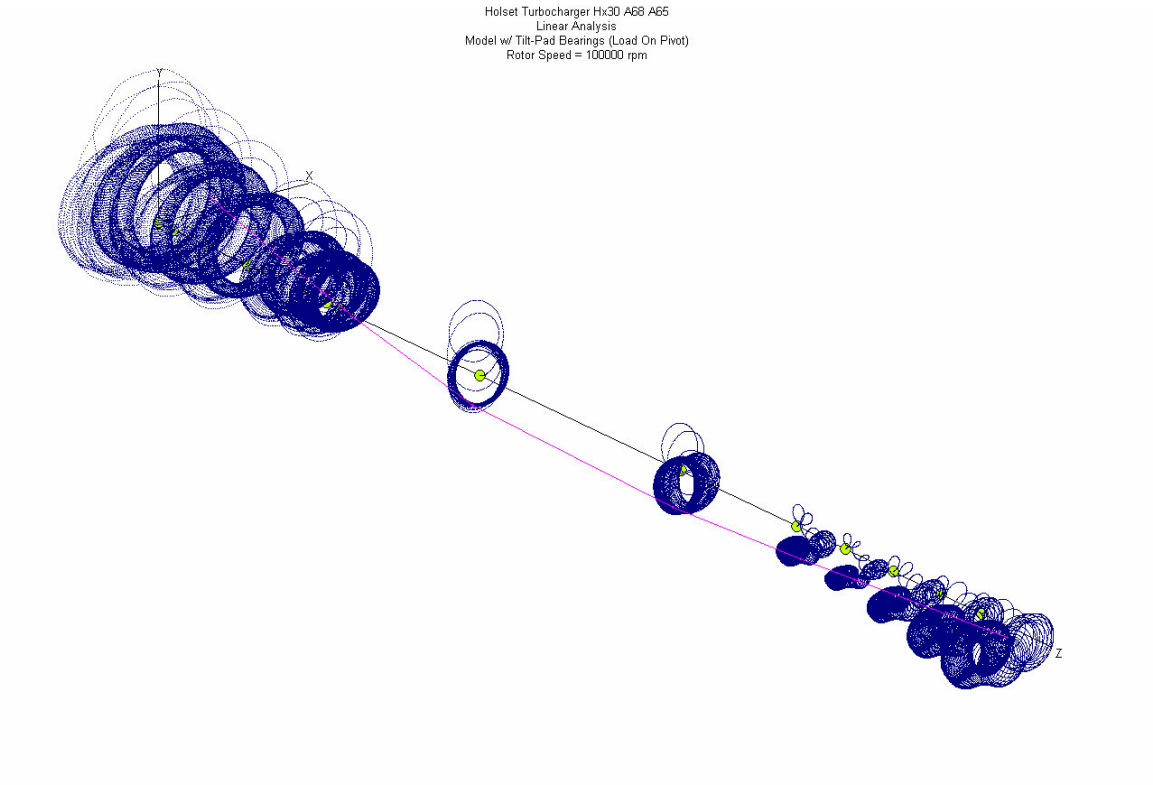

Figure 4.55 Turbo with Tilting-Pad Bearings (Load on Pivots) – Shaft Transient Response

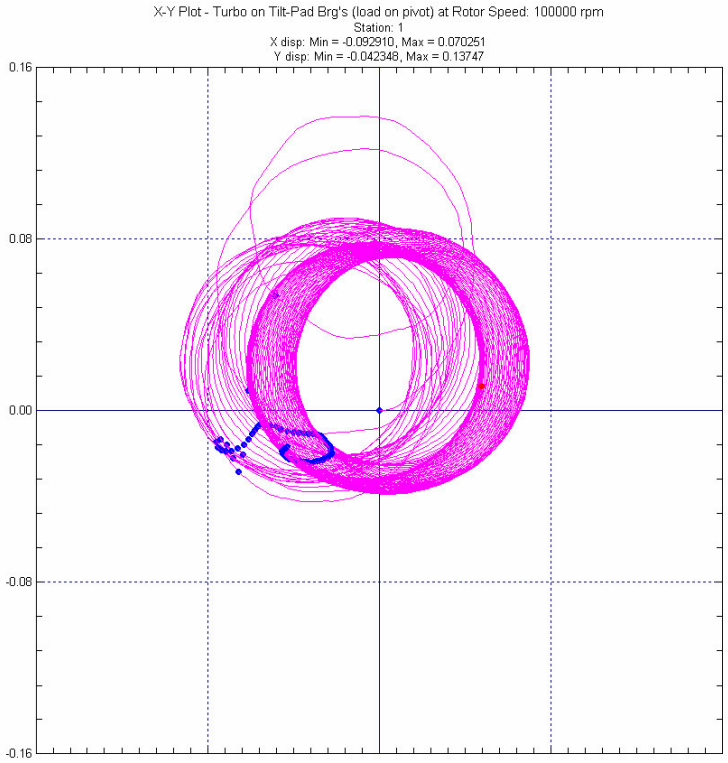

Figure 4.56 Turbo in Tilt-Pad Bearings (Load on Pivot) – X-Y Orbit at St1 (Compressor)

4.3 Stability Optimization Using Damped Support

Addition of external damping to restabilize high-speed rotors is a common practice by engineers. External damping can be achieved in several ways. Floating ring bearing is one method of adding external damping. The floating ring acts as a bearing with six-oil-groove, and the outer clearance acts as additional damper. Squeeze-film dampers are also another way of restabilizing rotors and they are widely used in turbomachinery.

This phase of the research will attempt to design external damping in order to stabilize the Holset HX30 turbocharger with six-oil-groove bearings. Damped supports (pedestal) are added at both six-oil-groove bearings with several stiffness and damping values. The turbocharger model will be similar to that in Figure 4.2 (a). The objective now is to find the optimum stiffness and damping values that will stabilize the system.

The stiffness values of the pedestal are assumed as:

$$K_P = \frac{K_{xx} + K_{yy}}{2}$$

where the *Kxx* and *Kyy* values are at both compressor and turbine bearings and in the analysis will be computed at speed 100,000 RPM.

The damping values of the pedestal are assumed as:

$$C_P = (0.1, 0.5, 1, 2, 5) \times \left(\frac{C_{xx} + C_{yy}}{2} \right)$$

where the *Cxx* and *Cyy* values are picked at speed 100,000 RPM from both bearings.

The *Kp* at 100,000 RPM is found to be 49.7 N/m at the compressor bearing and 444.5 N-s/m at the turbine bearings. The *Cp* values are (0.0345, 0.1725, 0.345, 0.69, 1.725) N-s/m at compressor bearings and (0.014, 0.07, 0.14, 0.28, 0.7) N-s/m. For each value of *Cp* with the value of *Kp*, the whiling analysis of the model will be computed. The first two unstable forward whirling modes will investigated, and the logarithmic decrement will be picked. The procedure will be repeated for values of 2**Kp* and 0.5**Kp*. In Figure 4.57, the real part of the root of the characteristic equation (derived from logarithmic decrement and running speed) for the first whirl mode is plotted against *Cp*'s values for each *Kp* value at the compressor bearing. The positive real part values means instability, whereas negative values is stability region. One can notice that acceptable values of *Cp* would be between 0.2 N-s/m and 0.8 N-s/m for any *Kp* value. In other words, the first whirling mode should be restabilized when the value of the pedestal damping is 0.2-0.8 N-s/m with any values of *Kp*'s (0.5**Kp*, *Kp* or 2**Kp*).

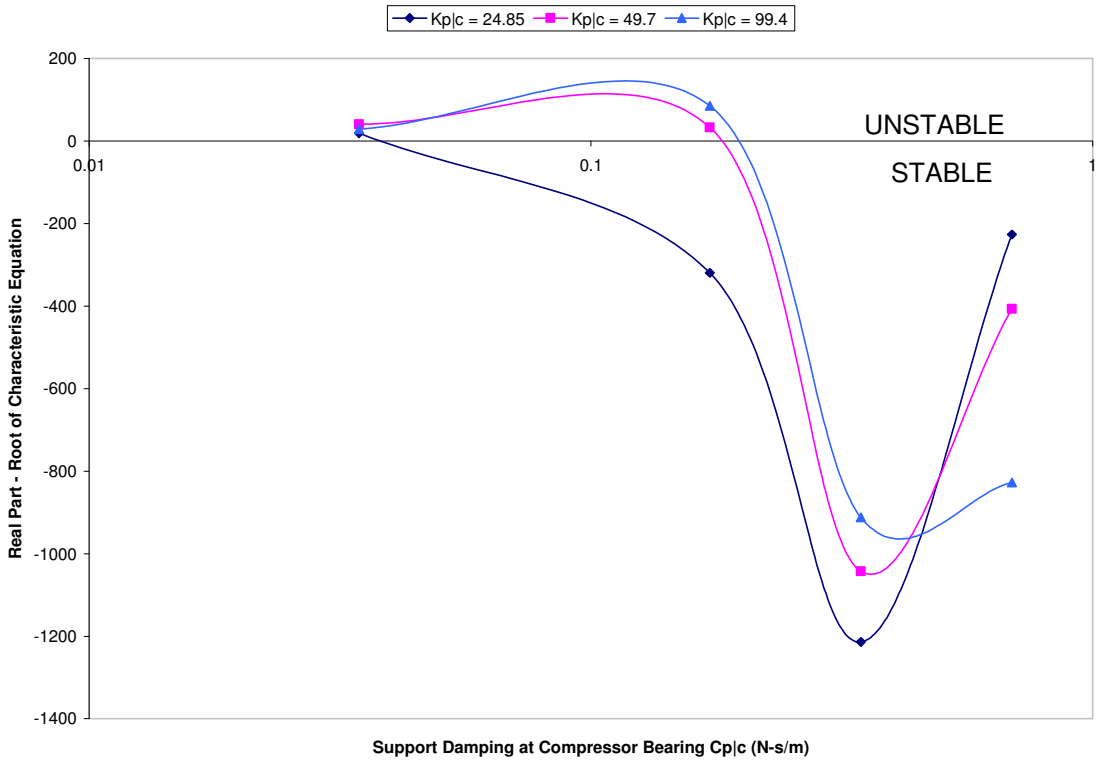

Figure 4.57 1st Whirling Mode Stability Optimization

The real parts of the eigenvalues of the second whirling mode were also plotted against the *Cp*'s values for each *Kp*, as shown in Figure 4.58. Unfortunately, the plot clearly shows that this mode did not stabilize in any trial of pedestal damping values. Though the second whirling mode tends to reach the stability region (Figure 4.58) at very low values of *Cp*, it still considered unstable. Even though the second mode restabilizes at much lower *Cp* values, the first whirling mode (Figure 4.57) will bound again in the instability reign.

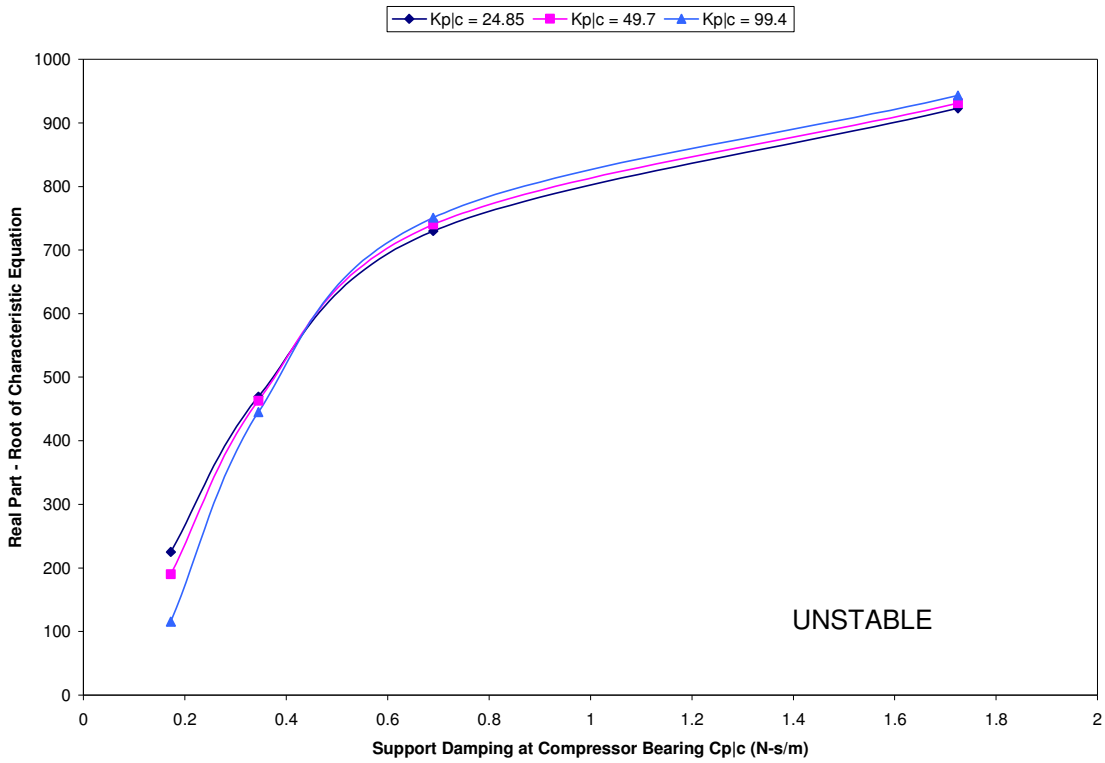

Figure 4.58 2nd Whirling Mode Stability Optimization

Flexible rotor stability optimization achieved by using damped support is a proven method in restabilizing turbomachinery. However, the above investigation can either tell that this approach is not applicable for the turbocharger case, or the very high running speed (100,000 RPM) requires some special considerations.

Chapter 5

Conclusions and Recommendations

The presented research has shown that turbochargers exhibit high subsynchronous vibrations and self-exited instabilities. Investigation of the dynamic stability of the rotor-bearing system was the main objective. Stability evaluation with linear bearing characteristics were conducted for several fluid film journal bearings using the capabilities of DyRoBeS© FEA code.

Analytical prediction of turbocharger rotor whirling with nonlinear floating ring bearings were first computed using DyRoBeS© as a reference to actual performance of the rotor-bearing system. The computations had predicted a good estimation to turbochargers real dynamical response. There are two unstable whirling modes persist during the turbocharger operation speed range. The first one is a rigid body mode of a conical mode shape where the compressor and turbine wheels moving forward out of phase. The second whirl mode has a cylindrical mode shape with slight bending in the shaft where the turbine and compressor wheels moving forward in-phase.

Linear analysis of the turbocharger rotordynamics is a reliable way to study the dynamic stability and whirling modes. Various linear bearings models were created and employed in the turbocharger model to examine the stability of the system. Though tilting-pad bearings provided stable turbocharger rotor-bearing system, they are still relatively expensive to produce. Other types of fluid-film journal bearings showed unaccepted instabilities in the linear running. However, the turbocharger with floating ring bearing has the least unstable whirling operation. The floating ring design introduced an external damping by the outer oil-film that restabilized the whirling modes. Hence, an attempt was made to find an optimum external damping for the turbocharger with a six-oil-groove bearing.

Although the turbocharger with linear floating ring bearings is dynamically unstable, nonlinearities in real operation could damp the destabilizing forces. However, high whirling running may cause permanent damage to bearings and casing.

The attempt to optimize the whirling modes by adding damped supports to the six-oil-groove bearing was not successful. The reason might be that the analysis was linear, though actual running is nonlinear. Therefore, it's recommended to run nonlinear models and try to optimize the stability again. Experimental investigations would be definitely a wise approach to assure the results.

There is also another recommended technique that might restabilize the turbocharger rotor-bearing system. Optimizing and redesigning the turbocharger rotor mass distribution could be a different route to give a better dynamical performance.

New bearing bore geometries need to be investigated to provide stability over the entire operation speed range. Promise of a distorted bore fixed geometry design [14] must be investigated both analytically and experimentally for the Holset HX30 turbocharger.

A low cost tilting lobe bearing must be designed to achieve a similar performance to the tilting pad bearing stability.

References

[1] AeroTwin™ Motors, "4-Stroke Aerobatic Engine", http://www.aerotwinmotors.com (Henderson, NV: AirScooter Corporation).

[2] Biljetina, R., "Natural Gas Engine", http://www.aircompressor.org (Washington, DC: Energy Solutions Center Inc.).

[3] Born, H. R., "Analytical & Experimental Investigation of the Stability of the Rotor-Bearing System of New Small Turbocharger", *Gas Turbine Conference and Exhibition*, Anaheim, California, May31-June4, 1987, 10p.

[4] Brown, S., "Turbocharging Simplified", http://www.turbochargedpower.com (Roswell, NM: Turbocharged Power Systems).

[5] Ehrich, F. F., *Handbook of Rotordynamics*, Revised edition (Malabar, FL: Krieger Pub. Co., 1999).

[6] Gunter, E. G. and Chen, W. J., "Dynamic Analysis of Turbocharger in Floating Bushing Bearings", To be presented on the *3rd International Symposium on Stability Control of Rotating Machinery (ISCORMA-3)*, Cleveland, Ohio, September 19-23, 2005.

[7] Gunter, E. G. and Chen, W. J., *DyRoBeS© - Dynamics of Rotor Bearing Systems User's Manual*, Revised edition (Charlottesville, VA: RODYN Vibration Analysis, Inc., 2000).

[8] Holmes, R., Brennan, M. J. and Gottrand, B., "Vibration of an Automotive Turbocharger – A Case Study", *Institute of Mechanical Engineers (IMechE)*, 2004, pp. 445-450.

[9] Kirk, R. G., "Stability and Damped Critical Speeds: How to Calculate and Interpret the Results", *Compressed Air and Gas Institute (CAGI) Technical Digest*, Vol. 12, No. 2, 1980, pp. 1-14.

[10] Li, C. H. and Rohde, S. M., "On the Steady State and Dynamic Performance Characteristics of Floating Ring Bearings" *Trans. ASME Journal of Lubrication Technology*, Vol. 103, 1981, pp. 389-397.

[11] NASA, "Turbocharger Cutaway", http://www.nasa.gov (Washington, DC: NASA).

[12] Pitstop, "Gargantuan Turbo", http://www.pitstopdevelopments.com (Littlehampton, UK: Pitstop Developments).

[13] Shaw, M. C. and Nussdorfer, T. J., "An Analysis of the Full-Floating Journal Bearing", *National Advisory Committee for Aeronautics (NACA)*, Report No. 866, 1947, pp. 95-107.

[14] Swanson, E., "Fixed-Geometry, Hydrodynamic Bearing with Enhanced Stability Characteristics", *Society of Tribologists and Lubrication Engineers (STLE) Tribology Transactions*, Vol. 48, No. 1, 2005, pp. 82-92.

[15] Tanaka, M., Hatakenaka, K. and Suzuki, K., "A Theoretical Analysis of Floating Bush Journal Bearing with Axial Oil Film Rupture Being Considered", *Trans. ASME Journal of Tribology*, Vol. 124, 2002, pp. 494-505.

[16] Turbotech, "Holset Medium Duty Turbochargers", *http://turbotech.com.au/holset3.htm* (Ascot, Western Australia: Turbotech Corporation).

[17] Wakefield, G., "The Axis Power® Turbo Diesel", *http://www.rocky-road.com/diesel.html* (Utah: Rocky Road, Inc.).

[18] Watson, N. and Janota, M. S., *Turbocharging the Internal Combustion Engine*, (New York: Wiley, 1982).

Appendix

Matlab Code

```
%       This is a sample Matlab code specially developed to create waterfall plots
%       using the time transient displacement response data generated from
%       DyRoBeS©.  The code also uses another code named hdrload.m
%       developed by Mathworks.com that separates the DyRoBeS© time
%       transient data from the heading text.

% Waterfall Plot: Station No. 1

clear all
close all

% Running Speed
s=[10e3 20e3 30e3 40e3 50e3 60e3 70e3 ...
   80e3 90e3 100e3 110e3 120e3 130e3 140e3 150e3];

% Importing the FFT Data Files
[h1, d1] = hdrload('FFTData10kStn1.dat');
[h2, d2] = hdrload('FFTData20kStn1.dat');
[h3, d3] = hdrload('FFTData30kStn1.dat');
[h4, d4] = hdrload('FFTData40kStn1.dat');
[h5, d5] = hdrload('FFTData50kStn1.dat');
[h6, d6] = hdrload('FFTData60kStn1.dat');
[h7, d7] = hdrload('FFTData70kStn1.dat');
[h8, d8] = hdrload('FFTData80kStn1.dat');
[h9, d9] = hdrload('FFTData90kStn1.dat');
[h10, d10] = hdrload('FFTData100kStn1.dat');
[h11, d11] = hdrload('FFTData110kStn1.dat');
[h12, d12] = hdrload('FFTData120kStn1.dat');
[h13, d13] = hdrload('FFTData130kStn1.dat');
[h14, d14] = hdrload('FFTData140kStn1.dat');
[h15, d15] = hdrload('FFTData150kStn1.dat');

% Creating a Speed Vector for each Running Speed FFT Data
S1=s(1)*ones(length(d1),1);
S2=s(2)*ones(length(d2),1);
S3=s(3)*ones(length(d3),1);
S4=s(4)*ones(length(d4),1);
S5=s(5)*ones(length(d5),1);
S6=s(6)*ones(length(d6),1);
S7=s(7)*ones(length(d7),1);
S8=s(8)*ones(length(d8),1);
```

```
S9=s(9)*ones(length(d9),1);
S10=s(10)*ones(length(d10),1);
S11=s(11)*ones(length(d11),1);
S12=s(12)*ones(length(d12),1);
S13=s(13)*ones(length(d13),1);
S14=s(14)*ones(length(d14),1);
S15=s(15)*ones(length(d15),1);

% Plottong Watefall for X-axis
figure (1)
hold on
title('FFT Waterfall - Compressor End')
xlabel('Frequency (Hz)')
ylabel('Rotor Speed (RPM)')
zlabel('X-Spectrum')
plot3(d1(:,1),S1,d1(:,2))
plot3(d2(:,1),S2,d2(:,2))
plot3(d3(:,1),S3,d3(:,2))
plot3(d4(:,1),S4,d4(:,2))
plot3(d5(:,1),S5,d5(:,2))
plot3(d6(:,1),S6,d6(:,2))
plot3(d7(:,1),S7,d7(:,2))
plot3(d8(:,1),S8,d8(:,2))
plot3(d9(:,1),S9,d9(:,2))
plot3(d10(:,1),S10,d10(:,2))
plot3(d11(:,1),S11,d11(:,2))
plot3(d12(:,1),S12,d12(:,2))
plot3(d13(:,1),S13,d13(:,2))
plot3(d14(:,1),S14,d14(:,2))
plot3(d15(:,1),S15,d15(:,2))
% Syncronous Speeds
thirdXrpm=(0.3/60)*s;
halfXrpm=(0.5/60)*s;
oneXrpm=(1/60)*s;
twoXrpm=(2/60)*s;
%Plotting Syncronous Speeds
plot3(thirdXrpm,s,zeros(1,length(s)),'r')
plot3(halfXrpm,s,zeros(1,length(s)),'r')
plot3(oneXrpm,s,zeros(1,length(s)),'r')
plot3(twoXrpm,s,zeros(1,length(s)),'r')
% Setting the proper View
VIEW(18,60)
XLIM([0 4000])
YLIM([0 150000])
ZLIM([0 0.6])
hold off
```

```
% Plottong Watefall for Y-axis
figure (2)
hold on
title('FFT Waterfall - Compressor End')
xlabel('Frequency (Hz)')
ylabel('Rotor Speed (RPM)')
zlabel('Y-Spectrum')
plot3(d1(:,1),S1,d1(:,3))
plot3(d2(:,1),S2,d2(:,3))
plot3(d3(:,1),S3,d3(:,3))
plot3(d4(:,1),S4,d4(:,3))
plot3(d5(:,1),S5,d5(:,3))
plot3(d6(:,1),S6,d6(:,3))
plot3(d7(:,1),S7,d7(:,3))
plot3(d8(:,1),S8,d8(:,3))
plot3(d9(:,1),S9,d9(:,3))
plot3(d10(:,1),S10,d10(:,3))
plot3(d11(:,1),S11,d11(:,3))
plot3(d12(:,1),S12,d12(:,3))
plot3(d13(:,1),S13,d13(:,3))
plot3(d14(:,1),S14,d14(:,3))
plot3(d15(:,1),S15,d15(:,3))
% Syncronous Speeds
thirdXrpm=(0.3/60)*s;
halfXrpm=(0.5/60)*s;
oneXrpm=(1/60)*s;
twoXrpm=(2/60)*s;
%Plotting Syncronous Speeds
plot3(thirdXrpm,s,zeros(1,length(s)),'r')
plot3(halfXrpm,s,zeros(1,length(s)),'r')
plot3(oneXrpm,s,zeros(1,length(s)),'r')
plot3(twoXrpm,s,zeros(1,length(s)),'r')
% Setting the proper View
VIEW(18,60)
XLIM([0 4000])
YLIM([0 150000])
ZLIM([0 0.6])
hold off
```

```
function [header, data] = hdrload(file)

% HDRLOAD Load data from an ASCII file containing a text header.
%     [header, data] = HDRLOAD('filename.ext') reads a data file
%     called 'filename.ext', which contains a text header.
%     This code developed by Mathworks.com

if nargin < 1
  error('Function requires one input argument');
elseif ~isstr(file)
  error('Input must be a string representing a filename');
end
fid = fopen(file);
if fid==-1
  error('File not found or permission denied');
  end
no_lines = 0;
max_line = 0;
ncols = 0;
data = [];
line = fgetl(fid);
if ~isstr(line)
  disp('Warning: file contains no header and no data')
  end;
[data, ncols, errmsg, nxtindex] = sscanf(line, '%f');
while isempty(data)|(nxtindex==1)
  no_lines = no_lines+1;
  max_line = max([max_line, length(line)]);
    eval(['line', num2str(no_lines), '=line;']);
  line = fgetl(fid);
  if ~isstr(line)
    disp('Warning: file contains no data')
    break
    end;
  [data, ncols, errmsg, nxtindex] = sscanf(line, '%f');
  end % while
data = [data; fscanf(fid, '%f')];
fclose(fid);
header = setstr(' '*ones(no_lines, max_line));
for i = 1:no_lines
  varname = ['line' num2str(i)];
eval(['header(i, 1:length(' varname ')) = ' varname ';']);
  end
eval('data = reshape(data, ncols, length(data)/ncols)'';', '');
```